Check for updates

Recent advances in enhancing the photodetector performance of 2D materials by combining them with organic thin films

Lei Guo, [a] Jiayue Han [ab] and Jun Wang [*ab]

Two dimension (2D) material-based photodetectors usually indicate excellent properties such as ultrafast and broadband response, but the atomic thickness of 2D materials usually leads to low absorption coefficient. Pure 2D material-based photodetectors also suffer from serious drawbacks such as short carrier lifetime, low optical absorption coefficient, and weak built-in field. Organic materials present excellent properties such as flexibility, high absorption coefficient, low cost and large area, which are very suitable for enhancing the detector performance of 2D materials. In this paper, the development of 2D material photodetectors by combining 2D materials with organic thin films since their proposal to date is reviewed. The 2D/organic photodetectors are classified into three categories (graphene-based, MoS_2-based and others), and their development history and research status are comprehensively summarized and reviewed. Organic thin films are categorized into small molecule organic thin films, organic polymer thin films, complex organic thin films, and bilayer organic thin films, and the device performance of each type of material and the mechanism behind the high performance are discussed in detail. Finally, the future development of 2D/organic photodetectors is envisaged. The aim of this paper is to provide new research ideas and directions for 2D/organic heterojunction photodetectors with ultra-high performance and promote the application of these combined photodetectors.

1. Introduction

In the field of modern technology, photodetectors play a key role, and their main function is to convert information-carrying optical signals into electronic signals for further processing and application in electronic devices.[1–3] This technology is widely used in the fields of image processing,[4,5] optical communication,[6,7] *etc.*, and has a profound impact on our daily life. For example, in smartphones, photodetectors enable automatic screen brightness adjustment; in cameras, charge-coupled devices help capture accurate images; infrared detectors play a key role in night observation and security surveillance;[8,9] and photodetectors are also used to acquire high-quality medical images.[10–12] Conventional photodetectors mainly utilize semiconductor materials, which can be divided into three according to the stages of development.[13] The first stage includes the monolithic semiconductors Si[14,15] and Ge;[16] the second stage includes the compound semiconductors GaAs,[17] InSb,[18] *etc.*, and the third stage includes

wide-bandwidth semiconductors GaN,[19] SiC,[20] and ZnO.[21] For a long time, traditional photodetector materials such as HgCdTe, Si, InGaAs, *etc.* have been dominating the global commercial photodetector market by virtue of their considerable detection performance as well as mature scale production and integration technologies.[22–24] The sensitivity, detection range, and detectivity of traditional material photodetectors can no longer meet the demands of military and civil products. There is an urgent need for novel materials to fabricate high-performance photodetectors.

Researchers are actively exploring novel materials, among which graphene[25] and other 2D materials have attracted much attention. Due to their excellent electronic properties and flexibility,[26] 2D materials have great potential for application in the field of improved photodetectors. 2D materials such as graphene have high mechanical strength and high optical transparency,[27] with potential use in fabricating transparent electrodes and flexible optoelectronic devices. The number of layers of 2D materials such as MoS_2 induces a change in the bandgap and has a low dielectric shielding effect internally, making them promising as stable carriers for electronic device applications.[2,28,29] The two-dimensional condition makes it possible to achieve arbitrary stacking between any materials, which is completely unaffected by the lattice mismatch of traditional 3D materials, and exhibits highly compatible

[a] *School of Optoelectronic Science and Engineering, University of Electronic Science and Technology of China, No. 2006, Xiyuan Ave, West Hi-Tech Zone, Chengdu 610054, P. R. China. E-mail: wjun@uestc.edu.cn*

[b] *State Key Laboratory of Electronic Thin Films and Integrated Devices, University of Electronic Science and Technology of China, Chengdu 610054, China*

This journal is © The Royal Society of Chemistry 2024

J. Mater. Chem. C, 2024, **12**, 1233–1267 | 1233

integration properties.[30] Therefore a large number of 2D materials have been applied in advanced optoelectronic devices,[31–33] including photodetectors,[1] optical modulators,[34] lasers,[35] and synaptic photonic chips.[36] In 2009, Xia *et al.* prepared the first graphene photodetector,[1] which initiated the large-scale application of graphene in photodetectors. In 2011, A. Kis *et al.* successfully realized the first single-layer MoS_2 field effect transistor,[37] with a current switching ratio of 10^8 in a device with HfO_2 as the top gate dielectric layer, and a subthreshold swing of 74 mV dec^{-1} for the field effect transistor at room temperature. However, 2D materials are usually less resistive, resulting in higher photodetector dark currents. Moreover, pure 2D material photodetectors have the disadvantages of short carrier lifetime, low light absorption coefficient, and weak built-in field. Therefore, further development on the basis of 2D photodetectors is necessary, and combining 2D materials with organic materials brings new development opportunities.[38]

Organic materials typically have low carrier mobility, high absorption coefficients and broader energy level structures, so photodetectors fabricated using organic materials typically have very low dark current[39] and high light sensitivity.[40] Combining 2D materials with organic materials results in ultra-high-performance photodetectors that can improve performance by several orders of magnitude.[41] Both 2D and organic materials contain a rich library of materials. Common 2D materials include graphene (semimetal),[25,26] MoS_2 (semiconductor),[2] h-BN (insulator),[42] FeTe (magnetic material),[43] *etc.*; common organic materials include pentacene (semiconductor),[44] PVCN (insulator),[45] CuPc (polymer),[46] C_8- BTBT (polymer),[47] *etc.* Although 2D materials show great potential in infrared photodetectors, the performance of photodetectors based on pure 2D materials is limited by weak light absorption and short carrier lifetime. 2D materials are capable of forming π–π stacked interfaces with organic materials, and 2D/organic heterojunctions have good compatibility.[48,49] In addition, the delocalization of Frenkel excitons in organic materials is beneficial to improve the quantum efficiency and operating wavelength of photodetectors. 2D/organic heterojunction photodetectors have been proved to be an effective alternative to improve the performance of photodetectors. 2D/organic heterojunction photodetectors usually exhibit the advantages of ultra-high responsivity, ultrahigh detectivity, ultra-fast response time, broadband spectral detection, ultra-high gain and ultra-high quantum efficiency. The first applications of 2D/organic heterojunctions are in field effect transistors, with the main objectives of improving dissociation efficiency, increasing responsivity and increasing gain.[50,51] For high-efficiency light generation or collection in graphene-based optoelectronic devices, the key challenges are to improve light absorption, construct appropriate band structures and improve the interface quality. Increasing the thickness of 2D material films significantly improves light absorption, but only a small fraction of carriers away from the interface can be collected.[52] The integration of 2D materials with other materials to improve light detection is an excellent strategy, and in particular the combination of organic materials with 2D materials is a breakthrough in photodetector performance.[48,53] Obtaining high-quality 2D/organic interfaces is also a challenge, which are easily contaminated during the fabrication process.[48,53] Heterojunction photovoltaic devices have far surpassed conventional photodetectors in terms of performance, but most of the research is only on individual devices, which have not realized large-scale applications, such as solar cells[54–56] and photodetectors, so heterojunction photovoltaic devices still have a sizeable developmental space.

There are five main physical mechanisms of 2D/organic heterojunction photodetectors: surface plasma-wave-assisted effect,[57] photovoltaic effect,[58] photoconductive effect,[59] photothermoelectric effect[60] and photobolometric effect.[61] A review of some 2D/organic devices, categorized according to the design strategy and physical mechanisms, was conducted by our group in 2019.[41] In this review, we present a comprehensive summary of recent advances in enhancing the photodetector performance of 2D materials by combining them with organic thin films from the materials perspective. Given the distinct properties of diverse materials, separate consideration is necessary concerning application areas, manufacturing processes, integration strategies, performance optimization, and research priorities. Categorizing 2D/organic heterojunction photodetectors based on material type aids in better comprehension and utilization of these materials' unique properties, facilitating the development of targeted application solutions. Initially, this paper classifies 2D/organic heterojunction photodetectors into three categories (graphene-based, MoS_2-based, and others) and discusses various photodetector technologies based on the materials' characteristics and advancements. Further, organic thin films are similarly categorized according to material type, and a comprehensive review of different material types of organic thin films is presented separately, revealing gaps in current research and future directions. This paper aims to systematically examine and discuss the latest advancements in the field of photodetectors, leveraging a material-based classification perspective. It offers an intuitive comparative framework, enabling readers to contrast the performance of detectors made from different materials easily. It is hoped that this review will provide readers with valuable information, which will guide the direction of future research and promote the further development of the field.

2. Two-dimensional (2D) materials and organic materials

Both 2D and organic materials contain a rich library of materials, which ensures the diversity of 2D/organic heterojunction photodetector design. Heterojunctions can also be designed from the structural aspect, such as type-I junction, type-II junction, type-III junction, Z scheme junction, Schottky junction and so on. Achieving effective energy band matching is the focal point of designing high-performance photodetectors, and the type of heterojunction charge transfer is mainly determined by the energy bands of 2D materials and organic materials.[62]

2.1.   Two-dimensional (2D) materials

Common materials used for photodetectors can be classified into four types: (1) zero-dimensional materials,[63] such as

quantum dots, clusters of atoms, *etc.*; (2) one-dimensional materials,[64] such as nanowires, nanorods, nanotubes, *etc.*; (3) two-dimensional materials,[1,2,25,26] such as graphene, MoS_2, *etc.*; and (4) three-dimensional materials, such as Si, Ge, and InSb. 2D materials are those with thickness reduced to the atomic level in one dimension and with larger sizes in the other two dimensions. Common 2D materials include graphene, MoS_2, black phosphorus (BP), $MoTe_2$, WSe_2, ReS_2, Bi_2Se_3, WS_2, *etc.*, and their structures are shown in Fig. 1. As a semimetal, graphene has the advantages of high mobility, broad light absorption spectrum, and ultrafast photogenerated carriers. As for semiconducting TMDs, they have a bandgap that varies with the number of layers (direct bandgap in the case of a single layer and indirect bandgap in the case of multilayers) and unique exciton properties. Graphene and TMDs are most widely used in photodetectors. This paper reports 2D/organic heterojunctions in three categories: graphene-based photodetectors, MoS_2-based photodetectors, and photodetectors of other 2D materials.

The crystal structure and energy band diagram of the 2D material graphene are given in Fig. 2(a) and (b). Graphene has a linear dispersion relation near the Dirac point, and the theoretical density of states at the Dirac point is zero.[65] Therefore, graphene is a semi-metallic material with a band gap of zero. The carriers in graphene can be described as massless Dirac fermions, and this unique property brings about many unique physical phenomena. For example, Dirac fermions can move at 1/300th of the speed of light in graphene. Most importantly, the carrier mobility in graphene can be as high as 20 000 cm^2 V^{-1} s^{-1}, much higher than that of commonly used semiconductor materials such as Si. Due to graphene's unique energy band structure, its zero band gap gives it uniform optical absorption over a broad spectrum (Fig. 2c and d), and its optical absorption range can be
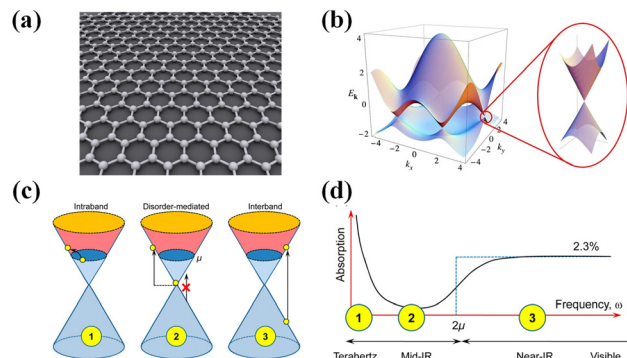

Fig. 2 2D material graphene. (a) Crystal structure of graphene.[65] Reproduced with permission.[65] Copyright 2015, Sciendo. (b) Energy band diagram of graphene.[26] Reproduced with permission.[26] Copyright 2009, American Physical Society. (c) Illustration of the various optical transition processes.[67] (d) Schematic diagram of the absorption spectrum of graphene, with the numbers corresponding to the dominant mechanism in part (c).[67] Reproduced with permission.[67] Copyright 2014, American Chemical Society.

extended from the UV to the terahertz band.[26,66,67] The optical absorption of graphene depends only on the structural parameters, and the intrinsic graphene absorbs only 2.3% of the light in the broad spectrum. Mechanically, Young's modulus of single-layer graphene is greater than 1 TPa. Since the thickness of a single layer is only 0.34 nm, it is very flexible and can be used to fabricate flexible devices, *e.g.*, as a flexible electrode material.

Unlike graphene, TMDs are a group of 2D materials that can have a band gap. Their common form is MX_2, where M is a transition metal (Mo, W, *etc.*) and X is a sulfur group element (S, Se, Te, *etc.*). MoS_2 is a typical TMD, and its crystal structure,
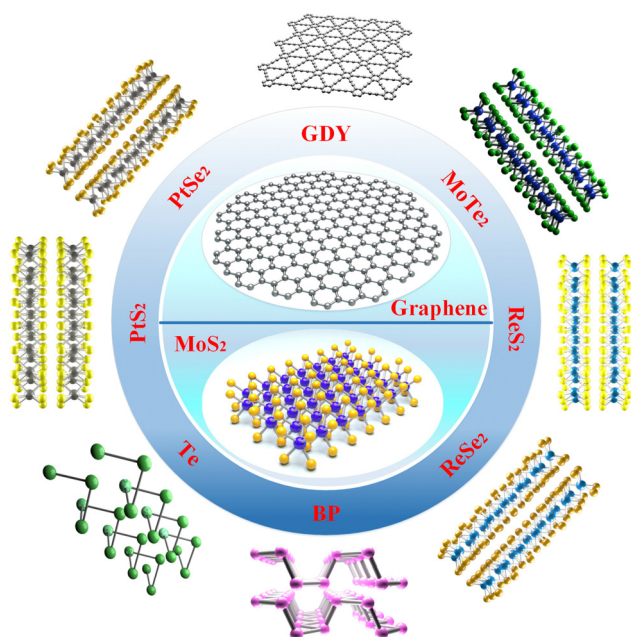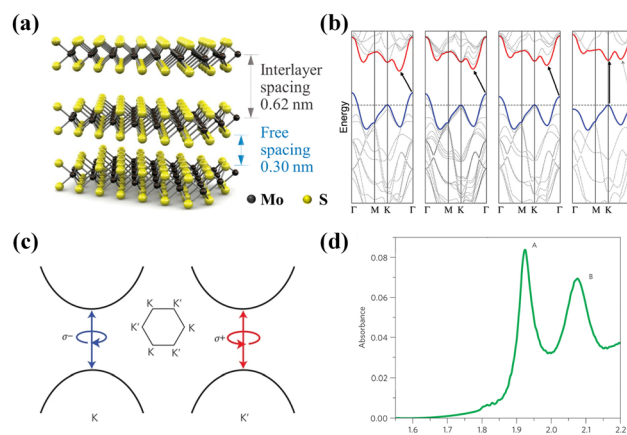

Fig. 1 Various 2D materials and their structures.

Fig. 3 Transition metal dichalcogenide MoS_2. (a) Crystal structure of MoS_2.[68] Reproduced with permission.[68] Copyright 2017, American Chemical Society. (b) Energy band diagram of MoS_2;[69] from left to right, block molybdenum, quadruple molybdenum, double molybdenum, and single molybdenum. Solid arrows indicate the lowest energy conversion. Reproduced with permission.[69] Copyright 2010, American Chemical Society. (c) Spin and valley coupling of MoS_2.[70] Reproduced with permission.[70] Copyright 2012, Nature Publishing Group. (d) Light absorption spectra of monolayer MoS_2 and A, B excitons.[71] Reproduced with permission.[71] Copyright 2012, Nature Publishing Group.

This journal is © The Royal Society of Chemistry 2024

J. Mater. Chem. C, 2024, **12**, 1233–1267 | **1235**

energy band structure, and spin–valley coupling are shown in Fig. 3(a)–(c) respectively. Thick-layer MoS_2 is an indirect bandgap semiconductor material, and the bandgap decreases as the layers become thicker. The band gap of thick-layer MoS_2 is 1.2 eV, whereas single-layer MoS_2 has a direct band gap of 1.9 eV. As shown in Fig. 3(d), which demonstrates the light absorption spectrum of MoS_2, the cleavage of the valence bands brings about two unique distinctive excitons, with the higher-energy exciton known as B-exciton and the lower-energy exciton known as A-exciton. In monolayer TMDs, the neutral exciton can also combine with an electron or hole to form a tri-exciton, and the concentration of tri-excitons in TMDs can be regulated by applying a gate voltage.

Researchers have been exploring the preparation method of high-quality, large-area, expandable, and stable 2D material films for a long time.[72] Currently, the main preparation methods include the following four: mechanical exfoliation,[73] chemical vapor deposition,[74] epitaxial growth[75] and reduction of graphene oxide.[76] 2D materials are unlikely to replace Si but can functionally complement the existing technologies. Microelectronic devices will continue to evolve in the direction of being faster, smaller, cheaper, and more functional. 2D materials are expected to lead the industrial transformation based on material innovation.

2.2. Organic materials

Organic materials mainly include small molecules, polymers, complexes, metal–organic frameworks (MOFs), and covalent organic frameworks (COFs). Organic semiconductor materials are widely used in organic light-emitting diodes (OLEDs) because of their low cost, flexibility, high fluorescence efficiency, and broad spectral coverage.[77–79] Organic thin film transistors are widely used in integrated circuits.[80–83] Polymer organic semiconductors were the first class of materials to be used in photodetector research, with a long history of research and extensive optimization experience. In general, polymers have good solubility and can be prepared as films by spin-coating, spraying, LB method, and other simple and inexpensive processes. Small molecule materials have inherent advantages over polymers. For example, they have a fixed molecular mass and physical properties, a fixed molecular structure, and a neat and regular crystal arrangement. The acene compounds possess flat and tight conjugated structures and are most frequently used in organic electronics research, such as benzotriazole, tetracene, pentacene, and rubrene, which have excellent properties. Among them, pentacene has become the most shining material in photodetector applications due to its good crystallinity, easy formation of large-size grains, and highly ordered single crystals. The molecular structure of phthalocyanines mainly consists of nitrogen-containing conjugated macrocycles with excellent planarity, and molecules with different properties can be synthesized by coordinating different metal elements. Phthalocyanine materials such as CuPc, CoPc, NiPc, $F_{16}CuPc$, etc. perform well in photodetectors. In addition to the above materials, many new high-performance organic semiconductor materials have also been developed and applied to photodetectors with good results, such as NTCDA, $PTCDI-C_8$, and C_{60}.

COFs are emerging crystalline porous organic polymers with light elements linked by covalent bonds. COFs have controllable properties in the material structure and electronics. COFs are formed by covalent bonding, and the 2D planes are usually stacked face-to-face, with strong π–π interactions between neighboring layers and in the 2D plane, which is very favorable for carrier migration.[84–86] 2D COFs with characteristic light absorption and exciton generation under light illumination have become a hot research topic. The coupling of optical and electrical properties leads to the application of 2D COFs in photodetectors with their unique advantages, and ultrathin 2D-COF nanosheets or thin films have gained a widespread interest as photodetectors. MOFs are a new class of crystalline nanoporous materials composed of inorganic secondary structural units and organic ligands via coordination bonds.[87] The intrinsic energy band structure and electronic properties of 2D MOFs can be systematically tuned by the reaction conditions of the coordination environment, organic ligands, and molecular building blocks during the assembly process.[88,89] MOFs have strong light absorption in the SWIR, and their structural and functional diversity and energy band tunability simultaneously provide more opportunities for their integration into photodetectors.

Common organic materials for heterojunction photodetectors are shown in Fig. 4. By choosing different 2D and organic materials, devices with different functions can be realized. The strategy of combining 2D materials with organic materials has excellent application prospects in the field of photodetectors.

2.3. Rational combination of 2D and organic materials

Photodetectors, as critical devices for information perception, have an indispensable position in modern information technology, and their main task is to convert optical signals into electrical signals efficiently. Optoelectronic devices adapted to different wavelength bands can be constructed by selecting
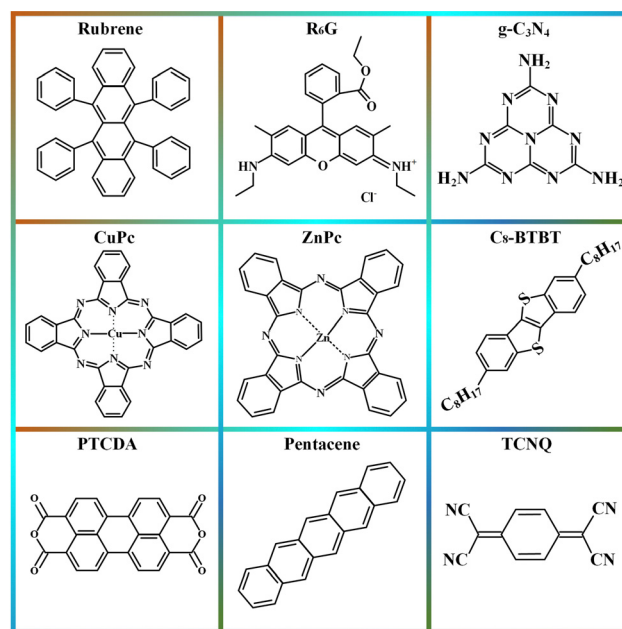

Fig. 4 Common organic materials in 2D/organic heterojunction photodetectors.

1236 | J. Mater. Chem. C, 2024, 12, 1233–1267

This journal is © The Royal Society of Chemistry 2024

semiconductor materials with different bandgaps. In recent years, 2D materials have been widely used in optoelectronic devices due to their wide variety and excellent electrical and optical properties. However, 2D materials suffer from limited light absorption capacity due to their ultrathin property, which limits their application in optoelectronics. Constructing 2D/organic heterojunctions is an advanced material design strategy (Fig. 5) that combines the advantages of 2D and organic materials, solves some of the problems of single-material systems, and significantly improves several material and device properties, especially in photovoltaic conversion and energy storage.

In order to construct high-performance heterojunction photodetectors, the energy band structures and properties of different materials need to be fully considered in order to select and match different materials. Fortunately, both 2D and organic materials are equipped with a rich library of materials, so researchers can flexibly select appropriate materials to achieve suitable heterostructures according to specific needs. Graphene has excellent electrical and thermal properties; the downside is that graphene has a zero band gap, which makes it more difficult to suppress its dark current. MoS_2 has an adjustable bandgap, which can be realized to suppress the dark current. However, the spectral response of MoS_2 is mainly concentrated in the visible range, and the response to bands such as infrared light is relatively poor. Graphene and MoS_2 are the most applied 2D materials in photodetectors.

When comparing Wannier excitons in 2D materials and Frenkel excitons in organic materials, Frenkel excitons have higher exciton binding energies, and delocalization of Frenkel excitons is beneficial for improving the quantum efficiency of photodetectors and broadening the operating wavelength range. Combining 2D and organic materials may result in "π–π stacked interfaces" and "ordered molecular orientations". The 2D materials have low-defect surfaces and show good compatibility with organic materials without the need to consider lattice matching. This provides a solid theoretical basis for the design and application of 2D/organic heterojunctions.[48,49]

As society enters the high-tech era, there is a growing demand for multifunctional photodetectors, such as in life sciences (X-rays,[90] MRIs,[91] CT scans,[92] and PET scans[93]), communications and information technology (fiber-optic communications,[94] LIDAR,[95] photonics computing,[96] and optical sensing[97]), security and military applications (night-vision,[98] infrared detection,[99] laser ranging,[100] and target identification[101]), industry and manufacturing[102] (measuring, detecting and monitoring various physical parameters), etc., which necessitates the development of new photodetectors, especially 2D/organic heterojunction detectors. 2D/organic heterojunctions face challenges in multifunctional, high-performance optoelectronic detection (e.g., interface engineering[103] and thin-film preparation techniques[104]), which can be overcome through materials engineering and technological innovation, enabling them to be useful in a variety of applications.

Combining 2D materials with organic materials offers the following advantages:

(1) Optoelectronic performance enhancement: 2D materials (e.g., graphene, TMDs, etc.) have excellent optoelectronic properties with high carrier mobility and wide spectral response range. Combining 2D materials with organic materials can extend the spectral response range of photodetectors and improve their sensitivity.

(2) Flexibility and malleability: organic materials are often very flexible and can be easily prepared on substrates of different shapes and sizes, thus making photodetectors more flexible. This is important for certain special applications such as wearable technology and flexible electronics.

(3) Low-cost production: organic materials typically have low preparation costs and can be prepared using simple processes such as printing and coating. Combining organic materials with 2D materials allows high performance photodetectors to be produced at low cost, which is very attractive for mass production.

(4) Energy efficiency: 2D materials possess high electron mobility, and thus combining them with organic materials can reduce power consumption and improve the energy efficiency of photodetectors, which is very important in mobile devices and sensor applications.

(5) Multifunctionality: organic materials can be chemically modified and functionalized to achieve a variety of functions, such as enhancing the stability, selectivity, and response speed of photodetectors. Thus, the combination of 2D and organic materials holds great promise for various specific applications.

3. Performance characterization of photodetectors

The following parameters are often used to measure the performance of a photodetector (Fig. 6): responsivity, gain,
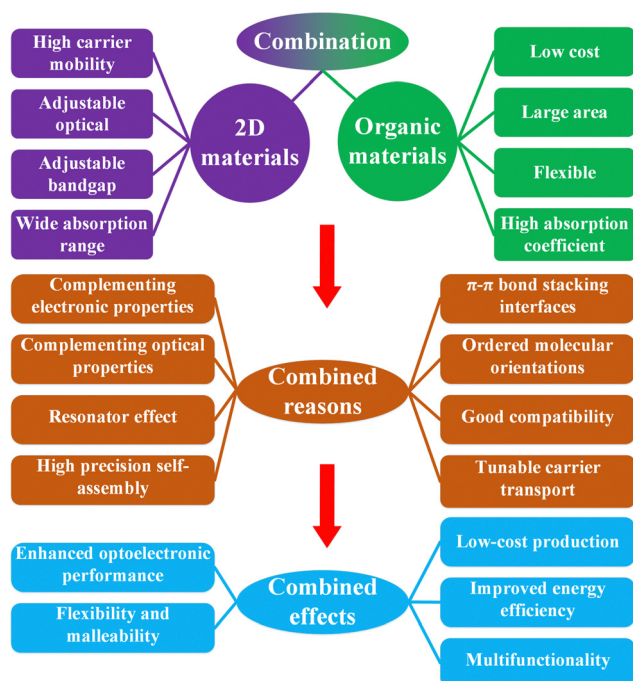

Fig. 5 Rational combination of 2D and organic materials.

This journal is © The Royal Society of Chemistry 2024

J. Mater. Chem. C, 2024, **12**, 1233–1267 | **1237**

response time, detectivity, noise equivalent power, and so on. These parameters are briefly described below.

3.1. Responsivity (R)

Responsivity (R), also known as sensitivity, describes the photoelectric conversion efficiency of a photodetector, which can characterize the magnitude of the photoelectric conversion capability and is an essential parameter for assessing the performance of a photodetector.[105] The responsivity refers to the ratio of the photocurrent generated under light conditions to the optical power of the effective area. The defining formula is

$$R = \frac{I_{ph}}{P_{in}} = \frac{I_{light} - I_{dark}}{P_{in}} \quad (1)$$

where I_{ph} denotes the photocurrent, I_{light} and I_{dark} denote the value of the current in the case of light and dark respectively, and P_{in} denotes the value of light power in the effective area. The performance of the detector is indicated by the magnitude of the value of R. A larger value of R indicates better performance.

3.2. Response time (τ)

Response time (τ) refers to the sensitivity of a photovoltaic device to an optical signal. Typically, the response time (τ) is defined as the time for the net photocurrent to rise from 10% to 90% when the light is switched on and off (rise time or response time) or the time for the net photocurrent to fall from 90% to 10% (fall time or recovery time). The rise time is determined by the transport of carriers and the fall time is determined by the collection of carriers by the electrodes.[106] The response time is affected by many factors, such as the equivalent intrinsic RC constant of the device and the defect in the 2D material.

3.3. Noise equivalent power (NEP)

Noise equivalent power (NEP), also called minimum measurable power, refers to the optical power required to produce a signal with one signal-to-noise ratio.[107] The NEP is defined as

follows:

$$NEP = \frac{P_{in}}{\sqrt{B}} = \frac{i_n}{R} \quad (2)$$

where P_{in} is the incident power at a signal-to-noise ratio of 1, B is the amplifier bandwidth, i_n represents the noise current, and R is the responsivity. The smaller the NEP, the smaller the noise, and the better the detector detection capability.

3.4. Detectivity (D^*)

Detectivity (D^*) represents the ability of the detector to capture weak signals[108] and is calculated as follows:

$$D^* = \frac{\sqrt{AB}}{NEP} = R\frac{\sqrt{AB}}{i_n} \quad (3)$$

where A denotes the effective illumination area (cm^2) and e is the elementary charge.

3.5. Gain (G)

Gain (G) can be expressed as the number of regenerated photoexcitons through a multiplication mechanism. For highly responsive photoconductive devices, researchers usually use multiple methods to capture one type of carrier to obtain a higher carrier lifetime, which multiplies the number of other types of carriers within the conducting channel.[109] Thus, the gain (G) stems from a longer carrier lifetime and can be defined as follows:

$$G = \frac{\tau_{life}}{\tau_{transit}} = \frac{\tau_{life}}{L^2/\mu V_{bias}} \quad (4)$$

where τ_{life} and $\tau_{transit}$ represent the excited carrier lifetime and carrier crossing time, respectively. L denotes the transmission channel length, μ denotes the carrier mobility, and V_{bias} denotes the bias voltage.

3.6. External quantum efficiency (EQE)

External quantum efficiency (EQE) is one of the main performance indicators of photodetectors and is defined as follows: when photons are irradiated onto the sensing surface of a photodetector, some of the photons will excite the photosensitive material to produce an electron–hole pair to form a photocurrent, and the ratio of the number of collected electrons to the number of all incident photons is called the external quantum efficiency (EQE).[110,111] The defining equation is as follows:

$$EQE = R \times \frac{hc}{e\lambda} \times 100\% \quad (5)$$

where h is Planck's constant, c represents the speed of light, and λ is the wavelength of the detected light. The external quantum efficiency (EQE) is proportional to responsivity (R).

4. Recent progress in 2D/organic heterojunction photodetectors

Modern optoelectronic devices, such as detectors, modulators, lasers, LEDs, and solar cells, are widely used daily. Modern optoelectronic devices are essential in imaging, display, optical

Fig. 6 Performance characterization of photodetectors.

1238 | *J. Mater. Chem. C*, 2024, **12**, 1233–1267

This journal is © The Royal Society of Chemistry 2024

communications, medicine, security, and energy. Photodetectors are popular optoelectronic devices used to convert optical signals into electrical signals. They play a key role in optics, communications, imaging, sensing and many other applications. The main principle of operation of photodetectors is to use light energy to excite charge carriers (electrons or holes) and convert them into current or voltage signals. Traditional photodetectors are usually manufactured based on traditional semiconductor materials such as Si, Ge, GaAs, *etc.*[13–21] The application fields of photodetectors are becoming increasingly extensive, and the corresponding requirements for photodetectors are also higher. Traditional photodetectors can no longer meet the demand, especially in medicine, quantum communication, and satellite radar, and other more stringent requirements.[90–97,99–102] The rise of 2D materials has brought new opportunities for the fabrication of photodetectors, especially since 2004 when Novoselov *et al.* obtained single-layer graphene by mechanical exfoliation.[112] 2D materials, including graphene and its derivatives (*e.g.*, graphene oxide, reduced graphene oxide), along with analogous materials (*e.g.*, TMDs, black phosphorus), demonstrate favorable compatibility with organic materials due to their distinct physical and chemical characteristics (low-defect surfaces, tunable surface chemistry, and the absence of a requirement for lattice matching considerations).[48,49] Constructing 2D/organic heterojunctions can enhance carrier separation efficiency and mobility, improve interface properties, and increase device flexibility and processability. Consequently, 2D/organic heterojunction photodetectors (Fig. 7) often exhibit ultra-high responsivity, ultra-sensitive optical response, ultra-fast response time, broadband spectral detection, ultra-high gain, and ultra-high quantum efficiency. With society entering the era of big data, there is an increasing demand for multifunctional photodetectors in various fields, including high-speed communication, optical memory, light modulation, and on-chip computational optoelectronics. Therefore, challenges and opportunities persist for 2D/organic heterojunctions in multifunctional and high-performance detection.

4.1. Graphene-based photodetectors

Photodetectors based on the 2D material graphene are a hot research topic in the field of photodetection. However, graphene's thickness of only one atomic layer results in low absorbance (only 2.7%), which limits its responsivity, which is usually on the order of mA W^{-1}. To solve this problem, we can combine graphene's property of high carrier mobility with the excellent light-absorbing properties of organic materials to prepare graphene photodetectors with excellent absorption properties (the summary of graphene/organic devices is shown in Table 1).

4.1.1. Combining with small molecule organic materials. Organic small-molecule materials can create thin film layers through thermal evaporation. This method offers ease of controlling parameters such as film thickness, making it particularly beneficial for conducting repetitive comparative experiments. Furthermore, films produced *via* thermal evaporation typically exhibit superior interface quality to alternative
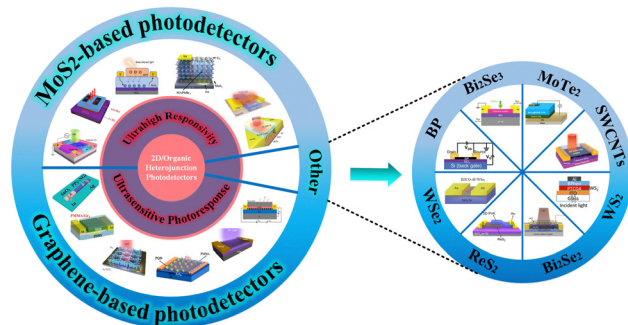

Fig. 7 2D/organic heterojunction photodetectors. Graphene-based photodetectors. Reproduced with permission.[126,139,148,152,157,169] Copyright 2018, Wiley-VCH; Copyright 2023, Wiley-VCH; Copyright 2018, Wiley-VCH; Copyright 2019, American Chemical Society; Copyright 2020, Wiley-VCH; Copyright 2017, American Chemical Society; Copyright 2022, American Chemical Society. MoS$_2$-based photodetectors. Reproduced with permission.[178,179,182,186,187,189] Copyright 2022, Nature Publishing Group; Copyright 2022, American Chemical Society; Copyright 2015, Wiley-VCH; Copyright 2019, Nature Publishing Group; Copyright 2022, Wiley-VCH; Copyright 2019, Wiley-VCH. Other photodetectors. Reproduced with permission.[191,193–198,200] Copyright 2017, American Chemical Society; Copyright 2020, Wiley-VCH; Copyright 2021, Wiley-VCH; Copyright 2021, Nature Publishing Group; Copyright 2022, American Chemical Society; Copyright 2022, Nature Publishing Group; Copyright 2022, Elsevier; Copyright 2022, Wiley-VCH.

techniques like spin coating. Dye molecules typically possess a high absorption cross-section, and their combination with graphene, which exhibits a broad absorption band, can significantly enhance the device's photocurrent and quantum efficiency. The primary mechanisms underlying the ultra-high performance of dye-sensitized graphene photodetectors involve enhanced light absorption and the amplification of photocurrent generated by optically excited charges. In this hybrid structure, the p-orbitals of dye molecules facilitate photoinduced charge transfer between the two materials. The graphene/dye R6G heterojunction photodetector[113] features a wide spectral range (400–1000 nm), high responsivity (460 A W^{-1}), and a high EQE (105%). Additionally, graphene/dye R6G can operate at low voltage, and its responsivity exhibits no significant attenuation in the detection region. Given the extensive variety of available dye molecules, they can be replaced as needed, providing a design strategy for high-performance photodetectors. In previous 2D/organic heterojunction phototransistors, graphene was often employed solely as a charge carrier transport layer, failing to exploit its broadband absorption characteristics fully. Graphene nanoribbons (GNRs) can open a bandgap near the charge neutrality point. However, this approach suffered from low photoresponsivity. Combining GNRs with graphene overcomes this limitation. The nanoribbon graphene/C$_{60}$ heterojunction photodetector[114] achieves tunable light responsivity in the MIR spectrum. C$_{60}$ captures the photogenerated charge carriers, while GNRs serve the dual roles of light detection and charge carrier transport. This leads to a broadband, high photocurrent, and high photoresponsivity photodetector. The principle of tunable light responsivity involves controlling the nanoribbon width to modulate the bandgap, which holds significant potential for application in fields such as infrared imaging.

Table 1 Summary of graphene-based 2D/organic devices

2D materials	Organic thin films	Published year	Active materials	Responsivity [A W^{-1}]	Response time [ms]	Detection range [nm]	Gain/ EQE [%]	Detectivity [Jones]	Ref.
Graphene	Small molecule organic thin films	2015	Graphene/dye R6G	460	<100	400–1000	10^5%	1.5×10^7	113
		2016	Nanoribbon graphene/C$_{60}$	0.4	4000	10 000	NA	NA	114
		2017	Graphene/Zn$_{0.9}$Mg$_{0.1}$O NPs/BET dye	8×10^3	≈ 1000	530	1.87×10^4%	1.7×10^{12}	115
		2017	Graphene/Zn$_{0.9}$Mg$_{0.1}$O NPs/N$_4$ dye	6.5×10^3	≈ 1000	460, 660	1.75×10^4%	1.3×10^{12}	115
		2017	Graphene/rubrene	10^7	100	400–600	10^9%	9×10^{11}	116
		2018	Graphene/C$_{60}$	10^7	<5	200–808	$>10^8$%	NA	117
		2018	Graphene/DPA	110	>1000	420	$>10^3$%	10^{13}	118
		2019	Graphene/R6G/graphene	500	30 000	400–1000	$>10^4$%	NA	119
		2019	Graphene/C$_{60}$	10^9	2.3	400–1100	10^9%	10^{15}	120
		2020	Graphene/C$_{60}$/graphene	3.4×10^5	23	405–1550	$>10^7$%	NA	121
		2020	Graphene/C$_{12}$TBP	2330	NA	400–850	$>10^5$%	1.9×10^9	122
		2021	Graphene/HAT-CN/Bi$_2$O$_2$Se	2000	0.197	488–1550	6×10^4	1.2×10^{11}	123
		2021	IGZO/graphene/CuPc	NA	NA	300–800	150%	NA	124
		2022	Graphene/pentacene	10^5	0.006/0.009	270–850	3.3%/10%	$>10^{11}$	128
		2022	Graphene/BUBD-1	7×10^5	0.33/0.49	295–658	NA	4×10^{14}	129
		2023	Rubrene/graphene	8×10^5	0.02/0.07	405	NA	$>10^{12}$	130
		2023	Pentacene/graphene/Au	$>10^4$	1	658	1.51%	NA	165
	Polymer organic thin films	2014	Graphene/P3HT/PZT	NA	180	325	10^3	NA	131
		2015	Graphene/P3HT	10^5	60	500	$>10^6$%	NA	132
		2016	Graphene/C$_8$-BTBT	10^4	25	355	1.89×10^8	10^8	133
		2017	Graphene/PTB7	1.8×10^5	7.8	450–800	$>10^6$%	NA	134
		2018	Graphene/PDA	556	NA	350–700	$>10^5$%	6×10^{11}	135
		2020	Graphene/J-aggregate TDBC cyanine dye	0.02	>1000	530–600	NA	NA	136
		2020	Graphene/PTCDI-C$_8$/Al	1.5×10^{-4}	NA	400–650	1.50%	4.5×10^9	166
		2021	Graphene/h-BN/J-aggregate PTCDI-C$_{13}$	10^3	>1000	550	$>10^5$%	10^{10}	137
		2021	Graphene/h-BN/PTCDI-C$_{13}$	180	<1000	550	$>10^3$%	10^{10}	137
		2021	Graphene/PDVF	70	NA	350–850	NA	10^{10}	138
		2021	Graphene/PTCDI-C$_8$ dimer	2×10^5	10	300–940	NA	10^{16}	167
		2023	PPy-NGr/SnO$_2$	4594.25	490/3040	<240	NA	6.47×10^{11}	139
	Complex organic thin films	2013	Graphene/chlorophyll	10^6	110	400–700	NA	NA	140
		2015	TiO$_x$/graphene/ P3HT:PCBM	≈ 0.1	≈ 1000	300–800	NA	NA	141
		2015	Graphene/CH$_3$NH$_3$PbI$_3$	180	87	400–800	2×10^4%	10^9	142
		2016	Graphene/CH$_3$NH$_3$PbI$_3$/ NPs	2×10^3	1500	532	$>10^6$%	NA	143
		2017	Graphene/ CH$_3$NH$_3$PbI$_3$:PCBM	8×10^5	2.5×10^3	400–750	NA	NA	144
		2018	Graphene/TCNQ	2×10^3	0.1	600–2000	NA	NA	145
		2018	Graphene/MOF	10^6	<150	300–700	5×10^8%	6.9×10^{14}	146
		2018	Graphene/ CH$_3$NH$_3$PbI$_3$:MoS$_2$	1.08×10^4	45	400–750	2×10^6%	4.28×10^{13}	147
		2019	Graphene/CH$_3$NH$_3$PbBr$_3$ QDs/graphene	10^9	0.02	350–850	1.2×10^{10}%	8.7×10^{15}	148
		2019	Graphene/P3HT:F4 TCNQ	6×10^5	NA	600–1500	$>10^7$%	NA	149
		2020	Graphene/GNSs/MAPbI$_3$	5.9×10^4	2500	460	1.59×10^7%	1.31×10^{13}	150
		2020	Graphene/TTF:CA	10^5	8	600–2200	6×10^6%	10^{13}	151
		2020	Graphene/COF	3.2×10^7	1.14	400–600	8.5×10^9%	6×10^{13}	152
		2021	Graphene/Au array/ (BA)$_2$(FA)$_{n-1}$Pb$_n$I$_{3n+1}$	18.71	330	300–800	$\approx 10^3$%	10^{13}	153
		2021	Graphene/ZnO/IEICO-4F:PTB7-Th	6.1×10^6	NA	488–1064	8.3×10^8%	2.43×10^{13}	154
		2021	Graphene/PBDB-T:PC$_{71}$BM	0.36	0.049	400–700	10^{13}	10^{13}	168
		2022	Graphene/PM6:Y6	2.8×10^6	0.02/8.4	450–1064	5.47×10^8%	1.47×10^{14}	155
	Bilayer organic thin films	2015	Graphene/PEDOT:PSS/ P3HT:PC$_{71}$BM	0.16	≈ 1000	300–650	NA	1.33×10^{12}	156
		2017	Graphene/P3HT/ CH$_3$NH$_3$PbI$_{3-x}$Cl$_x$	4.3×10^9	1000	400–1300	8.9×10^9	NA	157
		2017	Graphene/PTCDA/ pentacene	10^5	0.03	400–700	9%	NA	158
		2017	Graphene/pentacene/ PTCDI-C$_8$	0.007	NA	480–670	1.26×10^9	1.26×10^9	125
		2018	Graphene/C$_{60}$/pentacene	9127	0.275	405–1550	5.2×10^5	NA	126
		2019	Graphene/P3HT/ PEDOT:PSS	0.25	NA	400–650	NA	1.8×10^8	159
		2019	Graphene/PTCDA/C$_8$-BTBT	5.76×10^5	470	400–700	1.38×10^9	NA	160

Table 1 (*continued*)

2D materials	Organic thin films	Published year	Active materials	Responsivity [A W^{-1}]	Response time [ms]	Detection range [nm]	Gain/EQE [%]	Detectivity [Jones]	Ref.
		2021	Graphene/ZnPc:C$_{60}$/ZnPc	204	0.004	635	3.9×10^4	NA	161
		2021	Graphene/PTAA/CH$_3$NH$_3$PbI$_{3-x}$Cl$_x$	10^5	310	350–800	NA	10^{13}	162
		2021	Graphene/C$_{60}$/ZnPc	6537	0.007	405–980	1.4×10^5	NA	163
		2021	Graphene/C$_{60}$/pentacene	2010	<300	400–1100	NA	NA	127
		2022	Graphene/MOF/graphene/PVDF	1.3×10^3	0.22	530	3×10^{10}%	2.9×10^{15}	169
		2022	Graphene/C$_{60}$/PbPc	2.2×10^3	NA	405–980	NA	NA	164
		2022	Graphene/C$_{60}$/CuPc	NA	NA	NA	NA	NA	170

Narrowband photodetection has attracted extensive research, but previous strategies had noticeable drawbacks, such as reduced photoresponsivity, complex configurations, and lack of tunability. 2D/dye molecule heterojunction phototransistors[115] provide an ideal solution. The graphene/Zn$_{0.9}$Mg$_{0.1}$O NPs/BET dye combination achieves tunable narrowband detection in the range of 470–580 nm, while the graphene/Zn$_{0.9}$Mg$_{0.1}$O NPs/N$_4$ dye setup accomplishes narrowband photodetection at 400–500 nm and 610–700 nm. The responsivity reaches levels of 10^3, EQE reaches levels of 10^4%, and detectivity reaches levels of 10^{12}. Most importantly, these devices are compatible with flexible configurations. Organic dye molecules typically have distinct isolated energy levels, making them unique, high-absorption, inherently narrowband absorbers. Combining them with 2D materials, where the dye molecules are anchored on graphene, significantly enhances light absorption while mitigating linewidth broadening. Graphene serves as a narrowband hybrid transport layer. In summary, the high performance of these photodetectors results from the controlled adsorption of dye molecules, which suppresses dye–dye coupling and π-resonance, preserving the narrowband detection characteristics of the dye molecules. The rich library of available dye molecule materials enables the tunability of the photodetectors. Gareth *et al.* were the first to apply single-crystal organic semiconductor materials to 2D/organic heterojunctions, and the stacking within single crystals can promote exciton diffusion over several micrometers, which contributes to improving the phototransistor's EQE. The graphene/rubrene heterojunction phototransistor[116] achieves a responsivity of 10^7 A W^{-1} and a detectivity of 9×10^{11} Jones at room temperature. This performance is attributed to the long-range order in single-crystal "rubrene", which helps to efficiently transfer photogenerated charges to graphene. Furthermore, combining single crystals with 2D materials can enhance the response speed of 2D/organic heterojunction phototransistors, holding significant potential applications in optical storage. Qin *et al.*[117] were the first to introduce C$_{60}$ into 2D/organic heterojunction photodetectors. The authors synthesized an all-carbon hybrid film with solid, tunable ultraviolet spectral absorption. The graphene/C$_{60}$ heterojunction photodetector exhibits high photocurrent gain, elevated EQE, and exceptional ultraviolet sensitivity (covering 200–400 nm, $R > 10^7$ A W^{-1}). This is attributed to the well-organized assembly of C$_{60}$, which facilitates efficient exciton dissociation at the heterojunction interface. Notably, the device maintains its performance almost unchanged after two months of operation, demonstrating long-term stability and high reliability. The authors simultaneously fabricated a 5×5 array of devices, which holds significant potential for integrated optoelectronic applications.

Field-effect transistors have found wide applications due to their excellent optoelectronic properties. However, previously reported 2D/organic heterojunction vertical field-effect transistors did not perform well. DPA is an organic single-crystal material known for its advantages, such as the absence of impurities and defects, uniform molecular orientation, and high mobility. Combining DPA with graphene forms an excellent interface contact that effectively suppresses dark currents, enabling high photo-detection rates and a sizeable on–off ratio. The graphene/DPA heterojunction field-effect transistor,[118] by gently transferring the organic single crystal onto the graphene surface using soft contact gold electrodes, achieves a detectivity of 10^{13} Jones, a responsivity of 110 A W^{-1}, and a switching ratio of 1.5×10^3. This represents a significant enhancement in the performance of 2D/organic field-effect transistors, laying a solid foundation for developing vertical organic optoelectronic devices. Graphene/R6G/graphene (Fig. 8a and b)[119] adopts a sandwich structure with a rhodamine 6G (R6G) monolayer as the photoactive layer sandwiched between two graphene films acting as channels. R6G dye molecules possess favorable characteristics such as low cost, high stability, and a high fluorescence yield (0.95). Due to the solid π–π interaction between R6G and graphene interfaces, photo-excited electrons can transfer from graphene to the dye molecules. Compared to R6G/graphene, graphene/R6G/graphene exhibits a 40-fold increase in responsivity (10^3 A W^{-1}) (Fig. 8c). This enhancement results from the powerful π–π interaction, which reduces the intermolecular distance between the monolayer of R6G and the graphene, allowing photo-excited electrons from the top and bottom graphene layers to more effectively transfer to the encapsulated R6G monolayer. Of greater significance, graphene/R6G/graphene represents a three-layer ultra-thin structure, potentially serving as a critical component in the next generation of highly integrated optoelectronic devices.

Electrophoretic deposition technology aids in producing high-quality 2D/organic heterojunctions. Photodetectors fabricated using electrophoretic deposition technology, such as the graphene/C$_{60}$ heterojunction photodetector (Fig. 8d and e),[120] achieve an outstanding detectivity of 10^{15} Jones, an EQE of 10^9%, and a remarkably high responsivity of 10^9 A W^{-1} (Fig. 8f).

This journal is © The Royal Society of Chemistry 2024

J. Mater. Chem. C, 2024, **12**, 1233–1267 | **1241**

The exceptional performance of these photodetectors is primarily attributed to the doping enhancement of graphene upon adsorption of C_{60}, significantly promoting charge transport between the two components. This device capitalizes on C_{60}'s strong electron-accepting properties and graphene's high charge carrier mobility, enabling synergistic cooperation for efficient charge collection and, thus, the realization of high-performance photodetectors. Importantly, this device introduces electrophoretic deposition technology into manufacturing 2D/organic heterojunction photodetectors for the first time, extending the detection range to 400–1100 nm. This marks a pivotal advancement for broadband and NIR photodetection. The graphene/C_{60}/graphene heterojunction photodetector[121] proposed by our research group has also been utilized to fabricate phototransistor arrays. This approach enables tunability of multiple parameters, such as photocurrent, response

intensity, and response speed, making it feasible for wideband, large-scale array detection of an all-carbon material. Notably, graphene/C_{60}/graphene exhibits bidirectional response photocurrent, with the device displaying a negative response current in the 405–650 nm range and a positive response current in the 808–1550 nm range. The authors employed photolithography and deep reactive ion etching methods to achieve sensitivity (3.4105 A W^{-1}), rapid response (23 ms), and ultra-wideband coverage (405–1550 nm) in the phototransistor's characteristics. The significant contribution of this work lies in enabling the fabrication of large-scale, all-carbon array photodetectors.

The interface layer may have a different arrangement from the bulk material, leading to an unclear understanding of the interface layer's optoelectronic properties and photodetection performance. Shao *et al.* prepared high-performance
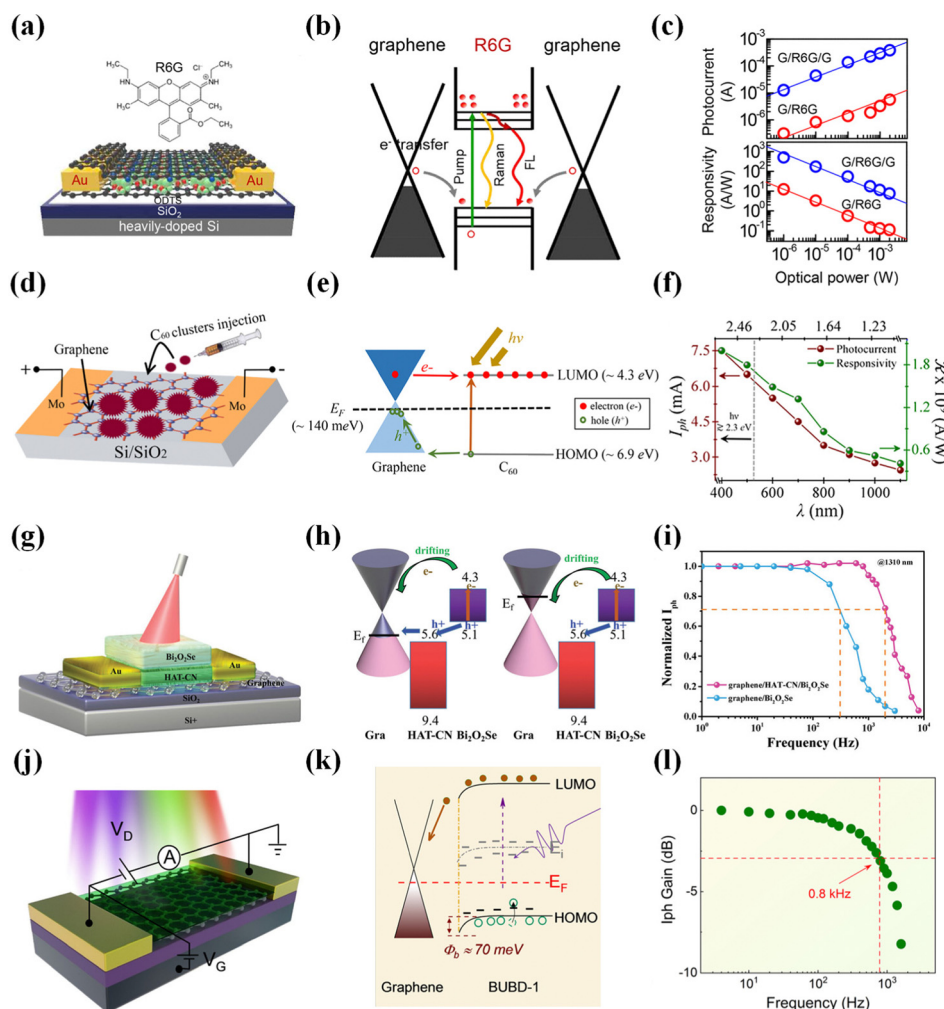

Fig. 8 Enhancing the photodetector performance of graphene by combining it with small molecule organic materials. (a) Schematic illustration of graphene/R6G/graphene.[119] (b) Schematic band structure.[119] (c) Responsivity and photocurrent as a function of incident light power density.[119] Reproduced with permission.[119] Copyright 2019, American Chemical Society. (d) Schematic representation of graphene/C_{60}.[120] (e) Band diagram.[120] (f) I_{ph} and responsivity as a function of λ.[120] Reproduced with permission.[120] Copyright 2019, American Chemical Society. (g) Schematic illustration of graphene/HAT-CN/Bi_2O_2Se.[123] (h) The charge transfer principle of type-III energy band alignment.[123] (i) Normalized amplitude as a function of frequency.[123] Reproduced with permission.[123] Copyright 2021, Royal Society of Chemistry. (j) Schematic of graphene/BUBD-1.[129] (k) Energy band diagram.[129] (l) Photocurrent gain as a function of frequency.[129] Reproduced with permission.[129] Copyright 2021, Royal Society of Chemistry.

1242 | *J. Mater. Chem. C*, 2024, **12**, 1233–1267

This journal is © The Royal Society of Chemistry 2024

graphene/C_{12}TBP heterojunction photodetectors (191 A W^{-1}, 3.9×10^{12} Jones)[122] using the *in situ* retro-Diels–Alder reaction. Notably, the authors investigated the impact of the interface layer stacking on photodetection capabilities and the underlying mechanism. They pointed out that the π–π stacking at the graphene/C_{12}TBP interface edges is critical in achieving ultra-high photodetection efficiency. More accurately, this is due to the adequate overlap of molecular orbitals in adjacent π–π stacked C_{12}TBP molecules, promoting the diffusion, dissociation, and separation of photogenerated charge carriers and charge transfer states. This work provides robust theoretical support for studying interface layer structures and electronic properties. Similar to the challenges in weak light detection in the NIR region, achieving a fast response in the optical communication band (@1310 nm) has been challenging. Our research group has proposed the graphene/HAT-CN/Bi_2O_2Se heterojunction phototransistor (Fig. 8g and h),[123] which demonstrates the capability of ultra-broadband detection (488–1550 nm) (Fig. 8i), covering the optical communication band, and exhibits a rapid response time (101 ms). This is attributed to the presence of HAT-CN, which efficiently transfers photogenerated holes in Bi_2O_2Se to the graphene layer, resulting in an enhanced responsivity of 2420 A W^{-1}. Additionally, the authors have achieved array detection, which holds significant potential for application in near-infrared focal plane detection and high-speed communication fields. Choi *et al.* harnessed the anti-ambipolar charge transport behavior of IGZO/graphene/CuPc heterojunction photodetectors[124] to achieve high-precision color selectivity. In other words, a monolithic tandem multicolor photodetector has enabled the functionality of an image sensor. This vertically stacked photodetector structure and wavelength-selective photodetection approach have paved the way for the development of image sensors.

Photodetectors based on pentacene and graphene have been manufactured for some time.[125–127] However, these devices typically feature relatively complex structures and modulation processes and exhibit limited weak light detection capabilities. The graphene/pentacene heterojunction photodetector proposed by Gan *et al.*[128] offers several advantages, including a simple structure and excellent self-powered weak light detection capabilities. This device exhibits high responsivity ($>10^5$ A W^{-1}), high detectivity ($>10^{11}$ Jones), and ultra-fast response times (0.006/0.009 ms). Its exceptional performance can be attributed to the low charge trap density and short carrier lifetime at the graphene/pentacene interface. Notably, the device achieves high-resolution single-pixel imaging in UV and VIS spectra. Overall, this work provides a design concept for self-powered photodetectors and holds great promise in integrating weak light detection devices and radio equipment. The performance of sensitized devices is highly correlated with the quality of the heterojunction interface, making the simplified production of high-quality heterojunction interfaces a challenging issue. Qin *et al.* have successfully fabricated a high-quality graphene/BUBD-1 heterojunction interface using a straightforward thermal evaporation technique. The graphene/BUBD-1 heterojunction photodetector (Fig. 8j and k)[129] exhibits a high responsivity (7×10^5 A W^{-1}), rapid response times (0.33/0.49 ms), and a

high detectivity (4×10^{14} Jones). The cutoff frequency at -3 dB, indicating where the photocurrent signal decreased by 2, was determined to be approximately 0.8 kHz under $V_G = -60$ V (Fig. 8l). Additionally, this device offers the capability for ultraviolet detection and tunable rise/decay times attributed to gate voltage adjustments of the barrier height. This direct growth preparation method holds significant potential for application in large-scale hybrid devices. Organic semiconductors exhibit high optical absorption coefficients, but amorphous and polycrystalline materials often reduce exciton dissociation efficiency due to short exciton diffusion lengths. They also typically struggle to achieve zero-bias photodetection. The use of single-crystal rubrene structures can address these challenges. While rubrene/graphene heterojunction photodetectors have been proposed previously,[116] they did not achieve self-powered capabilities. The rubrene/graphene heterojunction photodetector presented by Zhao *et al.*[130] offers self-powered photon detection, high responsivity (8×10^5 A W^{-1}), high detectivity ($>10^{12}$ Jones), and fast response times (20/70 µs). These attributes are primarily due to the long exciton diffusion length in the rubrene/graphene heterojunction's rubrene single crystal and graphene's high mobility. Furthermore, the asymmetric van der Waals stacking structure of the rubrene/graphene heterojunction forms a high-quality heterojunction interface, which holds significant promise in the field of wireless photon detection.

4.1.2. Combining with organic polymers. Organic polymer films are thin and uniform layers composed of organic polymeric materials. These films are typically prepared from solutions of organic polymers or melt-polymerized materials, or from methods such as vapor deposition. Organic polymer films find wide-ranging applications in various fields, including electronics, optoelectronics, photovoltaics, coating technologies, and biomedicine. These films offer numerous advantages, such as tunability, lightweight, flexibility, and solubility, making them an ideal choice in many applications. In the field of electronics, organic polymer films are used in the fabrication of devices like organic field-effect transistors (OFETs), organic light-emitting diodes (OLEDs), and organic photovoltaic solar cells (OPVs). They are also used in flexible electronic devices, such as flexible displays and sensors. The characteristics and performance of organic polymer films can be customized by adjusting the type of polymer, molecular structure, and processing conditions. This tunability makes them highly suitable for meeting the requirements of specific applications. At the same time, organic polymer films have some challenges, such as stability, long-term durability, and production costs. Researchers are continuously working to overcome these challenges to enhance their applicability.

Poly(3-hexylthiophene) (P3HT) demonstrates a high absorption coefficient, offering a solution to graphene's low absorption limitations. Moreover, P3HT possesses favorable attributes such as ease of manufacturing and cost-effectiveness. In 2014, Tan *et al.* introduced the graphene/P3HT/PZT heterojunction photodetector (Fig. 9a–c).[131] Photogenerated holes transfer from P3HT to graphene, while photogenerated electrons are retained within P3HT. The high hole mobility within graphene
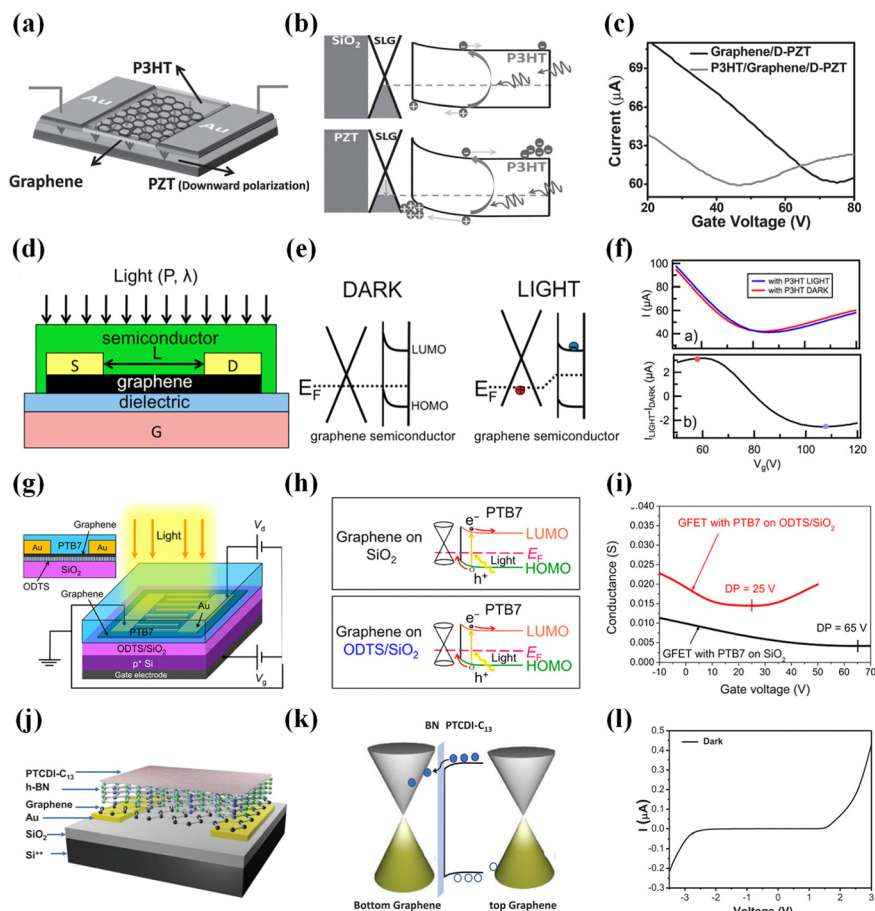
Fig. 9 Enhancing the photodetector performance of graphene by combining it with organic polymers. (a) Schematic view of graphene/P3HT/PZT.[131] (b) Band diagrams of P3HT/graphene/PZT: the lower Fermi level of graphene produces a higher built-in field by D-PZT than by the SiO_2 substrate.[131] (c) Drain current as a function of gate voltage.[131] Reproduced with permission.[131] Copyright 2014, Wiley-VCH. (d) Side view of graphene/P3HT.[132] (e) Energy level diagram of graphene/P3HT in the dark and under light.[132] (f) Source−drain and light-induced current as a function of gate voltage.[132] Reproduced with permission.[132] Copyright 2015, American Chemical Society. (g) Schematic illustration of graphene/PTB7.[134] (h) Schematic illustration of the photocarrier transfer.[134] (i) Channel conductance of PTB7-coated GFETs.[134] Reproduced with permission.[134] Copyright 2017, American Chemical Society. (j) Schematic of graphene/h-BN/J-aggregate PTCDI-C$_{13}$.[137] (k) Energy-band diagram under illumination at zero bias.[137] (l) I–V curve.[137] Reproduced with permission.[137] Copyright 2021, Wiley-VCH.

allows them to circulate efficiently before recombining with the electrons captured in P3HT. Consequently, photosensitivity is significantly enhanced. Variations in the confinement of the PZT substrate can have a crucial impact on P3HT/graphene photodetectors and substantially improve the light responsivity of the hybrid composite material. This photodetector exhibits an ultra-high gain of 10^3. Organic polymer thin films have the potential to enhance the performance of 2D phototransistors, but achieving high gain remains a challenging task. Everardus *et al.* fabricated graphene/P3HT heterojunction phototransistors (Fig. 9d–f),[132] obtaining phototransistors with ultra-high gain for the first time. By reducing the channel length and increasing the mobility, the transit time of charge carriers through graphene was minimized, thereby optimizing the optical gain of these devices. Organic semiconductors offer high spectral sensitivity, and graphene provides high charge carrier mobility. However, creating high-quality 2D/organic interfaces remains a challenge. Using van der Waals epitaxy

allows for producing single-layer organic semiconductors and high-quality interfaces. Even with just one layer of C$_8$-BTBT, the graphene/C$_8$-BTBT heterojunction phototransistor[133] still demonstrates outstanding performance, with a high responsivity (R) of up to 1.57×10^4 A W^{-1} and an ultra-high gain exceeding 10^8.

Most graphene-based hybrid photodetectors typically exhibit longer response times. However, the "assembled-monolayer (SAM)-functionalized" technique can improve devices' response time due to the enhanced interface quality. High-sensitivity photodetectors with short response times are of great importance in the field of photodetection. Graphene/PTB7 heterojunction (Fig. 9g–i)[134] photodetectors using SAM technology achieve an ultra-high responsivity of 1.8×10^5 A W^{-1} and a fast response time of 7.8 ms. High-quality interfaces are crucial for photodetector performance and represent an area that needs significant development in the future. Most current research focuses on visible to infrared light, with

relatively few studies addressing the ultraviolet part. PDA exhibits extensive strong absorption properties in the VIS and UV regions, offering significant potential in the field of flexible wideband UV-VIS photodetectors. PDA possesses advantages such as low manufacturing costs, flexibility, and ease of production. Therefore, the graphene/PDA heterojunction photodetector[135] achieves a responsivity of 556 A W^{-1} and a detectivity of 6 × 10^{11} Jones. The graphene/PDA detector maintains reliable sensing capabilities even after undergoing 25 000 bending rounds. This can be attributed to PDA serving as both a transfer support layer and a light-absorbing layer, allowing the production of near-perfect centimeter-scale graphene sheets. The device also possesses eco-friendly characteristics, similar to graphene/MOF. It holds significant potential for application in the field of flexible, portable, and wearable electronic devices. J-aggregates have very narrow absorption bands in the VIS and NIR regions, greatly enhancing the spectral sensitivity of photodetectors due to their rapid and coherent energy transfer capabilities. Therefore, this material holds promise for improving the spectral sensitivity of photodetectors, but effectively integrating it with graphene is a challenge. The graphene/J-aggregate TDBC cyanine dye heterojunction photodetector[136] is a VIS light-gated all-carbon phototransistor. While its performance is not outstanding, it offers an innovative thin film fabrication technique. This technique is simple and controllable, allowing the fabrication of thin films of various water-soluble materials on the desired substrate material's surface. It is worth noting that this transistor can reversibly write and erase charge doping in graphene using visible light, paving the way for applying J-aggregates in photodetectors.

In the field of biophysics, there is often a need to detect the colors of biomolecules, requiring high-performance narrowband photodetectors. Previous narrowband photodetectors have frequently sacrificed gain and responsivity. Using J-aggregate fluorescent molecules with narrowband absorption characteristics can address this issue. However, J-aggregates lack π–π interactions and exhibit low charge carrier mobility. Combining J-aggregates with graphene holds great promise. The graphene/h-BN/J-aggregate PTCDI-C$_{13}$ heterojunction photodetector (Fig. 9j–l)[137] achieves an ultra-narrow spectral response of 13 nm and a high responsivity of 10^3 A W^{-1}. Growing PTCDI-C$_{13}$ on an h-BN substrate ensures the device's narrowband absorption characteristics. This represents a significant advancement in the field of narrowband detection in 2019 and provides a new avenue for designing highly sensitive narrowband photodetectors. Taking the graphene/PDVF heterojunction photodetector presented by Yu et al. as an example,[138] the researchers demonstrated a technique for tuning the detection wavelength using thermal annealing. This device can alter the position of the Fermi level in the PDVF film through thermal annealing, thereby changing the barrier height and the detection wavelength. The device achieves tunable measurements in the 350–850 nm range, exhibiting varying photosensitivity under different temperature treatments. This provides valuable support for understanding the complex electronic processes near the interface.

2D/organic heterojunctions have been the subject of extensive research, primarily confined to the VIS and NIR regions, with limited progress in DUV detection. The DUV spectrum is an integral component of sunlight with potential antiviral and sterilization applications, making DUV detection highly meaningful. SnO$_2$, a wide-bandgap semiconductor material capable of sensing DUV light, can be combined with graphene to create high-performance DUV photodetectors. The PPy-NGr/SnO$_2$ heterojunction photodetector exhibits an exceptionally high responsivity (4594.25 A W^{-1}) and a high detectivity (6.47 × 10^{11} Jones).[139] These characteristics result from the substantial built-in electric field (NGr/SnO$_2$, PPy/SnO$_2$, and PPy-NGr/SnO$_2$), accelerating the efficient dissociation of photogenerated excitons. At the same time, NGr mitigates the valence band offset between PPy and SnO$_2$. This work provides a design approach for cost-effective and easily manufacturable DUV photodetectors.

4.1.3. Combining with complex organic materials. Complex organic thin films refer to thin film structures composed of multiple organic molecules or polymers, where these molecules or polymers come together to form the thin film of a composite material. Such films find utility in various applications, including electronic devices, solar cells, displays, sensors, barrier films, and more. The properties and performance of composite organic films can be tailored by adjusting material composition, film thickness, and processing methods to meet specific application requirements. The application of composite organic films in photodetectors continues to grow because of their advantages such as diversity, customizability, cost-effectiveness, and suitability for a wide range of wavelengths. This makes them useful in various fields, from communications to healthcare and industrial monitoring.

As mentioned earlier, pristine graphene exhibits a weak absorption rate as low as 2.3%, fundamentally limiting its applicability in photodetection. Chlorophyll is an organic semiconductor known for its exceptional light absorption properties. The graphene/chlorophyll phototransistor demonstrates high gain and responsivity through the integration of graphene and photosensitive chlorophyll molecules. This device's observed ultra-high light responsivity, reaching 10^6 A W^{-1},[140] can be attributed to charge transfer at the interface and the efficient light effect within the chlorophyll layer. One of the most significant challenges in graphene-based electronics is the control of carrier types and the modulation of carrier concentration in graphene through doping. The method of regulating the electrical performance of graphene transistors using photoexcitation has the advantages of controllability and reversibility. It would be exciting and appealing if the carrier transport types (either n- or p-type) of an optically induced graphene transistor could be selectively controlled by choosing specific optical excitation wavelengths, enabling tunable carrier transport in a graphene-based photonic device. The TiO$_x$/graphene/P$_3$HT:PCBM heterojunction photodetector[141] can determine whether the graphene transistor carries n-type or p-type carriers by choosing either UV or VIS light irradiation, achieving a degree of controllable and reversible n-type or p-type doping. The transistor device exhibits a negative shift in the charge neutrality point (CNP) value when illuminated with wavelengths less than 350 nm. Conversely, under illumination with wavelengths greater than 350 nm, a positive shift in the

CNP value is observed, confirming the selective n-type and p-type carrier transport phenomenon in graphene transistors.

Methylammonium lead halide, that is, $CH_3NH_3PbX_3$ (where X is a halogen), possesses excellent optoelectronic properties, and notably, these nanocrystals offer a simple manufacturing process and lower production costs. While $CH_3NH_3PbX_3$/graphene heterojunctions have long been applied in solar cells, their utilization in photodetectors has also yielded excellent results. The graphene/$CH_3NH_3PbI_3$ heterojunction photodetector[142] demonstrates a photoresponsivity of 180 A W^{-1}, an EQE of approximately 5×10^4%, a photodetection rate of around 10^9 Jones, and a broad spectral bandwidth in the VIS range, owing to efficient charge transfer from graphene to $CH_3NH_3PbI_3$. The transfer of electrons from the graphene layer to the proximate $CH_3NH_3PbI_3$ layer determines the occupied states in the $CH_3NH_3PbI_3$ valence band generated by photon absorption. The recombination of photoexcited electron–hole pairs in $CH_3NH_3PbI_3$ is restricted, allowing the photoexcited electrons to remain within the conduction band of $CH_3NH_3PbI_3$ without decay. While previous studies have successfully combined organic semiconductor materials with graphene, high-gain phototransistors have not been achieved. The plasmonic effect of metal nanostructures can significantly improve photodetector performance. Compared to graphene/$CH_3NH_3PbI_3$ heterojunction photodetectors, graphene/$CH_3NH_3PbI_3$/NPs (NPs refers to nanoparticles) heterojunction photodetectors[143] exhibit higher EQE and responsivity. This enhancement can be attributed to the surface plasmonic effects of NPs, which increase the light absorption cross-section of the surrounding $CH_3NH_3PbI_3$ material, thereby improving light capture within the $CH_3NH_3PbI_3$ layer. Introducing a combination of two distinct organic materials to form an organic heterojunction is a promising strategy for optimizing the performance of organic optoelectronic materials and expanding the range of applications for various optoelectronic devices. For example,

doping PCBM into $CH_3NH_3PbI_3$ can facilitate the separation of electron–hole pairs and selective charge capture, significantly enhancing the efficiency of electron–hole pair separation and the carrier lifetime in such organic heterojunctions. In the case of graphene/$CH_3NH_3PbI_3$:PCBM (Fig. 10a and b),[144] the electron lifetime is extended by four to five orders of magnitude compared to graphene/$CH_3NH_3PbI_3$, resulting in a 30-fold increase in photoresponsivity, reaching 10^6 A W^{-1}. Graphene/$CH_3NH_3PbI_3$:PCBM represents the first application of doped organic heterojunctions in 2D/organic photodetectors, opening up a new design strategy for high-performance photodetectors. Subsequently, a continuous stream of high-performance photodetectors based on doped organic heterojunctions has emerged.

Charge-transfer (CT) complex tetrathiafulvalene-tetracyanoquinodimethane (TTF-TCNQ) was discovered in 1973, and it possesses unique properties related to intermolecular electron transitions, offering substantial applications in high-performance photodetectors. The graphene/TCNQ heterojunction photodetector (Fig. 10c and d)[145] exhibits exceptionally high responsiveness between 600 and 2000 nm, with a peak exceeding 2000 A W^{-1}. This can be attributed to TCNQ's unique low-energy intermolecular electronic transitions that extend into the NIR region. Interactions between molecules lead to efficient charge separation, resulting in an extremely high photocurrent gain, thus holding significant value in photodetection applications. MOFs are characterized by high porosity and intrinsic tunability, making them excellent materials for wearable devices. Meeting the global demand for wearable devices such as electronic skin, flexible optoelectronic devices, and biomedical equipment requires environmentally friendly, highly stable devices. The graphene/MOF heterojunction photodetector (Fig. 10e and f)[146] is characterized by its non-toxic, stable, and environmentally friendly nature, making it highly suitable for wearable electronic devices. The high porosity of MOFs
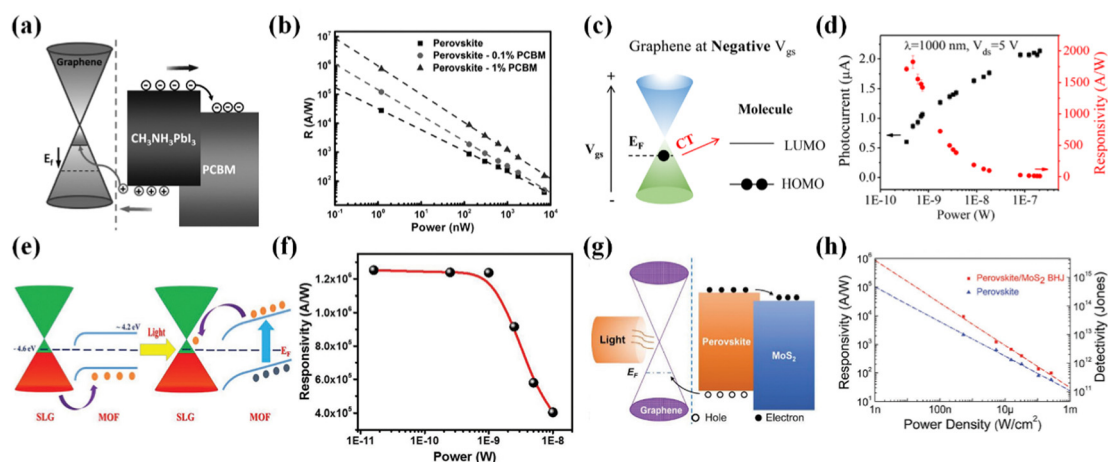

Fig. 10 Enhancing the photodetector performance of graphene by combining it with complex organic materials. (a) The energy level diagram of graphene/$CH_3NH_3PbI_3$:PCBM.[144] (b) Responsivity as a function of the incident light power.[144] Reproduced with permission.[144] Copyright 2017, Wiley-VCH. (c) Schematic illustration of charge-transfer transitions of graphene/TCNQ.[145] (d) Photocurrent and responsivity as a function of the incident light power.[145] Reproduced with permission.[145] Copyright 2018, American Chemical Society. (e) Energy band diagram of graphene/MOF.[146] (f) Variation of responsivity as a function of illumination power.[146] Reproduced with permission.[146] Copyright 2018, Wiley-VCH. (g) Energy level diagram of graphene/PDA.[147] (h) Dependence of responsivity and detectivity on the incident light power density.[147] Reproduced with permission.[147] Copyright 2018, Wiley-VCH.

results in strong light absorption, while graphene exhibits excellent optoelectronic properties and flexibility. Consequently, graphene/MOF exhibits remarkable attributes such as ultrafast response (<150 ms), ultra-high responsivity ($>10^6$ A W^{-1}), extremely high EQE ($>5 \times 10^8\%$), and extensibility. Combining MOFs with 2D materials paves the way for developing wearable and portable electronic products. Peng *et al.* introduced the graphene/CH$_3$NH$_3$PbI$_3$:MoS$_2$ heterojunction photodetector (Fig. 10g and h),[147] further advancing the development of multi-heterojunction photodetectors. In this device, CH$_3$NH$_3$PbI$_3$:MoS$_2$ serves as the light-absorbing layer, graphene functions as the charge carrier transport layer, and MoS$_2$ facilitates selective electron capture, thereby suppressing carrier recombination and increasing photocurrent. This photodetector exhibits a high responsivity (1.08×10^4 A W^{-1}), a high detectivity (4.28×10^{13} Jones), a high EQE ($2.0 \times 10^6\%$), and a rapid light response time (45 ms). Moreover, it is crucial to note that the graphene/CH$_3$NH$_3$PbI$_3$:MoS$_2$ device maintains high performance even when applied to flexible substrates, opening up significant opportunities for application in wearable and portable electronic devices.

With the continuous advancement of technology, there is a growing demand for simple, lightweight, integrated electronic devices, especially those capable of converting light into electricity and generating light from electricity, serving as dual-function optoelectronic devices. Prior to this, research combining photodetectors with light-emitting diodes was limited, and such combinations typically exhibited subpar performance. The graphene/CH$_3$NH$_3$PbBr$_3$ QDs/graphene heterojunction phototransistor (Fig. 11a and b)[148] represents a dual-function device with both light emission and photodetection capabilities, featuring a vertical stacked "sandwich" structure. This device exhibits a rapid response time (~ 20 μs), ultra-high responsivity ($\sim 3 \times 10^9$ A W^{-1}) (Fig. 11c), and a high EQE ($\sim 1.2 \times 10^{10}\%$), with the magnitude and direction of the photocurrent being adjustable by applying gate voltage. Compared to lateral phototransistors, vertical phototransistors leverage an internal electric field to modulate charge separation directly, significantly increasing photocurrent and enhancing responsivity. Highly stable dual-function light-emitting phototransistors hold great promise in the fields of displays and optical communications. Commercial NIR photodetectors rely on semiconductor materials such as InGaAs and InAs. Therefore, developing high-performance emerging NIR photodetectors remains essential. The graphene/P3HT:F4 TCNQ heterojunction photodetector[149] exhibits an ultra-high responsivity of 10^6 A W^{-1} in the NIR range and demonstrates broadband photoresponse from VIS to the NIR. This can be attributed to the photoinduced effects at the interface of charge transfer complexes and graphene molecules and the intermolecular electronic transitions of charge transfer complexes. Furthermore, the graphene/P3HT:F4 TCNQ structure exhibits tunable photoresponsivity, which can be flexibly
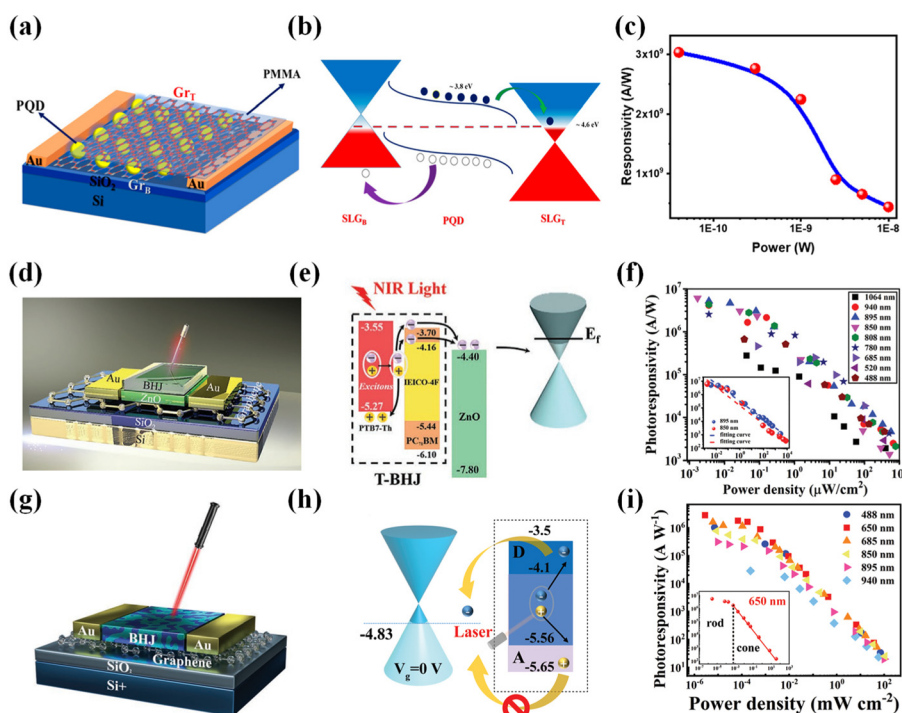

Fig. 11 Graphene/complex organic thin film photodetectors. (a) Schematic design of graphene/CH$_3$NH$_3$PbBr$_3$ QDs/graphene.[148] (b) Energy band representation.[148] (c) Illumination light power dependent photoresponsivity curve of graphene/CH$_3$NH$_3$PbBr$_3$ QDs/graphene.[148] Reproduced with permission.[148] Copyright 2019, American Chemical Society. (d) Schematic of graphene/ZnO/IEICO-4F:PTB7-Th.[154] (e) The energy level alignment and working mechanism diagrams.[154] (f) Responsivity as a function of input light power density.[154] Reproduced with permission.[154] Copyright 2021, Wiley-VCH. (g) Schematic device structure of graphene/PM6:Y6.[155] (h) Schematic diagram of the device energy level.[155] (i) Light power density dependent responsivity of graphene/PM6:Y6.[155] Reproduced with permission.[155] Copyright 2022, Wiley-VCH.

This journal is © The Royal Society of Chemistry 2024

J. Mater. Chem. C, 2024, 12, 1233–1267 | 1247

adjusted through the electrical gating of graphene. The development of this device contributes to the advancement of low-cost, high-performance NIR photodetectors.

The plasma effect can significantly enhance the responsivity of photodetectors. However, when combined with graphene, a single type of plasma structure is often used, which does not yield satisfactory results. Combining plasma nanomaterials with perovskites ($MAPbI_3$) can result in ineffective synergistic effects and insufficient device performance. The graphene/gold nanostars (GNSs)/$MAPbI_3$ heterojunction photodetector[150] provides a perfect solution to both issues. This device incorporates spherical plasma gold nanoparticles (GNSs) and $MAPbI_3$ materials. Due to the hybridization of tip and core plasma modes, GNSs generate a powerful local electric field, exhibiting a highly efficient light-capturing effect. The device demonstrates outstanding detection performance ($R = 58\,952$ A W^{-1}, $D^\star = 1.31 \times 10^{13}$ Jones, EQE $= 1.59 \times 10^7$%), signifying the effective integration of $MAPbI_3$ materials and GNSs into graphene. More importantly, even after undergoing 1000 repeated bends, the device maintains excellent performance and stability. Furthermore, the authors have fabricated a 10×10 array of photodetectors that exhibits high resolution in response to optical signals, laying the foundation for developing array detection devices. Tetrathiafulvalene–chloranil (TTF–CA) exhibits charge transfer electronic transitions down to 0.5 eV, making it an ideal absorber material for the shortwave infrared (SWIR) region. When combined with graphene as the charge transport layer, it produces an exceptionally high-performance graphene/TTF:CA photodetector ($D^\star = 10^{13}$ Jones, $R = 10^5$ A W^{-1}, $\tau = 2$–12 ms).[151] The photodetector's exceptional performance can be primarily attributed to optical photogating, which promotes delayed carrier recombination, leading to high gain and sensitivity. The critical contribution of this work is the discovery of charge transfer complex absorbers in the SWIR region, making low-cost and high-performance SWIR photodetectors feasible.

2D-COFs possess excellent properties such as thermal stability, permanent porosity, large surface area, diverse topological structures, and low mass density. Importantly, they feature a pre-designed π-electron framework and a highly ordered topological structure that enhances carrier transport. However, COFs are typically in solid powder form, making integration challenging. Xiong et al. successfully obtained COF thin films on graphene using chemical vapor deposition, forming an ordered graphene/COF heterojunction. Graphene/COF[152] exhibits high responsivity (3.2×10^7 A W^{-1}) and a fast response time (1.14 ms). Significantly, graphene/COF can be modulated by specific target molecules, attributed to COF's high surface area and polarity selectivity. The significant contribution of this work lies in providing a new research strategy for tunable multifunctional devices. Although perovskite materials have made substantial contributions in the field of solar cells, their use in photodetectors has been limited due to structural defects and grain boundaries often found in perovskite thin films, which hamper charge carrier transport capabilities. Additionally, perovskite materials have a low absorption coefficient in the NIR range, resulting in very small photocurrents. Hence,

there is a need for a high-quality interface to effectively integrate 2D perovskite $(BA)_2(FA)_{n-1}Pb_nI_{3n+1}$ with graphene. The utilization of hyperbolic gold nanostructures can address the issues above. Gold nanostructures exhibit light-capturing and electromagnetic field-enhancing effects, and the coupling effect between graphene, gold array, and $(BA)_2(FA)_{n-1}Pb_nI_{3n+1}$ significantly enhances their light response capabilities in the UV and NIR spectral regions. The graphene/gold array/$(BA)_2(FA)_{n-1}Pb_nI_{3n+1}$ heterojunction photodetector[153] achieves a detectivity of 2.21×10^{13} Jones and features a low dark current of 1.0×10^{-10} A, with a high on/off ratio of up to 10^4. They utilized Au array/$(BA)_2(FA)_{n-1}Pb_nI_{3n+1}$ as the photosensitive layer and graphene as the charge carrier transport layer, which maximizes light capture and photoinduced charge extraction. This represents an excellent strategy for combining two high-quality materials, namely, graphene and $(BA)_2(FA)_{n-1}Pb_nI_{3n+1}$. Introducing zinc oxide into the charge carrier extraction layer similarly enhances the sensitivity of the photodetector in the NIR range. The graphene/ZnO/IEICO-4F:PTB7-Th heterojunction photodetector (Fig. 11d and e)[154] proposed by our research group exhibits weak NIR light detection capabilities. It also features high-performance parameters ($R = 6.1 \times 10^6$ A W^{-1} (Fig. 11f) and $D^\star = 2.43 \times 10^{13}$ Jones). The IEICO-4F:PTB7-Th heterojunction shows strong absorption in the NIR spectral range, and ZnO suppresses charge carrier recombination processes effectively. This ingenious design addresses the deficiency in weak light detection by photodetectors in the NIR region. Even more importantly, this device accomplishes the detection of human pulse signals and heart rate, representing another advancement in applying photodetectors in the medical field. While conventional organic heterojunctions have addressed issues such as the low quantum efficiency of a single absorption layer, they still suffer from poor dissociation efficiency and limited weak light detection capabilities. The PM6:Y6 heterojunction proposed by our research group cleverly overcomes these limitations, presenting a donor–acceptor interpenetrating bulk heterojunction structure. The graphene/PM6:Y6 heterojunction phototransistor (Fig. 11g and h)[155] possesses the capability for weak light detection in the near-infrared region, along with high responsivity (2.86×10^6 A W^{-1}) (Fig. 11i) and high detectivity (1.47×10^{14} Jones). This can be attributed to the high dissociation efficiency of the PM6:Y6 heterojunction and the alignment of energy bands at the interface. Furthermore, the device exhibits bidirectional photoresponse and a broadband photosensitive range. The authors also fabricated a retinal vision chip based on graphene/PM6:Y6, capable of handling visual images spanning over six orders of magnitude. This device can also be used for real-time monitoring of human pulses, holding significant promise in the field of medicine.

4.1.4. Combining with bilayer organic thin films. Early experiments in heterojunction device research primarily focused on enhancing absorption using single-layer semiconductors, including colloidal quantum dots, $CH_3NH_3PbI_3$, organic polymers, organic single crystals, semiconductor two-dimensional materials, silicon, and other traditional materials. However, the quantum efficiency of such structures remained

1248 | J. Mater. Chem. C, 2024, **12**, 1233–1267

This journal is © The Royal Society of Chemistry 2024

relatively low. Recent research indicates that introducing P–N junction double-layer absorption has become a significant direction in heterojunction device research. This design strategy for double-layer absorption leverages the complementary properties of two semiconductor materials, offering numerous advantages. Introducing P–N junction double-layer absorption is a promising research direction that opens up new possibilities for improving heterojunction device performance and application range. With further research and technological innovations, we can expect the emergence of high-performance photodetectors based on this design strategy.

The production of highly conductive graphene films still faces significant challenges. Therefore, seeking alternative approaches for constructing highly conductive graphene films is a task of great significance and considerable challenges. Poly(3,4-ethylenedioxy thiophene):poly(styrene sulfonate) (PEDOT:PSS) (clevios PH1000) is a novel graphene solution that enables the fabrication of high-quality, large-area graphene films through spray coating. The graphene/PEDOT:PSS/P3HT:PC$_{71}$BM heterojunction photodetector[156] operates at an extremely low bias voltage, possibly working with low energy consumption. This photodetector exhibits characteristics of being "ultrathin" and "flexible" and can be attached to the surface of the human body, making it a promising candidate for wearable devices. The construction and utilization of multiple heterojunctions have substantially enhanced the performance of photodetectors. For instance, the graphene/P3HT/CH$_3$NH$_3$PbI$_{3-x}$Cl$_x$ heterojunction phototransistor[157] exhibited a responsivity of 4.3×10^9 A W^{-1} and a gain of 10^{10}, surpassing previous CH$_3$NH$_3$PbI$_{3-x}$Cl$_x$ phototransistors by several orders of magnitude. In this structure, CH$_3$NH$_3$PbI$_{3-x}$Cl$_x$ is the light-absorbing layer, P3HT is the hole transport layer that effectively separates electrons and holes, and graphene is the charge transport layer. The ultrahigh responsivity and gain are attributed to intense light absorption and efficient photogenerated charge carrier separation. Moreover, this phototransistor can detect infrared light with wavelengths exceeding 1300 nm.

Phototransistors with only one semiconductor light-absorbing layer lack a built-in electric field, which reduces quantum efficiency and bandwidth. The graphene/PTCDA/pentacene heterojunction phototransistor (Fig. 12a and b)[158] incorporates PTCDA/pentacene organic epitaxial heterostructures as the light-absorbing layer, resulting in the design of a high-performance phototransistor with optimized parameters such as responsivity (R) (Fig. 12c), carrier lifetime (τ), and EQE. The selection of PTCDA and pentacene as the light-absorbing layer is based on their complementary absorption spectra within the VIS light range. The high performance primarily stems from the inherent built-in electric field at the semiconductor interface that facilitates charge separation. This approach opens up a strategy for designing phototransistors, where organic heterojunctions as the light-absorbing layer can significantly enhance the performance of 2D/organic heterojunction phototransistors. Another promising design strategy is to create vertical Schottky barrier transistors by integrating two organic materials with graphene. The graphene/pentacene/PTCDI-C$_8$ heterojunction

photodetector (Fig. 12d and e)[125] effectively suppresses dark current density and enhances the device's photocurrent, crucial for improving photodiode performance. PTCDI-C$_8$ reduces the work function of graphene, preventing electron injection from graphene into pentacene and thus reducing dark current density. The reduced work function also improves the collection of photogenerated holes in pentacene, thereby increasing photocurrent density. As a result, the device's specific detectivity and responsivity (Fig. 12f) could be enhanced systematically by adjusting the gate bias. This represents the latest development in vertically stacked heterojunction devices integrated with graphene electrodes. The light response of 2D/organic heterojunction transistors is typically confined to a relatively narrow spectral range determined by the semiconductor's bandgap. Our research group introduced bidirectional (positive and negative) light response in organic heterojunctions for the first time. Previously reported graphene-based high-gain photodetectors had their spectral range typically limited to 400–700 nm. However, the graphene/C$_{60}$/pentacene heterojunction transistor (Fig. 12g and h)[126] extends the bandwidth to 405–1550 nm through bidirectional light response. It is important to note that the increased bandwidth is not achieved by altering the organic material's absorption unit. Instead, it leverages compassionate light responses in the visible spectrum. C$_{60}$/pentacene, as the light-absorbing layer with a significant built-in electric field, efficiently promotes charge dissociation. Graphene, functioning as both light-absorbing and transport layer, exhibits a responsivity of 9127 A W^{-1} (EQE = 11.5%) in the visible range (Fig. 12i) and a responsivity exceeding 1800 A W^{-1} (EQE = 0.063%) in the NIR range, with a shortened response time of 275 μs. The exceptional performance of this photodetector is attributed to bidirectional carrier transport, providing a new mechanism for broadband detection using graphene and a novel approach for creating stable and ultra-fast photodetectors.

P3HT, a widely recognized conjugated polymer for photovoltaic applications, possesses high electrical conductivity and absorption coefficient, but it suffers from drawbacks such as poor mechanical strength and stability. By overlaying it with graphene and PEDOT:PSS, a high-performance photodetector with a detectivity of 1.8×10^8 Jones was obtained.[159] It is worth noting that, similar to dark current, the photocurrent depends on the concentration of graphene, with the device's optimal performance achieved at a graphene concentration of 5%. This is because a small amount of graphene promotes charge carrier transport, while excess graphene can lead to particle aggregation, reducing the charge transfer rate. Furthermore, the device exhibits good photoresponse and bandwidth (0.624 MHz). A single absorption layer's limited spectral response bandwidth often constrains organic semiconductor/graphene photodetectors. This limitation can be effectively overcome by employing an organic heterojunction absorption layer strategy. PTCDA and C$_8$-BTBT exhibit complementary optical absorption characteristics in the ultraviolet and visible spectra. Incorporating them as the absorption layer through van der Waals vapor growth significantly enhances the performance of photodetectors. The graphene/PTCDA/C$_8$-BTBT heterojunction phototransistor[160] achieves a

This journal is © The Royal Society of Chemistry 2024

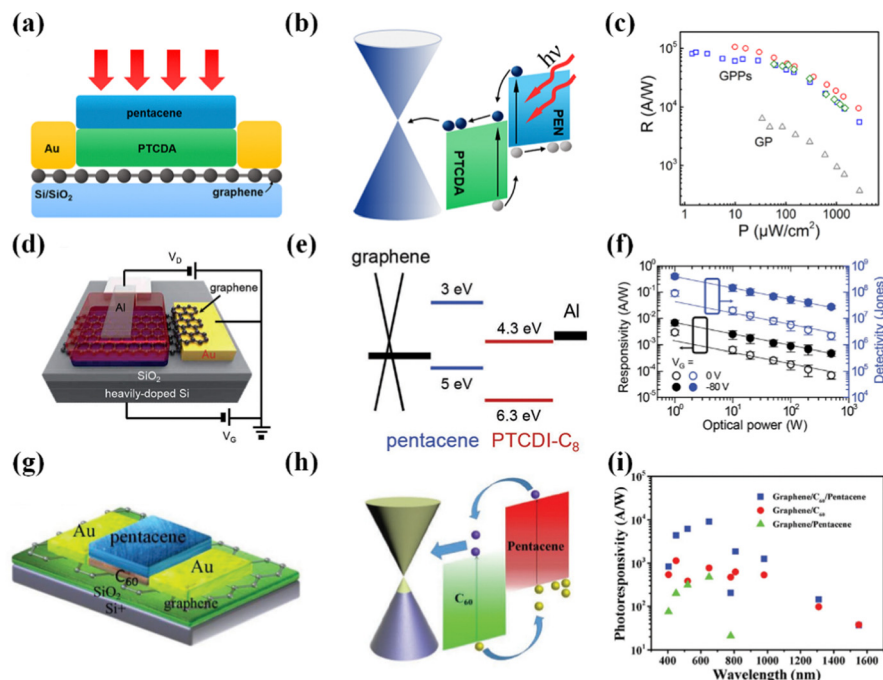*J. Mater. Chem. C*, 2024, **12**, 1233–1267 | **1249**

Fig. 12 Enhancing the photodetector performance of graphene by combining it with bilayer organic thin films. (a) Schematic illustration of graphene/PTCDA/pentacene.[158] (b) Energy band diagram.[158] (c) Responsivity as a function of laser power density.[158] Reproduced with permission.[158] Copyright 2017, American Chemical Society. (d) Schematic of graphene/pentacene/PTCDI-C$_8$.[125] (e) Energy band alignment.[125] (f) Responsivity and detectivity as a function of optical power.[125] Reproduced with permission.[125] Copyright 2017, Wiley-VCH. (g) 3D structure of graphene/C$_{60}$/pentacene.[126] (h) The photogenerated carrier transfer diagram of the whole device.[126] (i) Responsivity as a function of wavelength.[126] Reproduced with permission.[126] Copyright 2018, Wiley-VCH.

high photoresponsivity of up to 5.76 × 10^5 A W^{-1} and a high optical gain of 1.38 × 10^9. Importantly, this device achieves ultra-broadband detection spanning the UV, VIS, and NIR regions, attributed to the ultraviolet photosensitivity of C$_8$-BTBT and the high visible light absorption coefficient of PTCDA. The band alignment in the double heterojunction structure efficiently facilitates the transfer of photogenerated charge carriers (electrons) from the organic layer to the graphene layer. The high-quality interfaces produced through vacuum-based vapor deposition also contribute to efficient carrier transfer. This further advances the development of organic heterojunctions with complementary light absorption characteristics in photodetectors.

The response times of most 2D/organic heterojunction photodetectors are in the millisecond range. Lee *et al.* designed a graphene/ZnPc:C$_{60}$/ZnPc heterojunction photodetector[161] through the doping of organic semiconductor materials, achieving a response time in the microsecond range for the first time while maintaining high responsivity and high EQE. Electrons captured within C$_{60}$ can recombine with holes in ZnPc, reducing the transient photocurrent decay time from 5.8 ms to 19 μs, resulting in a 300-fold performance improvement. This can be attributed to the shortened carrier lifetime within the light-absorbing layer C$_{60}$, facilitating carrier mobility between C$_{60}$ and the graphene layer. This work has officially elevated the photodetector's performance to the microsecond level, providing a strategy for designing ultra-high-performance photodetectors. PTAA, with a wide bandgap of approximately −5.2 eV, serves as the hole transport layer in photodetectors.

The graphene/PTAA/CH$_3$NH$_3$PbI$_{3-x}$Cl$_x$ heterojunction photodetector[162] exhibits a high detectivity of 10^{13} Jones and a remarkable responsivity of 10^5 A W^{-1}. This is attributed to the role of the hole transport layer PTAA, which facilitates the movement of photogenerated charge carriers from the CH$_3$NH$_3$PbI$_{3-x}$Cl$_x$ layer to graphene while suppressing carrier recombination. The function of PTAA is akin to that of the ZnO/IEICO-4F:PTB7-Th heterojunction. However, the graphene/PTAA/CH$_3$NH$_3$PbI$_{3-x}$Cl$_x$ structure is more streamlined. Additionally, introducing a hydrophobic protective layer (PMMA) significantly enhances the device's stability and demonstrates exceptional durability under bending, making it suitable for application in imaging and sensing fields.

There has been limited research on the impact of organic semiconductor thickness on the performance of photodetectors. To investigate the multi-heterojunction photodetector response mechanism and the effect of film thickness on performance, our research group proposed the graphene/C$_{60}$/ZnPc heterojunction photodetector.[163] By varying the thickness of the C$_{60}$ film, an in-depth investigation was conducted into the relationship between film thickness and photocurrent, yielding two distinct heterojunction photodetector response mechanisms. This device exhibits a high responsivity of 6537 A W^{-1} and a rapid response time of 7.29 ms. Intriguingly, it exhibits bidirectional response characteristics attributed to the overlap in the responses of the graphene/C$_{60}$ heterojunction and the C$_{60}$/ZnPc heterojunction. The nodes between positive and negative responses are closely tied to the thickness of the

1250 | *J. Mater. Chem. C*, 2024, **12**, 1233–1267

This journal is © The Royal Society of Chemistry 2024

C_{60} film, allowing for tuning the switching points for positive and negative light responses by adjusting the C_{60} film thickness. This work establishes a foundational understanding of the charge transfer mechanisms in optoelectronic devices. The graphene/C_{60}/pentacene heterojunction photodetector,[126] proposed by our research group in 2018, has been further advanced by Nguyen et al.,[127] who introduced a self-assembled monolayer (SAM). SAM technology enhances the crystallinity of the C_{60} film, resulting in a fivefold performance improvement when compared to the direct deposition of C_{60} and pentacene on graphene. Image sensors are typically composed of at least four photodetectors, and the complexity of integration has posed limitations on the development of image sensors. In recent years, wearable optoelectronic devices have received extensive research interest; yet achieving versatile, single-polarization wearable optoelectronic technology remains challenging. Bera et al. introduced a graphene/MOF/graphene/PVDF heterojunction phototransistor,[164] offering a core technology for wearable integrated optoelectronic devices. The graphene/MOF/graphene/PVDF device exhibits self-powered ultra-high sensitivity (EQE $\approx$ 3 × 10^{10}%) and ultrafast response ($\tau \approx$ 220 μs), primarily attributed to the asymmetric Schottky junction formed between the MOF and graphene. Furthermore, this transistor offers tunable colors through electrical tuning. Additionally, the authors fabricated an optical strain sensor based on the graphene/MOF/graphene/PVDF heterojunction, operating on the principle of controlling the Dirac point of graphene by applying both upward and downward bending strains. This strain sensor exhibits excellent stretchability, making it highly suitable for wearable integrated optoelectronic devices. This work provides a promising direction for researching susceptible and ultrafast wearable devices. Typically, most graphene photodetectors exhibit lower responsivity in the near-infrared region. Graphene/C_{60}/PbPc[155] achieves tunable high photoresponsivity (2.2 × 10^3 A W^{-1}) and broadband response (405–980 nm) in the NIR region. This is attributed to PbPc's strong absorption in the near-infrared region and the high exciton dissociation efficiency of the PbPc/C_{60} heterojunction. Moreover, this device exhibits bidirectional photoresponse due to the appropriate band alignment of graphene/C_{60}. The authors further investigated the mechanism behind this bidirectional photoresponse, providing a novel approach for manufacturing broadband detection phototransistors with vast potential in the field of high-performance NIR photodetection.

Graphene-based 2D/organic heterojunction photodetectors have been the subject of approximately a decade of research, resulting in the continuous development of high-performance devices. In the future, these graphene-based 2D/organic heterojunctions still hold significant research value, given that graphene's broadband absorption characteristics are unparalleled by other 2D materials. Currently, there is limited research on long-wavelength detection, and graphene/organic heterojunction photodetectors are poised to excel in the field of long-wavelength detection.

4.2. MoS$_2$-based photodetectors

Transition metal dichalcogenides (TMDs) are similarly endowed with high charge carrier mobility. However, unlike graphene, which exhibits a zero bandgap, TMDs possess tunable bandgaps, allowing for the suppression of dark current generation. Among TMDs, MoS_2 stands out as a prominent representative, and photodetectors based on MoS_2 typically exhibit exceptional performance. Nevertheless, MoS_2 suffers from limited light absorption capabilities, making it an attractive candidate for synergistic combination with organic materials, opening up extensive development prospects (the summary of MoS_2/organic devices is provided in Table 2).

4.2.1. Combining with small molecule organic materials.
Organic small molecule thin films play a crucial role in enhancing the performance of MoS_2 photodetectors through diverse mechanisms. These contributions encompass increased carrier mobility, enhanced light absorption, and improved device stability. Specifically, the roles of organic small molecules involve (1) as charge transport layers, (2) improving light absorption, (3) modifying interfaces, (4) modulating charge injection and transport, (5) facilitating flexible device design, and (6) optimizing performance through interface modulation.

In 2014, Yu et al. pioneered the concept of 2D/organic heterojunction photodetectors based on MoS_2, achieving noteworthy results. The MoS_2/dye R6G heterostructure demonstrated a maximum photoresponsivity of 1.17 A W^{-1}, a detectivity of 1.5 × 10^7 Jones, and an external quantum efficiency (EQE) of 280%.[171] In comparison to the original MoS_2 photodetector, the performance of the MoS_2/dye R6G has been amplified by a factor of ten, primarily ascribed to the photoinduced charge transfer phenomena between MoS_2 and dye R6G. Furthermore, this device has broadened its detection spectrum into the NIR (405–980 nm). This study marks the pioneering introduction of MoS_2 into 2D/organic heterojunction photodetectors, ushering in a new era of research on MoS_2/organic heterojunctions. Heterojunction photodetectors based on van der Waals (vdW) interactions typically exhibit excellent performance. Combining rubrene with MoS_2 forms a vdW heterojunction photodetector,[172] achieving a photoresponsivity of approximately 500 mA W^{-1} and a rectification ratio of up to 10^5, demonstrating commendable rectifying properties and gate-tunability. This device presents a promising avenue for low-cost, high-performance photodetectors. Previous research showed a lack of clear understanding of charge transport between organic materials and MoS_2. Therefore, Jariwala et al. investigated the photodetection response of MoS_2/pentacene heterojunction photodetectors.[173] The results revealed that the MoS_2/pentacene heterojunction exhibits a type II band alignment photovoltaic effect, giving rise to asymmetric photocurrent transfer characteristics. The smaller size of pentacene compared to SiO_2 enhances the capture of photoexcited charge carriers, consequently accelerating the response time. This work underscores the potential of MoS_2 as a receptor material in photovoltaic applications.

Traditional organic photovoltaic materials such as phthalocyanines (Pcs) and their metal derivatives exhibit excellent chemical stability and, when combined with 2D materials, possess the attribute of rapid charge transfer. The MoS_2/ZnPc heterojunction photodetector (Fig. 13a and b)[174] showcases a

Table 2 Summary of MoS$_2$-based 2D/organic devices

2D materials	Organic thin films	Published year	Active materials	Responsivity [A W^{-1}]	Response time [ms]	Detection [nm]	Gain/EQE [%]	Detectivity [Jones]	Ref.
MoS$_2$	Small molecule organic thin films	2014	MoS$_2$/dye R6G	1.17	5.1×10^{-3}	405–980	280%	10^{10}	171
		2015	MoS$_2$/rubrene	0.5	5	450–700	$\approx 60\%$	NA	172
		2016	MoS$_2$/pentacene	NA	NA	500–700	NA	NA	173
		2018	MoS$_2$/ZnPc	1.4×10^4	8	532	NA	10^{11}	174
		2020	MoS$_2$/CuPc	3×10^3	0.436	500–650	483%	2×10^{10}	175
		2021	MoS$_2$/BTBT-SAM	475	5500	300–700	$1.4 \times 10^5\%$	NA	176
		2022	DPA/MoS$_2$(DMDM)	7.3×10^2	NA	365–550	NA	3.5×10^8	177
		2022	MoS$_2$/2DPI	390.5	400/430	405–1020	1.04×10^5	5.10×10^{12}	178
		2022	PbPc/MoS$_2$	1263.85	NA	808	194 066.7%	1.4×10^{13}	179
		2023	MoS$_2$/BTP-4F	3.2	0.332/0.274	500–700	756%	1.6×10^9	180
	Polymer and complex organic thin films	2015	MoS$_2$/C$_8$-BTBT	0.022	NA	Visible	$\approx 10\%$	NA	181
		2015	MoS$_2$/P(VDF-Tr18FE)	2570	1.8	500–1550	NA	$\approx 2.2 \times 10^{12}$	182
		2016	MoS$_2$/P3HT:PCBM/metasurface	NA	$<10^{-3}$	300–700	NA	NA	183
		2017	MoS$_2$/g-C$_3$N$_4$	4	50	270–700	$\approx 10^2\%$	4×10^{11}	184
		2019	MoS$_2$/PDPP3T	0.445	4	365–850	NA	3×10^8	185
		2019	MoS$_2$/P(VDF-TrFE) BJT	12	0.02	532	10^3	10^{13}	186
		2019	MoS$_2$/P(VDF-TrFE)	0.14	5.5	375–10 000	NA	9×10^{14}	187
		2022	(C$_6$H$_5$C$_2$H$_4$NH$_3$)$_2$PbBr$_4$/MoS$_2$	7.98×10^{-3}	42/38	405	10^3	NA	188
		2022	MAPbBr$_3$/MoS$_2$	0.368	252/260	532	8%	3.74×10^{12}	189
		2023	PSS/SnS$_2$/MoS$_2$	548.26/1389.08/457.47	NA	350/450/1150	$1.94 \times 10^5\%$/$3.82 \times 10^5\%$/$4.72 \times 10^4\%$	2.49×10^{12}/6.31×10^{12}/2.07×10^{12}	190

high responsivity (1.4×10^4 A W^{-1}) (Fig. 13c), swift response time (8 ms), and high sensitivity (10^{11} Jones). The MoS$_2$/ZnPc heterojunction establishes a van der Waals interface, enabling electron–hole pairs to spontaneously separate under illumination, with holes migrating to the ZnPc thin film layer. ZnPc is capable of utilizing the inherent capture states of MoS$_2$. This work, rooted in the surface assembly of organic molecules, provides a novel design approach for developing 2D/organic photodetectors. The Pcs family can maintain an idealized energy offset for ultrafast exciton dissociation. CuPc stands out as a distinguished representative within the Pcs family. The MoS$_2$/CuPc heterojunction constitutes an ideal type-II heterojunction, where CuPc can smooth the surface of MoS$_2$, suppressing the generation of dark current and accelerating charge transfer. The MoS$_2$/CuPc heterojunction photodetector[175] exhibits a high responsivity (3×10^3 A W^{-1}), a high detection rate (2×10^{10} Jones), a swift response time (0.436 ms), and an EQE of 483%. Compared to MoS$_2$ photodetectors, the response time has been improved by four orders of magnitude. This work advances the development of highly sensitive VIS light photodetectors. Self-assembled monolayers (SAM) significantly enhance the interface quality by allowing precise film thickness control, reducing charge scattering and recombination, and simplifying solution adsorption processes. The MoS$_2$/BTBT-SAM heterojunction proposed by Zhao et al.[176] represents the first realization of all 2D organic–inorganic hybrid vdW heterojunction phototransistors. The MoS$_2$/BTBT-SAM heterojunction photodetector demonstrates a high responsivity (475 A W^{-1}) and EQE ($1.45 \times 10^5\%$), primarily attributed to the photovoltaic effect. BTBT-SAM promotes charge transfer through π–π

interactions. This work advances the application of SAM technology in the field of photodetectors, providing more possibilities for the design of 2D atomic-molecular layers and fostering the development of novel heterostructures.

In 2022 and 2023, the performance of 2D/organic heterojunction photodetectors based on MoS$_2$ has demonstrated remarkable advancements. Photodetectors with bipolar charge transport characteristics have been developed,[177] and highly stable NIR photodetectors have been proposed.[178,179] The suppression of dark current has seen recent developments, with dark currents reduced to the pA level.[180] In contrast to heterojunctions, bilayer structures with independent channels can individually transport photogenerated excitons. 2,6-Diphenyl anthracene (DPA) is an outstanding representative in organic semiconductors, characterized by high hole mobility and electroluminescence properties. DPA/MoS$_2$(DMDM)[177] exhibits bipolar charge transport characteristics, with electrons and holes displaying distinct migration rates (holes at 0.13 cm^2 V^{-1} s^{-1} and electrons at 1.1 cm^2 V^{-1} s^{-1}). The key to achieving balanced electron and hole transport lies in bilayer structures and independently layered configurations with "ideal" clean interfaces. Research findings indicate that large interfaces within bilayer structures and unique band alignments are advantageous for carrier accumulation and recombination. Furthermore, reduced abnormal photocurrent has been observed, attributed to the differing light absorption ranges and band alignment structures of DPA and MoS$_2$. This work promotes the development of bipolar photodetectors, offering insights into the future development of organic–inorganic van der Waals heterojunction photodetectors. Achieving
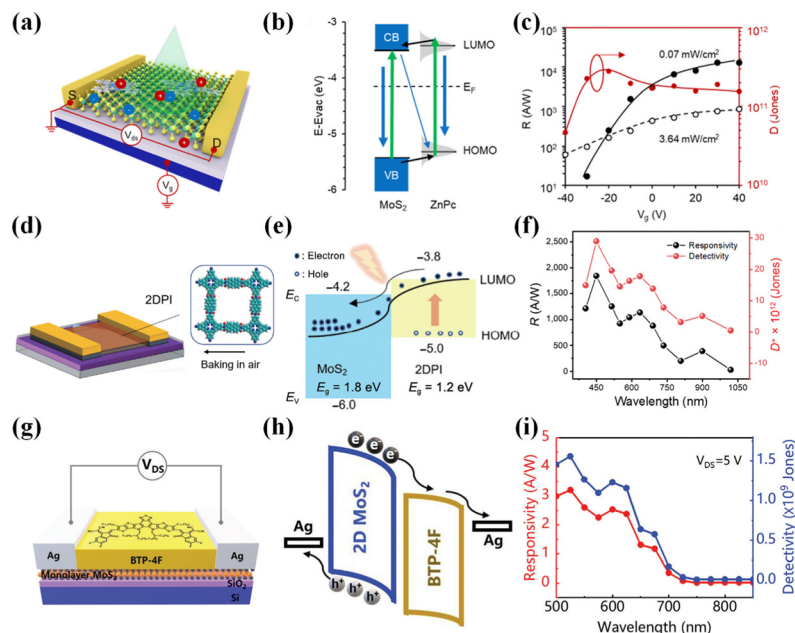
1252 | J. Mater. Chem. C, 2024, **12**, 1233–1267

This journal is © The Royal Society of Chemistry 2024

Fig. 13 Enhancing the photodetector performance of MoS_2 by combining it with small molecule organic materials. (a) Schematic illustration of MoS_2/ZnPc.[174] (b) Derived interfacial band alignment.[174] (c) Responsivity and detectivity as a function of V_g.[174] Reproduced with permission.[174] Copyright 2018, American Chemical Society. (d) Schematic diagram of MoS_2/2DPI.[178] (e) Band alignment and the injection process of photogenerated carriers.[178] (f) Responsivity and detectivity as a function of wavelength.[178] Reproduced with permission.[178] Copyright 2022, Nature Publishing Group. (g) Illustration of MoS_2/BTP-4F.[180] (h) Energy level matching.[180] (i) Responsivity and detectivity as a function of wavelength.[180] Reproduced with permission.[180] Copyright 2023, Wiley-VCH.

excellent and stable NIR photodetection is a meaningful yet challenging endeavor. MoS_2/2DPI (Fig. 13d and e)[178] accomplishes high-performance photodetection in the NIR region. The device exhibits high photoresponsivity (390.5 A W^{-1}) (Fig. 13f), a high detection rate (5.10×10^{12} Jones), and a broad response range (405–1020 nm). This is attributed to the type-II heterojunction's rational band structure and 2D PI's strong NIR light absorption. This work provides critical technology for high-performance detection in the NIR range using monolayer TMDCs sensitized with 2D covalent organic polymers.

PbPc is an exemplary member of the phthalocyanine family, with most metal phthalocyanine materials responding to light in the UV to VIS range. However, PbPc demonstrates excellent photovoltaic response in the NIR region. Under a mere 0.061 μW cm^{-2} NIR illumination, PbPc/MoS_2[179] exhibits an exceptionally high photoresponsivity (1263.85 A W^{-1}) and an extraordinarily high EQE (194 066.7%). This is attributed to the use of aluminum electrodes. From the perspective of energy level matching, the performance of gold electrodes should be far superior to that of aluminum electrodes. Paradoxically, this is because gold electrodes constitute Ohmic contacts, while aluminum electrodes form Schottky contacts. Schottky contacts have a significantly higher exciton dissociation efficiency than Ohmic contacts. This study elucidates the principles behind using materials such as Al, Au, Cu, and Ag as electrodes and analyzes the various factors contributing to exciton dissociation. It offers novel insights for enhancing the performance of 2D/organic devices. Organic materials with solubility properties are crucial for fabricating straightforward and high-performance

photodetectors. BTP-4F possesses solubility characteristics and features a low exciton dissociation energy, facilitating effective exciton dissociation. The MoS_2/BTP-4F heterojunction photodetector (Fig. 13g and h)[180] not only exhibits shallow dark currents (at the pA level) but also demonstrates high responsivity (3.2 A W^{-1}), elevated EQE (756%), remarkable detectivity (1.6×10^9 Jones) (Fig. 13i), and rapid response times (0.332/0.274 ms). This work advances the development of high-performance 2D/organic heterojunctions, providing a design paradigm for sensitive and rapidly responsive heterojunctions.

4.2.2. Combining with organic polymers or complex materials. Introducing organic polymers or complexes plays a vital role in improving the performance of MoS_2 photodetectors. The following three issues usually need to be focused on during device design and fabrication: (1) control of film thickness, (2) interface engineering optimization, and (3) preparation process optimization.

The epitaxial growth process offers notable advantages, including cleanliness, low-temperature operation, and precise morphological control. Photodetectors based on MoS_2/C_8-BTBT heterojunctions,[181] fabricated *via* epitaxial growth techniques, achieve a photoresponsivity of 22 mA W^{-1} and a rectification ratio as high as 10^5, primarily due to the photovoltaic effect inherent in the MoS_2/C_8-BTBT heterojunction. Both 2D and organic materials have a rich library of materials, which lays a solid foundation for developing 2D heterostructures. In traditional photodetectors, gate voltage and source–drain voltage are employed to enhance sensitivity, albeit at the cost of increased losses due to self-heating. P(VDF-TrFE) presents the

This journal is © The Royal Society of Chemistry 2024

J. Mater. Chem. C, 2024, **12**, 1233–1267 | 1253

ability to fine-tune the transport characteristics of the channel, thereby improving the detector's performance. The MoS$_2$/P(VDF-TrFE) heterojunction photodetector (Fig. 14a and b)[182] exhibits a high detectivity (2.2×10^{12} Jones) and a remarkable photoresponsivity (2570 A W^{-1}) (Fig. 14c), primarily attributed to P(VDF-TrFE) suppression of dark current in MoS$_2$ and the enhanced detector sensitivity brought about by stable residual polarization. Furthermore, this device can achieve detection in the NIR region (500–1550 nm). Plasma metasurface structures can enhance the light absorption of 2D materials. Petoukhoff et al. applied metasurface to MoS$_2$/P3HT:PCBM heterojunction photodetectors,[183] resulting in a six-fold increase in charge density and a broadening of the absorption bandwidth by 90 nm. This enhancement is attributed to the metasurface expediting the hole transfer from MoS$_2$ to P3HT:PCBM. This study underscores the synergistic effect between 2D/organic heterojunctions and metasurface, promising substantial applications in thin-film solar cells. 2D materials typically exhibit varying bandgaps and dark current characteristics. The cost-effective control and mitigation of dark current pose intriguing challenges. g-C$_3$N$_4$ is considered a promising candidate for integration with 2D materials due to its ability to suppress dark current in these materials. Furthermore, g-C$_3$N$_4$ facilitates rapid charge transfer between itself and 2D materials, improving the efficiency of photogenerated exciton dissociation. The MoS$_2$/g-C$_3$N$_4$ heterojunction photodetector[184] demonstrates a photoresponsivity of 4 A W^{-1}, a response time of 50 ms, 100% EQE, a detectivity of 4×10^{11} Jones, and

broadband responsiveness (270–700 nm). Notably, this device exhibits excellent flexibility, maintaining high performance even after hundreds of continuous bends, laying a solid foundation for developing low-cost, flexible photodetectors based on MoS$_2$.

While most of these heterojunctions primarily operate in the UV to VIS range, PDPP3T exhibits photosensitivity in the NIR region. The amalgamation of MoS$_2$ with PDPP3T promises to yield high-performance broadband photodetectors. The MoS$_2$/PDPP3T heterojunction phototransistor[185] demonstrates self-powered photoresponsivity at zero bias voltage, with high responsivity and a rapid response time of 4 ms. This is attributed to forming the MoS$_2$/PDPP3T heterojunction and creating an asymmetric source–drain configuration. Furthermore, PDPP3T's solubility facilitates its use in flexible photodetectors, rendering MoS$_2$/PDPP3T a highly flexible option with substantial potential for integration into wearable optical-electronic devices, presenting significant application value. Ferroelectric materials, such as P(VDF-TrFE) copolymers, exhibit exceptional properties in fabricating simple rotation layers. The MoS$_2$/P(VDF-TrFE) BJT heterojunction photodetector proposed by Lv et al. (Fig. 14d–f)[186] demonstrates self-powering and high gain characteristics, marking the first instance of improving the response time of MoS$_2$-based photodetectors to the microsecond level (20 μs). What's more, this device can easily tailor its reconfigurable features through finite element polarization switching. This reconfigurable device holds the potential to advance intelligent image window sensors. Its application in high-stability array detection is feasible.
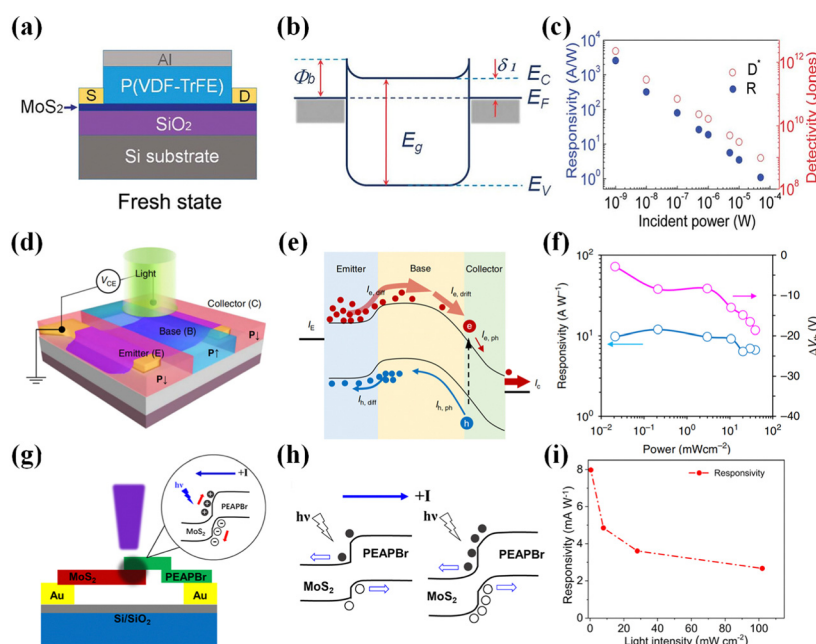

Fig. 14 Enhancing the photodetector performance of MoS$_2$ by combining it with organic polymers or complex materials. (a) The cross section structures of MoS$_2$/P(VDF-TrFE).[182] (b) Equilibrium energy band diagrams.[182] (c) Photoresponsivity and detectivity as a function of incident power.[182] Reproduced with permission.[182] Copyright 2015, Wiley-VCH. (d) Schematic illustration of MoS$_2$/P(VDF-TrFE).[186] (e) Energy band diagram.[186] (f) Responsivity and extracted threshold voltage shift as a function of incident power.[186] Reproduced with permission.[186] Copyright 2019, Nature Publishing Group. (g) Schematic illustrations of (C$_6$H$_5$C$_2$H$_4$NH$_3$)$_2$PbBr$_4$/MoS$_2$.[188] (h) Energy band diagrams of (C$_6$H$_5$C$_2$H$_4$NH$_3$)$_2$PbBr$_4$/MoS$_2$.[188] (i) Responsivity vs. light intensity.[188] Reproduced with permission.[188] Copyright 2022, American Chemical Society.

1254 | J. Mater. Chem. C, 2024, 12, 1233–1267

This journal is © The Royal Society of Chemistry 2024

Likewise utilizing P(VDF-TrFE) copolymers, Wang et al. introduced MoS_2/P(VDF-TrFE),[187] achieving ultrabroad detection ranging from UV to MIR with a high on–off ratio (10^3) and a fast response time (5.5 ms). This marks a groundbreaking development in 2D/organic heterojunction photodetectors, expanding the detection wavelength by 10 000 nm for the first time. This achievement is attributed to the thermoelectric effect of the MoS_2/P(VDF-TrFE) heterojunction and the significant enhancement of MoS_2's photodetection performance by the P(VDF-TrFE) polar field. P(VDF-TrFE) can suppress MoS_2's dark current and narrow MoS_2's bandgap, thus broadening the detection spectrum. This work provides a reliable approach for long-wave detection.

2D Ruddlesden–Popper (RP) phase perovskites exhibit excellent stability, and $(C_6H_5C_2H_4NH_3)_2PbBr_4/MoS_2$ proposed by Xu et al. (Fig. 14g–i)[188] demonstrates an ultra-low dark current (0.1 pA), owing to the low carrier density of $(C_6H_5C_2H_4NH_3)_2$-$PbBr_4$ and the reasonable band structure of the heterojunction. Furthermore, this device maintains excellent photodetection performance after over a thousand switching cycles. Notably, the device can operate at zero bias voltage, showcasing self-powering and self-driven capabilities. At illumination intensities below 0.5 mW cm^{-2}, the device exhibits excellent photoresponsivity even under zero bias conditions. This work underscores the significant potential of the 2D RP perovskite in weak light detection. $MAPbBr_3/MoS_2$ and $(C_6H_5C_2H_4NH_3)_2$-$PbBr_4/MoS_2$ demonstrate self-powered characteristics, maintaining excellent photodetection performance under zero bias voltage. $MAPbBr_3$ possesses favorable attributes such as low trap density, high absorption coefficient, and high photovoltaic conversion efficiency. With MoS_2 as the n-type semiconductor and $MAPbBr_3$ as the p-type semiconductor, the $MAPbBr_3/MoS_2$ heterojunction exhibits robust photovoltaic properties. Under zero bias conditions, $MAPbBr_3/MoS_2$[189] showcases a photoresponsivity of 368 mA W^{-1} and a photodetection rate of 3.74×10^{12} Jones. This work lays the foundation for the development of high-performance photovoltaic devices.

4.3. Photodetectors with other 2D materials

In addition to graphene and MoS_2, numerous 2D materials have been successfully employed in the fabrication of high-performance photodetectors (summarized in Table 3).[191–200] For instance, WS_2/poly-TPD:PCBM[192] has demonstrated self-powered capabilities, while SWCNTs/PQT-12:F4TCNQ,[194] Bi_2Se_3/MOF(Ni-CAT-1),[195] ReS_2/2D perovskite $((CH_3(CH_2)_3NH_3)_2(CH_3-NH_3)_4Pb_5I_{16})$,[196] IEICO-4F/$WSe_2$,[197] 3DG/P3HT:$PC_{71}$BM,[199] and graphite/$C_{60}$/BP,[200] among other devices, exhibit infrared detection capabilities. Notably, 3DG/P3HT:PC_{71}BM[199] can detect wavelengths exceeding 10 000 nm, expanding the detection range into the MIR region.

In 2017, the first 2D organic heterojunction photodetector based on WS_2 was introduced. WS_2/PTCDA[191] achieved an EQE of 1.8 ± 0.2% and an IQE of 11 ± 1%. The hybrid charge transfer excitons, formed through the interaction of Frenkel excitons in PTCDA and Wannier excitons in WS_2, subsequently dissociate into free charges, enhancing quantum efficiency. While the device may not exhibit outstanding hydrogen

sensitivity, this work has stimulated the extensive utilization of 2D materials in 2D/organic heterojunctions. In 2019, leveraging WS_2, Huang et al. introduced the WS_2/poly-TPD:PCBM heterojunction photodetector.[192] This device maintained a high responsivity (17 A W^{-1}), a high detection rate (1.1×10^{11} Jones), and a high on/off ratio even under zero bias voltage. The poly-TPD:PCBM heterojunction enhanced the light absorption coefficient, facilitating efficient dissociation of photogenerated excitons. Appropriate band structures and energy gaps also favored the separation of electron–hole pairs. Furthermore, the authors generated high-quality poly-TPD/PCBM and WS_2 films through a straightforward solution-coating technique and chemical vapor deposition. This provides relevant insights and design examples for creating high-performance 2D/organic heterojunctions. Prolonged photoconductivity is the primary challenge in high-speed imaging, which Pei et al. effectively addressed using the 2D material Bi_2Se_3. The Bi_2Se_3/rubrene heterojunction photodetector[193] exhibits a high responsivity (124 A W^{-1}) and fast response time (54 ms). This can be attributed to the rational band alignment structure and the built-in electric field in the Bi_2Se_3/rubrene heterojunction. Interestingly, the device also demonstrates a negative differential resistance effect and gate-tunable backward-like diode behavior, leading to the inversion of the Fermi level position. This work can potentially advance the application of 2D/organic devices in high-speed imaging. Infrared photodetection in the military sector is of paramount importance. The SWCNTs/PQT-12:F4TCNQ heterojunction photodetector proposed by Yang et al.[194] achieves broadband detection up to 2600 nm, with a high responsivity (2.75×10^6 A W^{-1}), a high detection rate (3.12×10^{14} Jones), and a high EQE (10^8%). The broadband detection can be attributed to the ultra-low intermolecular electronic transition energy in the SWCNT layer and the ultra-broadband absorption characteristics of the PQT-12:F4TCNQ layer. This device demonstrates outstanding stability, robustness, and flexibility, maintaining excellent optoelectronic performance even after 12 000 seconds of cyclic testing. Additionally, the authors demonstrated a noise reduction array, which holds significant potential for application in the field of biological synapses. Bi_2Se_3/MOF(Ni-CAT-1) (Fig. 15a and b)[195] exhibits broad-spectrum absorption characteristics (600–2000 nm). Unlike the reasons behind the broad-spectrum absorption in SWCNTs/PQT-12:F4TCNQ, Bi_2Se_3/MOF(Ni-CAT-1) achieves this due to the intense light absorption by the MOF(Ni-CAT-1) layer and the high charge carrier mobility of the Bi_2Se_3 layer. Specifically, this is attributed to the synergistic effect of Schottky barriers and the photovoltaic effect. The device maintains a high responsivity (4725 A W^{-1}) (Fig. 15c) and a high detectivity (3.5×10^{13} Jones) at 1500 nm, surpassing Bi_2Se_3 photodetectors by 2–3 orders of magnitude. This work highlights the enormous potential of MOF materials in infrared detection.

2D perovskites possess a wide bandgap, leading to a relatively poor spectral response. Surprisingly, $ReS_2/(CH_3(CH_2)_3-NH_3)_2(CH_3NH_3)_4Pb_5I_{16}$ has achieved exceptional photodetector performance. $ReS_2/(CH_3(CH_2)_3NH_3)_2(CH_3NH_3)_4Pb_5I_{16}$ (Fig. 15d–f)[196] exhibits characteristics of broad-spectrum response (2000 nm)

This journal is © The Royal Society of Chemistry 2024

J. Mater. Chem. C, 2024, **12**, 1233–1267 | **1255**

Table 3 Summary of other 2D/organic devices

2D materials	Published year	Active materials	Responsivity [A W^{-1}]	Response time [ms]	Detection [nm]	Gain/EQE [%]	Detectivity [Jones]	Ref.
Other 2D materials except graphene and MoS$_2$	2017	WS$_2$/PTCDA	NA	NA	400–600	NA	NA	191
	2019	WS$_2$/poly-TPD:PCBM	1.02	<181	450	8%	1.1×10^{11}	192
	2020	Bi$_2$Se$_3$/rubrene	124	58	532	>10^3%	NA	193
	2021	SWCNTs/PQT-12:F4TCNQ	2.75×10^6	9.7	400–2600	10^8%	3.12×10^{14}	194
	2021	Bi$_2$Se$_3$/MOF(Ni-CAT-1)	4725	130	600–2000	2.3×10^4%	3.5×10^{13}	195
	2022	ReS$_2$/(CH$_3$(CH$_2$)$_3$NH$_3$)$_2$(CH$_3$NH$_3$)$_4$Pb$_5$I$_{16}$	2.2	0.443/0.72	2000	68%	1.8×10^{14}	196
	2022	IEICO-4F/WSe$_2$	8.32	3.39/4.24	532–808	NA	4.65×10^{11}	197
	2022	MoTe$_2$/PBDB-T:ITIC	0.706	NA	656	133%	2.62×10^{10}	198
	2022	3DG/P3HT:PC$_{71}$BM	5.8×10^5	24	300–10 600	>10^6%	3×10^{15}	199
	2022	Graphite/C$_{60}$/BP	100	31.4	400–1060	NA	NA	200

due to the heterojunction's direct type-II bandgap of 0.4 eV. Furthermore, this device features self-powered capabilities, maintaining high detectivity (1.8×10^{14} Jones), high EQE (68%), and ultra-fast response times (0.443/0.72 ms) even at zero bias voltage. The sub-millisecond response time is attributed to the significant band offset at the heterojunction interface, ensuring efficient charge carrier separation. Moreover, the device demonstrates outstanding stability, retaining excellent photodetection performance after seven days of operation. This work provides an effective design strategy for high-performance and highly stable photodetectors. Zhu et al. designed an IEICO-4F/WSe$_2$ heterojunction photodetector.[197] By investigating the heterojunction's photoluminescence quenching behavior, they achieved a high-performance photodetector in the near-infrared range (808 nm) with a responsivity of 8.32 A W^{-1} and a detectivity of 4.65×10^{11} Jones. The

photodetection performance of this device is attributed to the effective separation of photogenerated charge carriers and charge transfer at the type-II heterojunction interface. While NIR detection has significantly developed, research on MIR detection remains limited. MIR detection has crucial value in various fields, such as biometrics and military applications, making it a meaningful and challenging endeavor. In 2022, Ge et al. introduced a 3DG/P3HT:PC$_{71}$BM heterojunction photodetector (Fig. 15g and h)[199] capable of ultra-broadband detection extending beyond 10 000 nm in the MIR spectrum. This device exhibits an exceptionally high responsivity (5.8×10^5 A W^{-1}) and a high detectivity (3×10^{15} Jones) (Fig. 15i). The PCBM layer and functional groups within the 3DG layer serve as electron trapping sites, extending the lifetime of charge carriers and enhancing the device's photoresponse and photocurrent. Furthermore, this device demonstrates outstanding
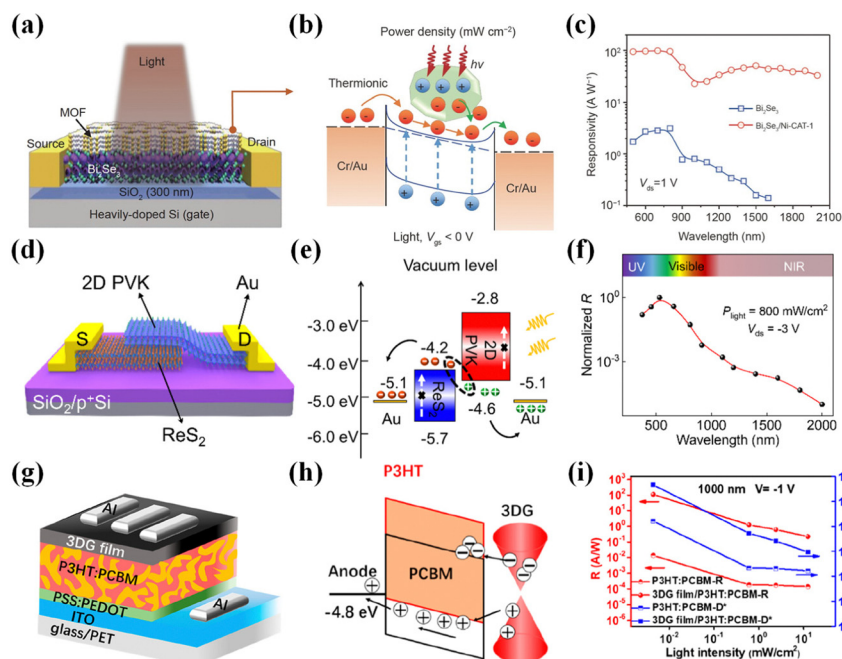

Fig. 15 Enhancing the photodetector performance of other 2D materials by combining them with organic thin films. (a) Schematic diagram of Bi$_2$Se$_3$/MOF(Ni-CAT-1).[195] (b) The carrier transport mechanism and band energy diagram at V_{gs} < 0.[195] (c) Responsivity as a function of wavelength.[195] Reproduced with permission.[195] Copyright 2021, Nature Publishing Group. (d) Schematic image of ReS$_2$/(CH$_3$(CH$_2$)$_3$NH$_3$)$_2$(CH$_3$NH$_3$)$_4$Pb$_5$I$_{16}$.[196] (e) Interlayer excitation under infrared light.[196] (f) Normalized wavelength-dependent responsivity.[196] Reproduced with permission.[196] Copyright 2022, American Chemical Society. (g) Schematic of 3DG/P3HT:PC$_{71}$BM.[199] (h) Working mechanism under infrared illumination.[199] (i) Power-dependent R and D^*.[199] Reproduced with permission.[199] Copyright 2022, American Chemical Society.

1256 | J. Mater. Chem. C, 2024, **12**, 1233–1267

This journal is © The Royal Society of Chemistry 2024

performance in weak light detection, easily detecting light at the pw level. It maintains excellent flexibility and mechanical stability, providing a core technology for designing highly stable wearable integrated optoelectronic devices.

4.4. Applications of 2D/organic heterojunctions in flexible photodetectors

Research into applying 2D/organic heterostructures in flexible devices is increasingly gaining attention, particularly in developing photodetectors. These photodetectors combine the exceptional electronic and optical properties of 2D materials with the flexibility and tunability of organic materials, offering an efficient and revolutionary photonic conversion solution in the realm of flexible electronics.[115,135,146,147,156,184,185,194,199]

In recent years, scientists have been advancing research on flexible photodetectors based on 2D/organic heterostructures to better meet the demand for flexible sensing and imaging technologies in electronic skin and flexible electronics applications. For instance, Gao et al. developed an organic dye/$Zn_{0.9}Mg_{0.1}O$ NPs/graphene photodetector (Fig. 16a),[115] showcasing exceptional photoresponse and mechanical flexibility by combining an organic dye, magnesium-doped zinc oxide, and graphene. Additionally, the graphene/MOF photodetector designed by Bera et al. (Fig. 16b)[146] demonstrated significant advantages such as non-toxicity, environmental friendliness, and stability, making it highly suitable for wearable and stretchable electronic devices. Furthermore, researchers have successfully developed various flexible 2D/organic heterostructure photodetectors, such as the cost-effective graphene/$CH_3NH_3PbI_3$:MoS_2 (Fig. 16c),[147] ultra-thin graphene/PEDOT:PSS/P3HT:PC_{71}BM (Fig. 16d),[156] exceptionally durable SWCNTs/PQT-12:F4TCNQ (Fig. 16e and f),[194] and low-light performing 3DG/P3HT:PC_{71}BM photodetectors (Fig. 16g and h).[199] These 2D/organic material photodetectors have demonstrated outstanding performance and high adaptability in flexible wearable devices.

Developing 2D/organic heterostructure photodetectors generally represents a significant breakthrough in materials science and electronic engineering. It opens up new possibilities for application in flexible electronic devices, particularly in areas like electronic skin, health monitoring, and environmental sensing. As future research progresses and technologies mature, these 2D/organic heterostructure photodetectors are poised to play an increasingly pivotal role in innovative materials and the next generation of electronic devices.

5. Summary of device performance

Photodetectors of organic materials suffer from the disadvantages of low photoelectron mobility, material instability, low photo-quantum efficiency, temperature dependence, short lifetime, and restricted sensitivity range.[201–203] Photodetectors of 2D materials suffer from drawbacks such as limited spectral response range, weak light detection capability, high thermal noise, poor stability, and physical size constraints.[204–206] Combining 2D materials with organic materials brings new

development opportunities.[38,41,207] It is undeniable that after a decade of development, 2D/organic heterojunction photodetectors have significantly improved the performance of photodetectors. However, taking 2D/organic heterojunction photodetectors to large-scale applications is still a long way to go. To date, graphene remains the best and most widely used 2D material, and graphene-based devices generally outperform other devices in terms of responsivity and detectivity (shown in Fig. 17a). The ultra-high responsivity and ultra-high detectability are mainly attributed to graphene's broadband spectral response, high carrier mobility, superior electrical conductivity, good mechanical flexibility, and excellent resistance to light fatigue.[208–210] MoS_2 has a tunable bandgap, which means that MoS_2 can achieve controllable switching and small dark current.[211,212] Moreover, MoS_2 possesses excellent chemical stability and can be grown over large areas using chemical vapor deposition.[213] Graphene-based 2D/organic heterojunction photodetectors typically have higher EQE, and MoS_2-based ones are usually excellent regarding response speed (shown in Fig. 17b). Some 2D materials have shown excellent performance in MIR wavelength detection up to 300 to 10 600 nm (shown in Fig. 17e). Organic/2D heterojunction photodetectors can achieve bandwidths up to 10^5 Hz and still reach 10^4 Hz while having a response rate of 10^9 A W^{-1} (Fig. 17c).

Graphene-based 2D/organic heterojunction photodetectors peaked their development rate in 2021 and have reached a relatively mature bottleneck. 2D/organic heterojunction photodetectors based on MoS_2 and other 2D materials are still developing rapidly (Fig. 17d). Devices[187,199] are available for detection in the NIR (Fig. 17e) but not in the FIR or longer wavelengths. Detection in the UV to NIR bands is well developed, but detection at long wavelengths is still understudied, and 2D/organic heterojunctions still have great potential for development in the field of long-wavelength detection.[48,214]

6. Future development

6.1. Long-wave and narrow-band detection

Long-wavelength and narrow-band detection are two dark clouds over 2D/organic heterojunction photodetectors and directions that must be vigorously researched and developed. Detection technology in the VIS to NIR bands is very mature, but the detection of FIR needs to be improved. The energy of photons is proportional to the frequency of electromagnetic radiation and inversely proportional to the wavelength. The photon energy can be expressed by the equation $E = h\nu = hc/\lambda$. The MIR and FIR energies are minimal, and the carrier energies are close to the molecular vibration or scattering, which are not easily collected and dissociated. 2D/charge transfer complex heterojunctions are considered an effective strategy to address long-wave detection, where the effect of donor–acceptor bonding and acceptor-induced negative anions in charge transfer complexes creates a new narrow bandgap, thus broadening the detection range.[215] The method can now easily detect the NIR and MIR bands, and further innovations and developments are needed for the detection of FIR.
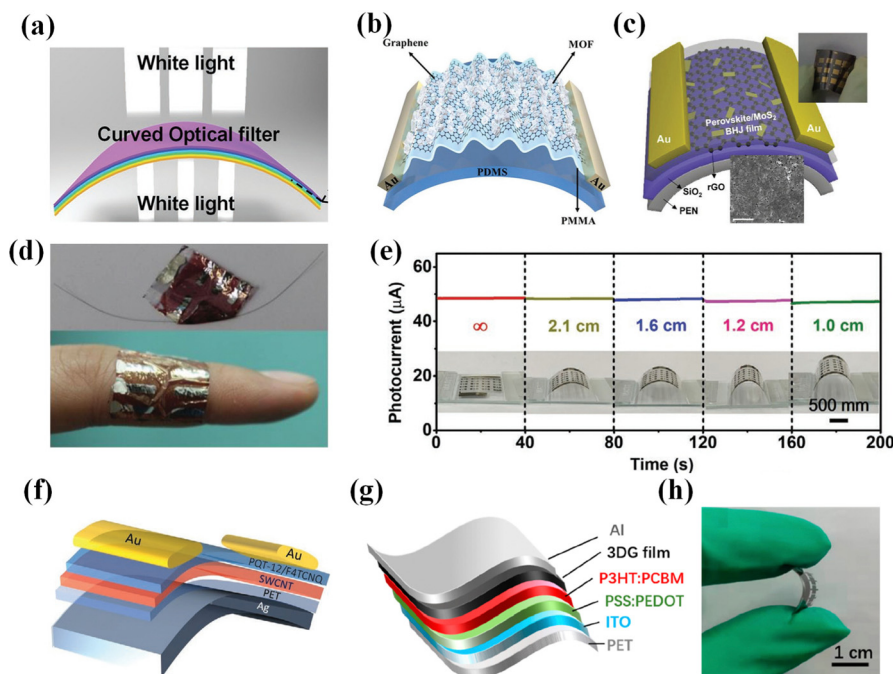
This journal is © The Royal Society of Chemistry 2024

J. Mater. Chem. C, 2024, **12**, 1233–1267 | **1257**

Fig. 16 Flexible 2D/organic heterojunction photodetectors. (a) Flexible graphene/Zn$_{0.9}$Mg$_{0.1}$O NPs/BET narrowband photodetector.[115] Reproduced with permission.[115] Copyright 2017, Wiley-VCH. (b) Schematic illustration of graphene/MOF under bending strain.[146] Reproduced with permission.[146] Copyright 2018, Wiley-VCH. (c) Flexible graphene/CH$_3$NH$_3$PbI$_3$:MoS$_2$ hybrid photodetector.[147] Reproduced with permission.[147] Copyright 2018, Wiley-VCH. (d) Ultrathin and flexible graphene/PEDOT:PSS/P3HT:PC$_{71}$BM photodetector.[156] (e) Photocurrent of SWCNTs/PQT-12:F4TCNQ under different bending radii.[194] (f) Flexible SWCNTs/PQT-12:F4TCNQ phototransistor.[194] Reproduced with permission.[194] Copyright 2021, Wiley-VCH. (g) Flexible 3DG/P3HT:PC$_{71}$BM photodetector.[199] (h) Photocurrent for flexible 3DG/P3HT:PC$_{71}$BM as a function of cycle number.[199] Reproduced with permission.[199] Copyright 2022, American Chemical Society.

Narrow-band detectors are typically used to detect or receive signals in a specific frequency range and are widely used in communication, radar, and medical systems.[216–218] Narrowband detection has triggered much research, but previous related strategies have more obvious drawbacks, such as reduced responsivity, complex configuration, and non-tunability. Although narrowband detection has been achieved in 2D/organic heterojunction photodetectors such as graphene/Zn$_{0.9}$Mg$_{0.1}$O NPs/BET dye,[115] graphene/h-BN/J-aggregate PTCDI-C$_{13}$,[137] graphene/PDVF,[138] *etc.*, the performance of these devices is not satisfactory ($R \approx 10^2$–10^3 A W^{-1}, $\tau \approx 1000$ ms). Therefore, it is still challenging to realize high-performance narrowband photodetectors, and more 2D/organic heterojunction photodetectors with advanced materials, functions, and structures are needed in the future.

6.2. New organic materials and structure

Currently, 2D materials commonly used in 2D/organic heterojunction photodetectors include graphene and TMDs, and organic materials mainly include COFs, MOFs, ferroelectrics (P(VDF-TrEE)),[182,186,187] semiconductors (pentacene),[125–127,129,158,165,173] insulators (PVCN)[45] and photochromic molecules (DAE). More 2D and organic, exceedingly narrow bandgap materials must be developed to develop high-performance long-wave and narrowband detectors. Another way to reduce the bandgap is through modulation: for example, inter-doping TCNQ with MOF

Ru$_2$(C$_6$H$_5$COO)$_4$Cl to reduce the bandgap of the MOF from 0.625 eV to 0.175 eV.[219] Narrow bandgap is the basis for long-wave detection, and materials such as MOFs, COFs, topological Dirac semimetals, and topological insulators have good prospects for development.

Heterostructures, mainly in stacking and doping, usually contain only 1–2 organic materials as the absorbing layer and one 2D material as the absorbing layer. In the future, more complex heterostructures are needed to enhance the performance of photodetectors, such as s-scheme heterojunctions,[220] double charge transfer heterojunctions[221,222] and heterojunctions with more layers. In addition, higher-performance photodetectors can be obtained by combining several approaches, such as local field coupling combined with built-in electric fields. Overall, the effective trapping and efficient dissociation of carriers should be enhanced, the energy loss should be reduced, and the charge decomposition efficiency should be improved.[223] Also, high-quality heterogeneous interfaces that are easy to implement should also be emphasized.[224]

6.3. Exploring the 2D/organic interface: new horizons in materials science

In materials science, heterostructures constitute systems composed of different material layers, with interfaces between these layers possessing unique electronic, optical, and chemical properties.[225] Research on interfaces in 2D/organic

1258 | *J. Mater. Chem. C*, 2024, **12**, 1233–1267

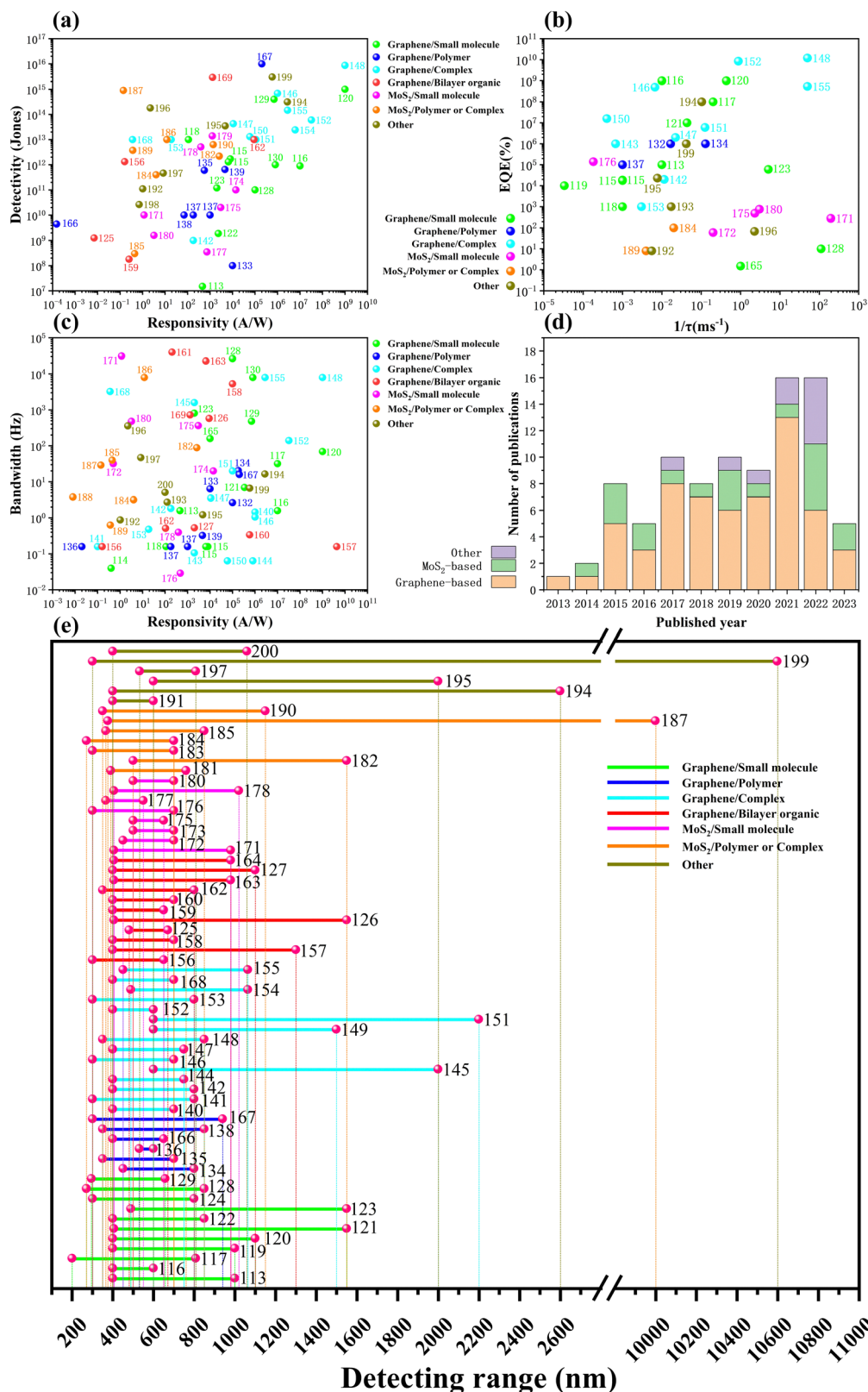This journal is © The Royal Society of Chemistry 2024

Fig. 17 (a) Responsivity and detectivity of 2D/organic heterojunction photodetectors. (b) EQE and $1/\tau$ of 2D/organic heterojunction photodetectors. (c) Bandwidth and responsivity of 2D/organic heterojunction photodetectors. (d) The number of publications of 2D/organic heterojunction photodetectors. (e) The detection range of 2D/organic heterojunction photodetectors. Note: bandwidth = $1/(2\pi\tau)$.

This journal is © The Royal Society of Chemistry 2024

J. Mater. Chem. C, 2024, **12**, 1233–1267 | **1259**

heterojunctions has long been a focal point. Effective interface formation between 2D materials and organic materials enables efficient charge transfer, thereby enhancing the efficiency of solar cells or photodetectors. Additionally, investigating interfaces in 2D/organic heterojunctions involves studying molecular arrangements, charge recombination, band alignment, and other microscale mechanisms at these interfaces, all representing current focal points in materials science.[33,226]

6.3.1. New opportunities at the 2D atom/organic molecule interface. The emergence of "highly ordered 2D atom/organic molecule interfaces" presents new opportunities in materials science. 2D materials, owing to their atomic-level thickness and highly ordered lattice structure, provide a unique and precisely controllable platform for the self-assembly of organic molecules.[49] At the interface of 2D/organic materials, organic molecules can form highly ordered structures on the surface of 2D materials through intermolecular forces such as hydrogen bonding, van der Waals forces, and π–π stacking, among others.[48] This ordered structure relies not only on the design and functionality of the organic molecules themselves but is also strongly influenced by the underlying surface properties of the 2D materials. For instance, graphene's flat and chemically inert surface can serve as an ideal template, promoting the regular arrangement of organic molecules. Earlier devices were based on the growth of organic single crystals on graphene surfaces, achieving a photo-responsivity of 110 A W^{-1} and a detectivity of 10^{13} Jones in the visible light spectrum.[118]

In organic photovoltaic materials, the high binding energy of excitons often stands as a crucial limiting factor in their performance. Combining 2D materials with organic materials enables the formation of novel electronic states at the interface, reducing excitons' binding energy and promoting their separation—an essential aspect for enhancing photovoltaic conversion efficiency.[50,227] For instance, Shao et al. employed edge-on C_{12}TBP, stacked in a π–π configuration with graphene, inducing orbital coupling and hybridization to improve electron transfer at the interface.[122] Liu et al. achieved high-quality interfaces by epitaxially depositing several layers of the organic small molecule C_8-BTBT onto graphene, resulting in devices exhibiting high internal quantum efficiency (41%) and responsivity (1.8×10^5 A W^{-1}).[133] Similarly, heterojunctions such as the self-assembled BTBT with MoS_2 have been explored.[176] However, the exciton dissociation efficiency in planar 2D/organic heterojunctions still falls short of the requirements, necessitating a further enhancement of the built-in electric field. Vertical P–N structures (combination of p-type and n-type semiconductors) have emerged as a solution.[172–174,181] These structures can generate a strong built-in electric field at their interface, aiding in the effective separation of excitons. When an external voltage is applied, this field can be further strengthened, leading to more efficient separation of electrons and holes and enhancing charge collection efficiency. In practical applications, this implies that designing and optimizing the interface structure between 2D materials and organic materials and introducing suitable P–N structures can improve the performance of photodetectors and other optoelectronic

devices. For instance, effective P–N structures can be formed by introducing appropriate doping layers between 2D and organic layers or by introducing additional semiconductor materials. Such structural designs enhance the built-in electric field and improve the transport and collection of charge carriers. In the future, integrating the unique properties of 2D materials with the advantages of traditional P–N structures could lead to the development of more efficient and higher-performance photovoltaic systems.

The research on highly ordered 2D atomic/organic molecular interfaces holds significant importance in developing new nanoelectronic devices, sensors, optoelectronic materials, and more.[48,49] Precise control over molecular arrangement and interactions at interfaces enables manipulating the electronic properties of the materials, facilitating the design and optimization of device performance at the nanoscale. Moreover, this research domain offers insights into understanding and simulating complex biological interfaces; for instance, similar π–π stacking phenomena exist in protein–cell membrane interactions.[228–230] Therefore, in-depth exploration of interfaces between graphene-like 2D materials and organic substances holds significance for materials science and nanotechnology. It offers novel perspectives and applications in various biochemistry and molecular biology fields.

6.3.2. Trade-offs: orderliness vs. photovoltaic conversion efficiency. The challenge faced by 2D/organic heterojunctions lies in balancing the interface's orderliness with the photovoltaic conversion efficiency (PCE).[231,232] In 2D/organic heterojunctions, small molecular materials, due to their highly ordered stacking and precisely controlled interfaces, facilitate efficient charge transfer. However, this high degree of ordered structure might limit charge diffusion and transport within the material, resulting in a relatively low PCE of approximately 10%.[233,234] This limitation arises because while the interface for charge transfer is of high quality, the ordered structure might constrain the distance for excitons to reach the interface, thereby reducing effective exciton separation. In contrast, bulk heterojunctions possess relatively disordered structures, but their mixed distribution creates more interfaces that traverse the material, enhancing exciton separation efficiency. Although this disordered structure may lead to a loss in charge transfer efficiency, the improved exciton dissociation significantly boosts the overall PCE of solar cells, exceeding 17%.[235,236] Hence, the trade-off between interface orderliness and solar cell efficiency stands as a crucial consideration in solar cell design and material selection. Future research might optimize material structures to enhance exciton dissociation efficiency while maintaining high-quality charge transfer interfaces, aiming for higher photovoltaic conversion efficiencies. Deeper understanding and innovative design of material interfaces and microstructures offer promising prospects for achieving more efficient photodetector technologies.

6.4. Development and application of 2D/organic devices

In recent years, the development of organic solar cells has been rapid, and more organic systems with higher conversion efficiencies and more excellent stability have been proposed, which will continue to promote the development of

1260 | J. Mater. Chem. C, 2024, **12**, 1233–1267

This journal is © The Royal Society of Chemistry 2024

Fig. 18 The future developing trends.

graphene/organic heterojunction detectors and even a more extensive range of 2D/organic heterojunctions.[237–241] In addition, novel biosynaptic, low-energy functional photodetector devices, photonic chips for on-chip computing, and susceptible biomonitoring detectors have been the trend in recent years.[242–246] At present, more and more new structures and materials better reduce the gap between the energy bands of organic materials and reduce the energy loss in transmission, such as heterojunctions with double donor–acceptor groups and supramolecular systems with double donor–acceptor groups, and in the future, these new materials and structures will be combined with graphene for in-depth exploration in order to improve the performance of graphene/organic photodetectors (Fig. 18).

Although graphene/organic charge transfer complexes have made some progress in long-wave detection, their responsivity is still at a low level, which is because the new energy bands generated by organic charge transfer complexes have a small band gap, which makes it challenging to match the energy bands, leading to difficulties in the efficient dissociation process. Therefore, the overall efficiency of most organic charge transfer complexes at long wavelengths is low, which limits their further application and development. In the future, optimizing the long-wave detection depth of organic charge transfer complexes and improving the structure and energy band matching to prepare high-performance graphene/organic charge transfer complex heterojunction detectors is necessary.

While 2D/organic heterojunction photodetectors have had some success, more research into applications is still needed. This is mainly attributed to the fact that the design and preparation of 2D/organic heterojunction photodetectors involves a wide range of materials and processes and often requires highly sophisticated techniques and equipment. This complexity may make research and development even more challenging. In addition, some organic materials may be unstable or prone to degradation, limiting the devices' long-term stability. Future research and development will likely focus on optimizing materials, improving preparation processes, enhancing performance, and reducing costs to facilitate the widespread use of these technologies.

Author contributions

All authors contributed to the writing of the manuscript.

Conflicts of interest

There are no conflicts to declare.

Acknowledgements

This journal is © The Royal Society of Chemistry 2024

J. Mater. Chem. C, 2024, **12**, 1233–1267 | **1261**

References

1 F. N. Xia, T. Mueller, Y. M. Lin, A. Valdes-Garcia and P. Avouris, *Nat. Nanotechnol.*, 2009, **4**, 839–843.

2 Q. H. Wang, K. Kalantar-Zadeh, A. Kis, J. N. Coleman and M. S. Strano, *Nat. Nanotechnol.*, 2012, **7**, 699–712.

3 O. Lopez-Sanchez, D. Lembke, M. Kayci, A. Radenovic and A. Kis, *Nat. Nanotechnol.*, 2013, **8**, 497–501.

4 V. N. Fomin, V. M. Nikitin, E. B. Zhbakov, V. A. Sautkin and E. K. Suyazova, *Phys. Wave Phenom.*, 2014, **22**, 125–131.

5 C. H. Chen, Z. Y. Li and L. Fu, *Light: Sci. Appl.*, 2023, **12**, 77.

6 S. Watson, W. K. Zhang, J. Tavares, J. Figueiredo, H. Cantu, J. Wang, E. Wasige, H. Salgado, L. Pessoa and A. Kelly, *Microw Opt. Technol. Lett.*, 2019, **61**, 1121–1125.

7 P. D. Grant, S. R. Laframboise, R. Dudek, M. Graf, A. Bezinger and H. C. Liu, *Electron. Lett.*, 2009, **45**, 952–953.

8 Y. Zhou, X. Qiu, Z. A. Wan, Z. H. Long, S. Poddar, Q. P. Zhang, Y. C. Ding, C. L. J. Chan, D. Q. Zhang, K. M. Zhou, Y. J. Lin and Z. Y. Fan, *Nano Energy*, 2022, **100**, 107516.

9 T. Dong, J. Simoes and Z. C. Yang, *Adv. Mater. Interfaces*, 2020, **7**, 1901657.

10 T. Zhang, C. C. Ling, X. M. Wang, B. X. Feng, M. Cao, X. Xue, Q. Z. Xue, J. Q. Zhang, L. Zhu, C. A. K. Wang, H. P. Lu and W. P. Liu, *Adv. Mater. Technol.*, 2022, **7**, 2200250.

11 P. Buechele, M. Richter, S. F. Tedde, G. J. Matt, G. N. Ankah, R. Fischer, M. Biele, W. Metzger, S. Lilliu, O. Bikondoa, J. E. Macdonald, C. J. Brabec, T. Kraus, U. Lemmer and O. Schmidt, *Nat. Photonics*, 2015, **9**, 843–848.

12 W. W. Moses, *Nucl. Instrum. Methods Phys. Res., Sect. A*, 2009, **610**, 11–15.

13 J. L. Wang, H. H. Fang, X. D. Wang, X. S. Chen, W. Lu and W. D. Hu, *Small*, 2017, **13**, 1700894.

14 W. Lang, *Mater. Sci. Eng. R-Rep.*, 1996, **17**, 1–55.

15 B. Jalali and S. Fathpour, *J. Lightwave Technol.*, 2006, **24**, 4600–4615.

16 R. E. Camacho-Aguilera, Y. Cai, N. Patel, J. T. Bessette, M. Romagnoli, L. C. Kimerling and J. Michel, *Opt. Express*, 2012, **20**, 11316–11320.

17 R. I. Macdonald, *Appl. Opt.*, 1981, **20**, 591–594.

18 N. Koguchi, S. Takahashi and T. Chikyow, *J. Cryst. Growth*, 1991, **111**, 688–692.

19 D. B. Li, X. J. Sun, H. Song, Z. M. Li, Y. R. Chen, H. Jiang and G. Q. Miao, *Adv. Mater.*, 2012, **24**, 845–849.

20 M. Ruff, H. Mitlehner and R. Helbig, *IEEE Trans. Electron Devices*, 1994, **41**, 1040–1054.

21 B. Zhao, F. Wang, H. Y. Chen, L. X. Zheng, L. X. Su, D. X. Zhao and X. S. Fang, *Adv. Funct. Mater.*, 2017, **27**, 1700264.

22 D. L. Smith and C. Mailhiot, *J. Appl. Phys.*, 1987, **62**, 2545–2548.

23 M. Casalino, G. Coppola, M. Iodice, I. Rendina and L. Sirleto, *Sensors*, 2010, **10**, 10571–10600.

24 Y. K. Su, C. L. Lin, S. M. Chen, J. R. Chang and D. H. Jaw, *J. Appl. Phys.*, 1997, **81**, 7529–7532.

25 A. K. Geim and K. S. Novoselov, *Nat. Mater.*, 2007, **6**, 183–191.

26 A. H. Castro Neto, F. Guinea, N. M. R. Peres, K. S. Novoselov and A. K. Geim, *Rev. Mod. Phys.*, 2009, **81**, 109–162.

27 S. Stankovich, D. A. Dikin, G. H. B. Dommett, K. M. Kohlhaas, E. J. Zimney, E. A. Stach, R. D. Piner, S. T. Nguyen and R. S. Ruoff, *Nature*, 2006, **442**, 282–286.

28 S. Gopalan, M. L. van de Put, G. Gaddemane and M. V. Fischetti, *Phys. Rev. Appl.*, 2022, **18**, 054062.

29 K. F. Mak, C. Lee, J. Hone, J. Shan and T. F. Heinz, *Phys. Rev. Lett.*, 2010, **105**, 136805.

30 Y. Kim, S. S. Cruz, K. Lee, B. O. Alawode, C. Choi, Y. Song, J. M. Johnson, C. Heidelberger, W. Kong, S. Choi, K. Qiao, I. Almansouri, E. A. Fitzgerald, J. Kong, A. M. Kolpak, J. Hwang and J. Kim, *Nature*, 2017, **544**, 340–343.

31 S. J. Kang, D. H. Lee, J. Kim, A. Capasso, H. S. Kang, J. W. Park, C. H. Lee and G. H. Lee, *2D Mater.*, 2020, **7**, 022003.

32 J. R. An, X. Y. Zhao, Y. N. Zhang, M. X. Liu, J. Yuan, X. J. Sun, Z. Y. Zhang, B. Wang, S. J. Li and D. B. Li, *Adv. Funct. Mater.*, 2022, **32**, 2110119.

33 F. X. Yang, S. S. Cheng, X. T. Zhang, X. C. Ren, R. J. Li, H. L. Dong and W. P. Hu, *Adv. Mater.*, 2018, **30**, 1702415.

34 X. T. Gan, D. Englund, D. Van Thourhout and J. L. Zhao, *Appl. Phys. Rev.*, 2022, **9**, 021302.

35 J. S. He, L. L. Tao, H. Zhang, B. Zhou and J. B. Li, *Nanoscale*, 2019, **11**, 2577–2593.

36 L. Liu, Z. Q. Cheng, B. Jiang, Y. X. Liu, Y. L. Zhang, F. Yang, J. H. Wang, X. F. Yu, P. K. Chu and C. Ye, *ACS Appl. Mater. Interfaces*, 2021, **13**, 30797–30805.

37 B. Radisavljevic, A. Radenovic, J. Brivio, V. Giacometti and A. Kis, *Nat. Nanotechnol.*, 2011, **6**, 147–150.

38 J. Y. Han, F. K. Wang, S. Han, W. J. Deng, X. Y. Du, H. Yu, J. Gou, Q. J. Wang and J. Wang, *Adv. Funct. Mater.*, 2022, **32**, 2205150.

39 L. S. Li, Y. Y. Huang, J. B. Peng, Y. Cao and X. B. Peng, *J. Mater. Chem. C*, 2014, **2**, 1372–1375.

40 Y. Higashi, K. S. Kim, H. G. Jeon and M. Ichikawa, *J. Appl. Phys.*, 2010, **108**, 034502.

41 J. Wang, J. Y. Han, X. Q. Chen and X. R. Wang, *InfoMat*, 2019, **1**, 33–53.

42 L. Song, L. J. Ci, H. Lu, P. B. Sorokin, C. H. Jin, J. Ni, A. G. Kvashnin, D. G. Kvashnin, J. Lou, B. I. Yakobson and P. M. Ajayan, *Nano Lett.*, 2010, **10**, 3209–3215.

43 T. Miyake, K. Nakamura, R. Arita and M. Imada, *J. Phys. Soc. Jpn.*, 2010, **79**, 044705.

44 C. Pramanik and G. P. Miller, *Molecules*, 2012, **17**, 4625–4633.

45 J. Y. Jang, S. H. Kim, S. Nam, D. S. Chung, C. W. Yang, W. M. Yun, C. E. Park and J. B. Koo, *Appl. Phys. Lett.*, 2008, **92**, 143306.

46 J. S. Jung, J. W. Lee, K. Kim, M. Y. Cho, S. G. Jo and J. Joo, *Chem. Mater.*, 2010, **22**, 2219–2225.

47 S. Shaari, S. Naka and H. Okada, *J. Photopolym. Sci. Technol.*, 2016, **29**, 363–368.

1262 | *J. Mater. Chem. C*, 2024, **12**, 1233–1267

This journal is © The Royal Society of Chemistry 2024

48 H. Y. Wang, Z. X. Li, D. Y. Li, P. Chen, L. J. Pi, X. Zhou and T. Y. Zhai, *Adv. Funct. Mater.*, 2021, **31**, 2103106.

49 M. Gobbi, E. Orgiu and P. Samorì, *Adv. Mater.*, 2018, **30**, 1706103.

50 J. Y. Han and J. Wang, *Chin. Phys. B*, 2019, **28**, 017103.

51 H. W. Li, Z. Dong, Y. Zhang, L. Q. Li, Z. C. Wang, C. Wang, K. Zhang and H. Zhang, *2D Mater.*, 2021, **8**, 012001.

52 X. Q. Chen, K. Shehzad, L. Gao, M. S. Long, H. Guo, S. C. Qin, X. M. Wang, F. Q. Wang, Y. Shi, W. D. Hu, Y. Xu and X. R. Wang, *Adv. Mater.*, 2020, **32**, 1902039.

53 K. Pei and T. Y. Zhai, *Cell Rep. Phys. Sci.*, 2020, **1**, 100166.

54 P. Cheng, G. Li, X. W. Zhan and Y. Yang, *Nat. Photonics*, 2018, **12**, 131–142.

55 N. Gasparini, A. Salleo, I. McCulloch and D. Baran, *Nat. Rev. Mater.*, 2019, **4**, 229–242.

56 P. Sonar, J. P. F. Lim and K. L. Chan, *Energy Environ. Sci.*, 2011, **4**, 1558–1574.

57 Y. Liu, R. Cheng, L. Liao, H. L. Zhou, J. W. Bai, G. Liu, L. X. Liu, Y. Huang and X. F. Duan, *Nat. Commun.*, 2011, **2**, 579.

58 X. C. Miao, S. Tongay, M. K. Petterson, K. Berke, A. G. Rinzler, B. R. Appleton and A. F. Hebard, *Nano Lett.*, 2012, **12**, 2745–2750.

59 G. Rao, M. Freitag, H. Y. Chiu, R. S. Sundaram and P. Avouris, *ACS Nano*, 2011, **5**, 5848–5854.

60 M. Buscema, J. O. Island, D. J. Groenendijk, S. I. Blanter, G. A. Steele, H. S. J. van der Zant and A. Castellanos-Gomez, *Chem. Soc. Rev.*, 2015, **44**, 3691–3718.

61 P. L. Richards, *J. Appl. Phys.*, 1994, **76**, 1–24.

62 W. Z. Yu, S. J. Li, Y. P. Zhang, W. L. Ma, T. Sun, J. Yuan, K. Fu and Q. L. Bao, *Small*, 2017, **13**, 1700268.

63 J. C. Norman, D. Jung, Y. T. Wan and J. E. Bowers, *Appl. Photon.*, 2018, **3**, 030901.

64 H. Li, P. L. Xu, D. Liu, J. Y. He, H. L. Zu, J. J. Song, J. Zhang, F. H. Tian, M. J. Yun and F. Y. Wang, *Nanotechnology*, 2021, **32**, 375202.

65 M. Czerniak-Reczulska, A. Niedzielska and A. Jedrzejczak, *Adv. Mater. Sci.*, 2015, **15**, 67.

66 T. Sattar, *Top. Curr. Chem.*, 2019, **377**, 1–45.

67 T. Low and P. Avouris, *ACS Nano*, 2014, **8**, 1086–1101.

68 Z. Y. Wang and B. X. Mi, *Environ. Sci. Technol.*, 2017, **51**, 8229–8244.

69 A. Splendiani, L. Sun, Y. B. Zhang, T. S. Li, J. Kim, C. Y. Chim, G. Galli and F. Wang, *Nano Lett.*, 2010, **10**, 1271–1275.

70 H. L. Zeng, J. F. Dai, W. Yao, D. Xiao and X. D. Cui, *Nat. Nanotechnol.*, 2012, **7**, 490–493.

71 K. F. Mak, K. L. He, C. Lee, G. H. Lee, J. Hone, T. F. Heinz and J. Shan, *Nat. Mater.*, 2013, **12**, 207–211.

72 H. A. Li, Y. Li, A. Aljarb, Y. M. Shi and L. J. Li, *Chem. Rev.*, 2018, **118**, 6134–6150.

73 C. Knieke, A. Berger, M. Voigt, R. N. K. Taylor, J. Röhrl and W. Peukert, *Carbon*, 2010, **48**, 3196–3204.

74 H. J. Park, J. Meyer, S. Roth and V. Skákalová, *Carbon*, 2010, **48**, 1088–1094.

75 Y. X. Yan, F. Z. Nashath, S. R. Chen, S. Manickam, S. S. Lim, H. T. Zhao, E. Lester, T. Wu and C. H. Pang, *Nanotechnol. Rev.*, 2020, **9**, 1284–1314.

76 J. G. Song, X. Z. Wang and C. T. Chang, *J. Nanomater.*, 2014, **2014**, 6.

77 A. Dodabalapur, *Solid State Commun.*, 1997, **102**, 259–267.

78 S. Reineke, M. Thomschke, B. Lüssem and K. Leo, *Rev. Mod. Phys.*, 2013, **85**, 1245–1293.

79 G. M. Farinola and R. Ragni, *Chem. Soc. Rev.*, 2011, **40**, 3467–3482.

80 H. Sirringhaus, T. Kawase, R. H. Friend, T. Shimoda, M. Inbasekaran, W. Wu and E. P. Woo, *Science*, 2000, **290**, 2123–2126.

81 T. Yasuda, T. Goto, K. Fujita and T. Tsutsui, *Appl. Phys. Lett.*, 2004, **85**, 2098–2100.

82 H. Sirringhaus, N. Tessler and R. H. Friend, *Science*, 1998, **280**, 1741–1744.

83 C. D. Sheraw, L. Zhou, J. R. Huang, D. J. Gundlach, T. N. Jackson, M. G. Kane, I. G. Hill, M. S. Hammond, J. Campi, B. K. Greening, J. Francl and J. West, *Appl. Phys. Lett.*, 2002, **80**, 1088–1090.

84 A. P. Côté, A. I. Benin, N. W. Ockwig, M. O'Keeffe, A. J. Matzger and O. M. Yaghi, *Science*, 2005, **310**, 1166–1170.

85 S. Y. Ding and W. Wang, *Chem. Soc. Rev.*, 2013, **42**, 548–568.

86 S. Bhunia, K. A. Deo and A. K. Gaharwar, *Adv. Funct. Mater.*, 2020, **30**, 2002046.

87 Z. J. Lin, J. Lu, M. Hong and R. Cao, *Chem. Soc. Rev.*, 2014, **43**, 5867–5895.

88 G. Maurin, C. Serre, A. Cooper and G. Féreyd, *Chem. Soc. Rev.*, 2017, **46**, 3104–3107.

89 M. S. Yao, W. H. Li and G. Xu, *Coord. Chem. Rev.*, 2021, **426**, 213479.

90 T. Agostinelli, M. Campoy-Quiles, J. C. Blakesley, R. Speller, D. D. C. Bradley and J. Nelson, *Appl. Phys. Lett.*, 2008, **93**, 203305.

91 F. Stuker, C. Baltes, K. Dikaiou, D. Vats, L. Carrara, E. Charbon, J. Ripoll and M. Rudin, *IEEE Trans. Med. Imaging*, 2011, **30**, 1265–1273.

92 C. M. M. Paschoal, D. D. Souza and L. A. P. Santos, *IEEE Trans. Nucl. Sci.*, 2013, **60**, 735–738.

93 G. Llosá, N. Belcari, M. G. Bisogni, G. Collazuol, S. Marcatili, P. Barrillon, C. de la Taille, S. Bondil-Blin, N. Dinu, M. Melchiorri, A. Tarolli, C. Piemonte and A. Del Guerra, *IEEE Trans. Nucl. Sci.*, 2009, **56**, 2586–2593.

94 E. Suematsu and N. Imai, *IEEE Trans. Microw Theory Technol.*, 1996, **44**, 133–143.

95 B. Zhang, Y. Q. Guan, L. H. Xia, D. X. Dong, Q. Chen, C. Xu, C. Wu, H. X. Huang, L. B. Zhang, L. Kang, J. Chen and P. H. Wu, *Supercond. Sci. Technol.*, 2021, **34**, 034005.

96 X. Huang, Y. L. Guo and Y. Q. Liu, *Chem. Commun.*, 2021, **57**, 11429–11442.

97 B. H. Park, S. D. Baek, J. Y. Kim, J. Bae, H. Han and O. Kwon, *Opt. Eng.*, 2002, **41**, 1339–1345.

98 J. F. Huang, J. Lee, J. Vollbrecht, V. V. Brus, A. L. Dixon, D. X. Cao, Z. Y. Zhu, Z. F. Du, H. B. Wang, K. Cho, G. C. Bazan and T. Q. Nguyen, *Adv. Mater.*, 2020, **32**, 1906027.

This journal is © The Royal Society of Chemistry 2024

J. Mater. Chem. C, 2024, **12**, 1233–1267 | **1263**

99 Y. Zhai, G. R. Gu and X. J. Lu, *Micromachines*, 2019, **10**, 4.

100 X. F. Yin, G. Y. Liu and S. L. Cao, *J. Nanoelectron. Optoelectron.*, 2020, **15**, 1508–1517.

101 J. Xue, Z. F. Zhu, X. B. Xu, Y. Gu, S. L. Wang, L. M. Xu, Y. S. Zou, J. Z. Song, H. B. Zeng and Q. Chen, *Nano Lett.*, 2018, **18**, 7628–7634.

102 Z. Alaie, S. M. Nejad and M. H. Yousefi, *Mater. Sci. Semicond. Process.*, 2015, **29**, 16–55.

103 M. Ding, Z. Guo, X. H. Chen, X. R. Ma and L. Q. Zhou, *Nanomaterials*, 2020, **10**, 362.

104 F. Zhong, H. Wang, Z. Wang, Y. Wang, T. He, P. S. Wu, M. Peng, H. L. Wang, T. F. Xu, F. Wang, P. Wang, J. S. Miao and W. D. Hu, *Nano Res.*, 2021, **14**, 1840–1862.

105 F. C. Liu, H. Shimotani, H. Shang, T. Kanagasekaran, V. Zólyomi, N. Drummond, V. I. Fal'ko and K. Tanigaki, *ACS Nano*, 2014, **8**, 752–760.

106 M. Yang, J. Wang, J. Y. Han, J. W. Ling, C. H. Ji, X. Kong, X. C. Liu, Z. H. Huang, J. Gou, Z. J. Liu, F. X. Xiu and Y. D. Jiang, *ACS Photonics*, 2018, **5**, 3438–3445.

107 V. Mackowiak, J. Peupelmann, Y. Ma and A. Gorges, Thorlabs, Inc, 2015, 56.

108 Z. X. Zou, J. W. Liang, X. H. Zhang, C. Ma, P. Xu, X. Yang, Z. X. S. Zeng, X. X. Sun, C. G. Zhu, D. L. Liang, X. J. Zhuang, D. Li and A. L. Pan, *ACS Nano*, 2021, **15**, 10039–10047.

109 Z. Q. Xu, Y. P. Zhang, Z. Y. Wang, Y. T. Shen, W. C. Huang, X. Xia, W. Z. Yu, Y. Z. Xue, L. T. Sun, C. X. Zheng, Y. R. Lu, L. Liao and Q. L. Bao, *2D Mater.*, 2016, **3**, 041001.

110 J. Gilot, M. M. Wienk and R. A. J. Janssen, *Adv. Funct. Mater.*, 2010, **20**, 3904–3911.

111 K. T. Ly, R. W. Chen-Cheng, H. W. Lin, Y. J. Shiau, S. H. Liu, P. T. Chou, C. S. Tsao, Y. C. Huang and Y. Chi, *Nat. Photonics*, 2017, **11**, 63–68.

112 K. S. Novoselov, A. K. Geim, S. V. Morozov, D. Jiang, Y. Zhang, S. V. Dubonos, I. V. Grigorieva and A. A. Firsov, *Science*, 2004, **306**, 666–669.

113 Y. Lee, S. H. Yu, J. Jeon, H. Kim, J. Y. Lee, H. Kim, J.-H. Ahn, E. Hwang and J. H. Cho, *Carbon*, 2015, **88**, 165–172.

114 X. Yu, Z. Dong, J. K. W. Yang and Q. J. Wang, *Optica*, 2016, **3**, 979–984.

115 L. Gao, C. Ge, W. Li, C. Jia, K. Zeng, W. Pan, H. Wu, Y. Zhao, Y. He, J. He, Z. Zhao, G. Niu, X. Guo, F. P. G. de Arquer, E. H. Sargent and J. Tang, *Adv. Funct. Mater.*, 2017, **27**, 1702360.

116 G. F. Jones, R. M. Pinto, A. De Sanctis, V. K. Nagareddy, C. D. Wright, H. Alves, M. F. Craciun and S. Russo, *Adv. Mater.*, 2017, **29**, 1702993.

117 S. Qin, X. Chen, Q. Du, Z. Nie, X. Wang, H. Lu, X. Wang, K. Liu, Y. Xu, Y. Shi, R. Zhang and F. Wang, *ACS Appl. Mater. Interfaces*, 2018, **10**, 38326–38333.

118 J. Liu, K. Zhou, J. Liu, J. Zhu, Y. Zhen, H. Dong and W. Hu, *Adv. Mater.*, 2018, **30**, 1803655.

119 Y. Lee, H. Kim, S. Kim, D. Whang and J. H. Cho, *ACS Appl. Mater. Interfaces*, 2019, **11**, 23474–23481.

120 S. Chugh, N. Adhikari, J. H. Lee, D. Berman, L. Echegoyen and A. B. Kaul, *ACS Appl. Mater. Interfaces*, 2019, **11**, 24349–24359.

121 R. Pan, J. Han, X. Zhang, Q. Han, H. zhou, X. Liu, J. Gou, Y. Jiang and J. Wang, *Carbon*, 2020, **162**, 375–381.

122 M.-Y. Shao, M. Yu, M. Suzuki, H. Yamada, Y.-P. Wang, Y. Chen, C. Lu, D. Wang and Z.-Y. Yang, *ACS Appl. Electron. Mater.*, 2020, **2**, 3459–3467.

123 J. Han, C. Zhang, S. Peng, X. Zhang, X. Liu, H. Zhou, H. Yu and J. Wang, *J. Mater. Chem. C*, 2021, **9**, 13963–13971.

124 Y. J. Choi, S. B. Jo and J. H. Cho, *Adv. Mater.*, 2021, **33**, 2102725.

125 J. S. Kim, Y. J. Choi, H. J. Woo, J. Yang, Y. J. Song, M. S. Kang and J. H. Cho, *Adv. Funct. Mater.*, 2017, **27**, 1704475.

126 J. Han, J. Wang, M. Yang, X. Kong, X. Chen, Z. Huang, H. Guo, J. Gou, S. Tao, Z. Liu, Z. Wu, Y. Jiang and X. Wang, *Adv. Mater.*, 2018, **30**, 1804020.

127 N. N. Nguyen, H. C. Lee, K. Baek, M. S. Yoo, H. Lee, H. Lim, S. Choi, C. J. Kim, S. Nam and K. Cho, *Adv. Funct. Mater.*, 2020, **31**, 2008813.

128 Y. Gan, S. Qin, Q. Du, Y. Zhang, J. Zhao, M. Li, A. Wang, Y. Liu, S. Li, R. Dong, L. Zhang, X. Chen, C. Liu, W. Wang and F. Wang, *Adv. Sci.*, 2022, **9**, 2204332.

129 S. Qin, X. Qin, Q. Du, Y. Gan, Y. Zhang, A. Wang, X. Yan, R. Dong, Y. Liu, S. Li, C. Liu, W. Wang and F. Wang, *J. Mater. Chem. C*, 2022, **10**, 11710–11718.

130 J. Zhao, Q. Du, X. Zheng, Y. Liu, S. Li, W. Wang, F. Wang and S. Qin, *ACS Photonics*, 2023, **10**, 2955–2963.

131 W. C. Tan, W. H. Shih and Y. F. Chen, *Adv. Funct. Mater.*, 2014, **24**, 6818–6825.

132 E. H. Huisman, A. G. Shulga, P. J. Zomer, N. Tombros, D. Bartesaghi, S. Z. Bisri, M. A. Loi, L. J. Koster and B. J. van Wees, *ACS Appl. Mater. Interfaces*, 2015, **7**, 11083–11088.

133 X. Liu, X. Luo, H. Nan, H. Guo, P. Wang, L. Zhang, M. Zhou, Z. Yang, Y. Shi, W. Hu, Z. Ni, T. Qiu, Z. Yu, J. B. Xu and X. Wang, *Adv. Mater.*, 2016, **28**, 5200–5205.

134 P.-H. Chang, Y.-C. Tsai, S.-W. Shen, S.-Y. Liu, K.-Y. Huang, C.-S. Li, H.-P. Chang and C.-I. Wu, *ACS Photonics*, 2017, **4**, 2335–2344.

135 Q.-M. Wang and Z.-Y. Yang, *Carbon*, 2018, **138**, 90–97.

136 O. Yakar, O. Balci, B. Uzlu, N. Polat, O. Ari, I. Tunc, C. Kocabas and S. Balci, *ACS Appl. Nano Mater.*, 2019, **3**, 409–417.

137 B. Sun, G. Zhou, Y. Wang, X. Xu, L. Tao, N. Zhao, H. K. Tsang, X. Wang, Z. Chen and J. B. Xu, *Adv. Opt. Mater.*, 2021, **9**, 2100158.

138 M. Yu, Y. Chen, Y. G. Chen, Z. Y. Yang, W. F. Zhang and G. Yu, *Adv. Mater. Interfaces*, 2021, **8**, 2100770.

139 S. Fu, R. Song, Y. Wang, Y. Han, C. Gao, J. Ma, H. Xu, B. Li, A. Shen and Y. Liu, *Adv. Mater. Interfaces*, 2023, **10**, 2202488.

140 S. Y. Chen, Y. Y. Lu, F. Y. Shih, P. H. Ho, Y. F. Chen, C. W. Chen, Y. T. Chen and W. H. Wang, *Carbon*, 2013, **63**, 23–29.

141 P. H. Ho, S. S. Li, Y. T. Liou, C. Y. Wen, Y. H. Chung and C. W. Chen, *Adv. Mater.*, 2015, **27**, 282–287.

142 Y. Lee, J. Kwon, E. Hwang, C. H. Ra, W. J. Yoo, J. H. Ahn, J. H. Park and J. H. Cho, *Adv. Mater.*, 2015, **27**, 41–46.

1264 | *J. Mater. Chem. C*, 2024, **12**, 1233–1267

This journal is © The Royal Society of Chemistry 2024

143 Z. Sun, L. Aigouy and Z. Chen, *Nanoscale*, 2016, **8**, 7377–7383.

144 L. Qin, L. Wu, B. Kattel, C. Li, Y. Zhang, Y. Hou, J. Wu and W. L. Chan, *Adv. Funct. Mater.*, 2017, **27**, 1704173.

145 M. Cui, Y. Guo, Y. Zhu, H. Liu, W. Wen, J. Wu, L. Cheng, Q. Zeng and L. Xie, *J. Phys. Chem. C*, 2018, **122**, 7551–7556.

146 K. P. Bera, G. Haider, M. Usman, P. K. Roy, H. I. Lin, Y. M. Liao, C. R. P. Inbaraj, Y. R. Liou, M. Kataria, K. L. Lu and Y. F. Chen, *Adv. Funct. Mater.*, 2018, **28**, 1804802.

147 Z. Y. Peng, J. L. Xu, J. Y. Zhang, X. Gao and S. D. Wang, *Adv. Mater. Interfaces*, 2018, **5**, 1800505.

148 K. P. Bera, G. Haider, Y. T. Huang, P. K. Roy, C. R. Paul Inbaraj, Y. M. Liao, H. I. Lin, C. H. Lu, C. Shen, W. Y. Shih, W. H. Shih and Y. F. Chen, *ACS Nano*, 2019, **13**, 12540–12552.

149 M. A. Iqbal, M. Cui, A. Liaqat, R. faiz, M. Hossain, X. Wang, S. Hussain, C. Dang, H. Liu, W. Wen, J. Wu and L. Xie, *Nanotechnology*, 2019, **30**, 254003.

150 Y. H. Lee, S. Park, Y. Won, J. Mun, J. H. Ha, J. H. Lee, S. H. Lee, J. Park, J. Yeom, J. Rho, H. Ko and J. H. Oh, *NPG Asia Mater.*, 2020, **12**, 79.

151 M. A. Iqbal, A. Liaqat, S. Hussain, X. Wang, M. Tahir, Z. Urooj and L. Xie, *Adv. Mater.*, 2020, **32**, 2002628.

152 Y. Xiong, Q. Liao, Z. Huang, X. Huang, C. Ke, H. Zhu, C. Dong, H. Wang, K. Xi, P. Zhan, F. Xu and Y. Lu, *Adv. Mater.*, 2020, **32**, 1907242.

153 F. Feng, T. Wang, J. Qiao, C. Min, X. Yuan and M. Somekh, *ACS Appl. Mater. Interfaces*, 2021, **13**, 61496–61505.

154 Z. He, J. Han, X. Du, L. Cao, J. Wang, C. Zheng, H. Lin and S. Tao, *Adv. Funct. Mater.*, 2021, **31**, 2103988.

155 C. Han, X. Liu, X. Han, M. He, J. Han, H. Zhang, X. Hou, H. Zhou, H. Yu, Z. Wu, J. Gou and J. Wang, *Adv. Funct. Mater.*, 2022, **32**, 2209680.

156 Z. Liu, K. Parvez, R. Li, R. Dong, X. Feng and K. Mullen, *Adv. Mater.*, 2015, **27**, 669–675.

157 C. Xie and F. Yan, *ACS Appl. Mater. Interfaces*, 2017, **9**, 1569–1576.

158 X. Chen, X. Liu, B. Wu, H. Nan, H. Guo, Z. Ni, F. Wang, X. Wang, Y. Shi and X. Wang, *Nano Lett.*, 2017, **17**, 6391–6396.

159 A. Yadav, A. Upadhyaya, S. K. Gupta, A. S. Verma and C. M. S. Negi, *Thin Solid Films*, 2019, **675**, 128–135.

160 X. Liu, X. Chen, J. Yi, Z. Luo, H. Nan, H. Guo, Z. Ni, Y. Ding, S. Dai and X. Wang, *Org. Electron.*, 2019, **64**, 22–26.

161 Y. Lee, S. Cha and C. Kim, *Adv. Mater. Interfaces*, 2021, **8**, 2100478.

162 G. Zhou, R. Sun, Y. Xiao, G. Abbas and Z. Peng, *Adv. Electron. Mater.*, 2021, **7**, 2000522.

163 M. He, J. Han, X. Han, J. Gou, M. Yang, Z. Wu, Y. Jiang and J. Wang, *Carbon*, 2021, **178**, 506–514.

164 Q. Dai, G. Hu, W. Lv, S. Xu, L. Sun, G. F. Schneider, L. Jiang and Y. Peng, *Adv. Mater. Interfaces*, 2022, **9**, 2200116.

165 M. Li, S. Qin, X. Zheng, Q. Du, Y. Liu, S. Li, H. Li, W. Wang and F. Wang, *ACS Appl. Mater. Interfaces*, 2023, **15**, 48442–48451.

166 Y. J. Choi, H. J. Woo, S. Kim, J. Sun, M. S. Kang, Y. J. Song and J. H. Cho, *J. Ind. Eng. Chem.*, 2020, **89**, 233–238.

167 Y. Yao, Q. Ou, K. Wang, H. Peng, F. Fang, Y. Shi, Y. Wang, D. I. Asperilla, Z. Shuai and P. Samori, *Nat. Commun.*, 2021, **12**, 3667.

168 D. U. Lim, S. B. Jo and J. H. Cho, *J. Am. Chem. Soc.*, 2021, **143**, 879–890.

169 K. P. Bera, Y.-G. Lee, M. Usman, R. Ghosh, K.-L. Lu and Y.-F. Chen, *ACS Appl. Electron. Mater.*, 2022, **4**, 2337–2345.

170 G. Hu, H. Zhu, Q. Dai, C. Jiang, Y. Peng, W. Lv, S. Xu, L. Sun, L. Jiang and G. F. Schneider, *Appl. Phys. Lett.*, 2022, **121**, 123501.

171 S. H. Yu, Y. Lee, S. K. Jang, J. Kang, J. Jeon, C. Lee, J. Y. Lee, H. Kim, E. Hwang, S. Lee and J. H. Cho, *ACS Nano*, 2014, **8**, 8285–8291.

172 F. Liu, W. L. Chow, X. He, P. Hu, S. Zheng, X. Wang, J. Zhou, Q. Fu, W. Fu, P. Yu, Q. Zeng, H. J. Fan, B. K. Tay, C. Kloc and Z. Liu, *Adv. Funct. Mater.*, 2015, **25**, 5865–5871.

173 D. Jariwala, S. L. Howell, K. S. Chen, J. Kang, V. K. Sangwan, S. A. Filippone, R. Turrisi, T. J. Marks, L. J. Lauhon and M. C. Hersam, *Nano Lett.*, 2016, **16**, 497–503.

174 Y. Huang, F. Zhuge, J. Hou, L. Lv, P. Luo, N. Zhou, L. Gan and T. Zhai, *ACS Nano*, 2018, **12**, 4062–4073.

175 Z. H. Xu, L. Tang, S. W. Zhang, J. Z. Li, B. L. Liu, S. C. Zhao, C. J. Yu and G. D. Wei, *Mater. Today Phys.*, 2020, **15**, 100273.

176 B. Zhao, Z. Gan, M. Johnson, E. Najafidehaghani, T. Rejek, A. George, R. H. Fink, A. Turchanin and M. Halik, *Adv. Funct. Mater.*, 2021, **31**, 2105444.

177 J. Li, S. Ding, X. Ren, Q. Sun, L. Sun, L. Zheng, F. Li, W. Zhu and W. Hu, *ACS Mater. Lett.*, 2022, **4**, 1483–1492.

178 Q. Luo, G. Feng, Y. Song, E. Zhang, J. Yuan, D. Fa, Q. Sun, S. Lei and W. Hu, *Nano Res.*, 2022, **15**, 8428–8434.

179 S. Xu, D. Yang, L. Sun, W. Lv, X. Wu, Y. Wei, X. Fang, X. Song, Y. Wang, Y. Tang and Y. Peng, *ACS Appl. Electron. Mater.*, 2022, **4**, 2777–2786.

180 Z. Xu, M. He, Q. Wu, C. Wu, X. Li, B. Liu, M. C. Tang, J. Yao and G. Wei, *Adv. Sci.*, 2023, **10**, 2207743.

181 D. He, Y. Pan, H. Nan, S. Gu, Z. Yang, B. Wu, X. Luo, B. Xu, Y. Zhang, Y. Li, Z. Ni, B. Wang, J. Zhu, Y. Chai, Y. Shi and X. Wang, *Appl. Phys. Lett.*, 2015, **107**, 183103.

182 X. Wang, P. Wang, J. Wang, W. Hu, X. Zhou, N. Guo, H. Huang, S. Sun, H. Shen, T. Lin, M. Tang, L. Liao, A. Jiang, J. Sun, X. Meng, X. Chen, W. Lu and J. Chu, *Adv. Mater.*, 2015, **27**, 6575–6581.

183 C. E. Petoukhoff, M. B. Krishna, D. Voiry, I. Bozkurt, S. Deckoff-Jones, M. Chhowalla, D. M. O'Carroll and K. M. Dani, *ACS Nano*, 2016, **10**, 9899–9908.

184 D. B. Velusamy, M. A. Haque, M. R. Parida, F. Zhang, T. Wu, O. F. Mohammed and H. N. Alshareef, *Adv. Funct. Mater.*, 2017, **27**, 1605554.

185 M. Sun, P. Yang, D. Xie, Y. Sun, J. Xu, T. Ren and Y. Zhang, *Adv. Electron. Mater.*, 2018, **5**, 1800580.

186 L. Lv, F. Zhuge, F. Xie, X. Xiong, Q. Zhang, N. Zhang, Y. Huang and T. Zhai, *Nat. Commun.*, 2019, **10**, 3331.

187 X. Wang, H. Shen, Y. Chen, G. Wu, P. Wang, H. Xia, T. Lin, P. Zhou, W. Hu, X. Meng, J. Chu and J. Wang, *Adv. Sci.*, 2019, **6**, 1901050.

This journal is © The Royal Society of Chemistry 2024

J. Mater. Chem. C, 2024, **12**, 1233–1267 | **1265**

188 Y. Hao, C. He, J. Xu, Y. Bao, H. Wang, J. Li, H. Luo, M. An, M. Zhang, Q. Zhang, J. Qiu and Y. Yang, *J. Phys. Chem. C*, 2022, **126**, 16349–16356.

189 Z. Xu, Y. Zeng, F. Meng, S. Gao, S. Fan, Y. Liu, Y. Zhang, S. Wageh, A. A. Al-Ghamdi, J. Xiao, Z. Guo and H. Zhang, *Adv. Mater. Interfaces*, 2022, **9**, 2200912.

190 A. K. Dwivedi, S. Jit and S. Tripathi, *IEEE Trans. Electron Devices*, 2023, **70**, 4694–4699.

191 X. Liu, J. Gu, K. Ding, D. Fan, X. Hu, Y. W. Tseng, Y. H. Lee, V. Menon and S. R. Forrest, *Nano Lett.*, 2017, **17**, 3176–3181.

192 F. Huang, J. Li, Z. Xu, Y. Liu, R. Luo, S. W. Zhang, P. Nie, Y. Lv, S. Zhao, W. Su, W. D. Li, S. Zhao, G. Wei, H. C. Kuo and F. Kang, *Nanomaterials*, 2019, **9**, 1312.

193 K. Pei, F. Wang, W. Han, S. Yang, K. Liu, K. Liu, H. Li and T. Zhai, *Small*, 2020, **16**, 2002312.

194 B. Yang, Y. Wang, L. Li, J. Zhang, J. Wang, H. Jiao, D. Hao, P. Guo, S. Zeng, Z. Hua and J. Huang, *Adv. Funct. Mater.*, 2021, **31**, 2103787.

195 F. Wang, J. Wu, Y. Zhang, S. Yang, N. Zhang, H. Li and T. Zhai, *Sci. China-Mater.*, 2021, **65**, 451–459.

196 W. Su, S. Zhang, C. Liu, Q. Tian, X. Liu, K. Li, Y. Lv, L. Liao and X. Zou, *Nano Lett.*, 2022, **22**, 10192–10199.

197 Q. Zhu, Y. Chen, T. Chen, L. Zuo, Y. Sun, R. Wang and M. Xu, *Nano Res.*, 2022, **15**, 8595–8602.

198 D. Vikraman, S. Hussain, H. Liu, S. H. Abbas Jaffery, K. Karuppasamy, J.-H. Lee, A. Kathalingam, J. Jung and H.-S. Kim, *J. Mater. Res. Technol.*, 2022, **17**, 2875–2887.

199 Z. Ge, N. Xu, Y. Zhu, K. Zhao, Y. Ma, G. Li and Y. Chen, *ACS Photonics*, 2022, **9**, 59–67.

200 T. K. Yun, Y. Lee, M. J. Kim, J. Park, D. Kang, S. Kim, Y. J. Choi, Y. Yi, B. Shong, J. H. Cho and K. Kim, *Small*, 2022, **18**, 2105916.

201 D. Z. Yang and D. G. Ma, *Adv. Opt. Mater.*, 2019, **7**, 1800522.

202 L. L. Shi, Q. B. Liang, W. Y. Wang, Y. Zhang, G. H. Li, T. Ji, Y. Y. Hao and Y. X. Cui, *Nanomaterials*, 2018, **8**, 713.

203 J. L. Miao and F. J. Zhang, *Laser Photon. Rev.*, 2019, **13**, 1800204.

204 J. S. Miao and C. Wang, *Nano Res.*, 2021, **14**, 1878–1888.

205 Q. X. Qiu and Z. M. Huang, *Adv. Mater.*, 2021, **33**, 2008126.

206 A. Bablich, S. Kataria and M. C. Lemme, *Electronics*, 2016, **5**, 13.

207 J. Sun, Y. Choi, Y. J. Choi, S. Kim, J. H. Park, S. Lee and J. H. Cho, *Adv. Mater.*, 2019, **31**, 1803831.

208 D. H. Shin and S. H. Choi, *Micromachines*, 2018, **9**, 350.

209 M. A. Khan, A. Kumar, J. Zhang and M. Kumar, *J. Mater. Chem. C*, 2021, **9**, 8129–8157.

210 H. J. Geng, D. Yuan, Z. Yang, Z. J. Tang, X. W. Zhang, K. Yang and Y. Su, *J. Mater. Chem. C*, 2019, **7**, 11056–11067.

211 A. Taffelli, S. Dirè, A. Quaranta and L. Pancheri, *Sensors*, 2021, **21**, 2758.

212 H. S. Nalwa, *RSC Adv.*, 2020, **10**, 30529–30602.

213 M. Chhowalla, H. S. Shin, G. Eda, L. J. Li, K. P. Loh and H. Zhang, *Nat. Chem.*, 2013, **5**, 263–275.

214 K. Ulman and S. Y. Quek, *Nano Lett.*, 2021, **21**, 8888–8894.

215 M. T. Fontana, D. A. Stanfield, D. T. Scholes, K. J. Winchell, S. H. Tolbert and B. J. Schwartz, *J. Phys. Chem. C*, 2019, **123**, 22711–22724.

216 K. H. Li, Y. Lu, X. K. Yang, L. C. Fu, J. G. He, X. T. Lin, J. J. Zheng, S. C. Lu, C. Chen and J. Tang, *InfoMat*, 2021, **3**, 1145–1153.

217 X. C. Tan, H. Zhang, J. Y. Li, H. W. Wan, Q. S. Guo, H. B. Zhu, H. Liu and F. Yi, *Nat. Commun.*, 2020, **11**, 5245.

218 L. L. Li, Y. H. Deng, C. X. Bao, Y. J. Fang, H. T. Wei, S. Tang, F. J. Zhang and J. S. Huang, *Adv. Opt. Mater.*, 2017, **5**, 1700672.

219 J. H. Kim, A. Liess, M. Stolte, A. M. Krause, V. Stepanenko, C. W. Zhong, D. Bialas, F. C. Spano and F. Würthner, *Adv. Mater.*, 2021, **33**, 2100582.

220 Q. L. Xu, L. Y. Zhang, B. Cheng, J. J. Fan and J. G. Yu, *Chem*, 2020, **6**, 1543–1559.

221 J. S. Kim, Y. J. Choi, H. J. Woo, J. Yang, Y. J. Song, M. S. Kang and J. H. Cho, *Adv. Funct. Mater.*, 2017, **27**, 1704475.

222 N. N. Nguyen, H. C. Lee, K. Baek, M. S. Yoo, H. Lee, H. Lim, S. Choi, C. J. Kim, S. Nam and K. Cho, *Adv. Funct. Mater.*, 2021, **31**, 2008813.

223 S. L. Zhang, Q. J. Wang, P. Zhang, J. Wang, Y. Li, C. Lu, M. T. Sarwar, X. B. Dong, Q. H. Zhao, A. D. Tang, L. J. Fu and H. M. Yang, *Small*, 2023, **19**, 2300770.

224 B. Wu, Y. H. Zhao, H. Y. Nan, Z. Y. Yang, Y. H. Zhang, H. J. Zhao, D. W. He, Z. L. Jiang, X. L. Liu, Y. Li, Y. Shi, Z. H. Ni, J. L. Wang, J. B. Xu and X. R. Wang, *Nano Lett.*, 2016, **16**, 3754–3759.

225 R. H. Dong, T. Zhang and X. L. Feng, *Chem. Rev.*, 2018, **118**, 6189–6235.

226 Y. L. Huang, Y. J. Zheng, Z. B. Song, D. Z. Chi, A. T. S. Wee and S. Y. Quek, *Chem. Soc. Rev.*, 2018, **47**, 3241–3264.

227 X. P. Xu, Y. Li and Q. Peng, *Adv. Mater.*, 2022, **1**, 311–326.

228 W. R. Zhuang, Y. Wang, P. F. Cui, L. Xing, J. Lee, D. Kim, H. L. Jiang and Y. K. Oh, *J. Controlled Release*, 2019, **294**, 311–326.

229 C. D. M. Churchill, L. R. Rutledge and S. D. Wetmore, *Phys. Chem. Chem. Phys.*, 2010, **12**, 14515–14526.

230 P. G. Song, Z. G. Xu, Y. P. Wu, Q. F. Cheng, Q. P. Guo and H. Wang, *Carbon*, 2017, **111**, 807–812.

231 Z. X. Liu Lau, G. Q. Zhou, S. X. Li, J. Ren, S. K. Das, R. X. Xia, G. Wu, H. M. Zhu, X. H. Lu, L. Yip, H. Z. Chen and C. Z. Li, *Nano Energy*, 2019, **63**, 103807.

232 A. Wadsworth, Z. Hamid, J. Kosco, N. Gasparini and I. McCulloch, *Adv. Mater.*, 2020, **32**, 2001763.

233 Q. Zhang, B. Kan, F. Liu, G. K. Long, X. J. Wan, X. Q. Chen, Y. Zuo, W. Ni, H. J. Zhang, M. M. Li, Z. C. Hu, F. Huang, Y. Cao, Z. Q. Liang, M. T. Zhang, T. P. Russell and Y. S. Chen, *Nat. Photonics*, 2015, **9**, 35–41.

234 N. N. Liang, D. Meng, Z. T. Ma, B. Kan, X. Y. Meng, Z. Zheng, W. Jiang, Y. Li, X. J. Wan, J. H. Hou, W. Ma, Y. S. Chen and Z. H. Wang, *Adv. Energy Mater.*, 2017, **7**, 1601664.

235 L. L. Zhan, S. X. Li, T. K. Lau, Y. Cui, X. H. Lu, M. M. Shi, C. Z. Li, H. Y. Li, J. H. Hou and H. Z. Chen, *Energy Environ. Sci.*, 2020, **13**, 635–645.

236 J. Yao, B. B. Qiu, Z. G. Zhang, L. W. Xue, R. Wang, C. F. Zhang, S. S. Chen, Q. J. Zhou, C. K. Sun, C. Yang,

1266 | *J. Mater. Chem. C*, 2024, **12**, 1233–1267

This journal is © The Royal Society of Chemistry 2024

M. Xiao, L. Meng and Y. F. Li, *Nat. Commun.*, 2020, **11**, 2726.

237 L. Liu, H. R. Xiao, K. Jin, Z. Xiao, X. Y. Du, K. Y. Yan, F. Hao, Q. Y. Bao, C. Y. Yi, F. Y. Liu, W. T. Wang, C. T. Zuo and L. M. Ding, *Nano-Micro Lett.*, 2023, **15**, 23.

238 B. Minnaert and P. Veelaert, *Materials*, 2012, **5**, 1933–1953.

239 T. Zhu, L. Y. Zheng, Z. Xiao, X. Y. Meng, L. Liu, L. M. Ding and X. Gong, *Sol. RRL*, 2019, **3**, 1900322.

240 P. P. Kumavat, P. Sonar and D. S. Dalal, *Renewable Sustainable Energy Rev.*, 2017, **78**, 1262–1287.

241 X. Fan, M. L. Zhang, X. D. Wang, F. H. Yang and X. M. Meng, *J. Mater. Chem. A*, 2013, **1**, 8694–8709.

242 Z. H. Zhang, S. Y. Wang, C. S. Liu, R. Z. Xie, W. D. Hu and P. Zhou, *Nat. Nanotechnol.*, 2022, **17**, 27–32.

243 L. J. Pi, P. F. Wang, S. J. Liang, P. Luo, H. Y. Wang, D. Y. Li, Z. X. Li, P. Chen, X. Zhou, F. Miao and T. Y. Zhai, *Nat. Electron.*, 2022, **5**, 248–254.

244 P. S. Wu, T. He, H. Zhu, Y. Wang, Q. Li, Z. Wang, X. Fu, F. Wang, P. Wang, C. X. Shan, Z. Y. Fan, L. Liao, P. Zhou and W. D. Hu, *InfoMat*, 2022, **4**, 12275.

245 N. Ilyas, J. Y. Wang, C. M. Li, D. Y. Li, H. Fu, D. E. Gu, X. D. Jiang, F. C. Liu, Y. D. Jiang and W. Li, *Adv. Funct. Mater.*, 2022, **32**, 2110976.

246 Y. Z. Luo, Y. Q. Xie, X. Ye and Y. Wang, *Phys. Chem. Chem. Phys.*, 2019, **21**, 7613–7617.